USGS
science for a changing world

Prepared in cooperation with the Department of the Interior Southeast Climate Science Center

Sea-Level Rise Modeling Handbook: Resource Guide for Coastal Land Managers, Engineers, and Scientists

Professional Paper 1815

U.S. Department of the Interior
U.S. Geological Survey

Sea-Level Rise Modeling Handbook: Resource Guide for Coastal Land Managers, Engineers, and Scientists

By Thomas W. Doyle, Bogdan Chivoiu, and Nicholas M. Enwright

Prepared in cooperation with the Department of the Interior
Southeast Climate Science Center

Professional Paper 1815

U.S. Department of the Interior
U.S. Geological Survey

U.S. Department of the Interior
SALLY JEWELL, Secretary

U.S. Geological Survey
Suzette M. Kimball, Acting Director

U.S. Geological Survey, Reston, Virginia: 2015

For more information on the USGS—the Federal source for science about the Earth, its natural and living resources, natural hazards, and the environment—visit http://www.usgs.gov or call 1–888–ASK–USGS.

For an overview of USGS information products, including maps, imagery, and publications, visit http://www.usgs.gov/pubprod/.

Suggested citation:
Doyle, T.W., Chivoiu, Bogdan, and Enwright, N.M., 2015, Sea-level rise modeling handbook—Resource guide for coastal land managers, engineers, and scientists: U.S. Geological Survey Professional Paper 1815, 76 p., http://dx.doi.org/10.3133/pp1815.

ISSN 2330-7102 (online)

Acknowledgments

The authors are grateful to student interns Nathan Burks and Cory Groover for data management and Internet research in support of this effort. The authors are indebted to the many government and university colleagues who contributed invaluable assistance with resource material, data, analysis, and model development including Darren Johnson, Rick Putnam, Ken Miller, Lorraine Lisiecki, Michelle Kominz, Joseph Donoghue, Laurie Rounds, Gary Mitchum, John Tirpak, and Gerald McMahon. Federal scientists and engineers Eric Glisch (U.S. Army Corps of Engineers), Martha Segura (National Park Service), and John Tirpak and Kristen Kordecki (U.S. Fish and Wildlife Service) provided valuable technical reviews.

The authors also thank Don DeAngelis and Michael Osland (U.S. Geological Survey) for providing valuable technical reviews.

Contents

Figures

Tables

Conversion Factors

Inch/Pound to International System of Units

Multiply	By	To obtain
	Length	
inch (in.)	2.54	centimeter (cm)
inch (in.)	25.4	millimeter (mm)
foot (ft)	0.3048	meter (m)
mile (mi)	1.609	kilometer (km)
yard (yd)	0.9144	meter (m)
	Area	
acre	4,047	square meter (m^2)
acre	0.4047	hectare (ha)
acre	0.004047	square kilometer (km^2)
square mile (mi^2)	259.0	hectare (ha)
square mile (mi^2)	2.590	square kilometer (km^2)
	Volume	
gallon (gal)	3.785	liter (L)
gallon (gal)	0.003785	cubic meter (m^3)
	Flow rate	
cubic foot per second (ft^3/s)	0.02832	cubic meter per second (m^3/s)
inch per year (in/yr)	25.4	millimeter per year (mm/yr)
mile per hour (mi/h)	1.609	kilometer per hour (km/h)
	Mass	
ton per year (ton/yr)	0.9072	metric ton per year

Conversion Factors—Continued

International System of Units to Inch/Pound

Multiply	By	To obtain
	Length	
centimeter (cm)	0.3937	inch (in.)
millimeter (mm)	0.03937	inch (in.)
meter (m)	3.281	foot (ft)
kilometer (km)	0.6214	mile (mi)
meter (m)	1.094	yard (yd)
	Area	
square meter (m^2)	0.0002471	acre
hectare (ha)	2.471	acre
square kilometer (km^2)	247.1	acre
square meter (m^2)	10.76	square foot (ft^2)
hectare (ha)	0.003861	square mile (mi^2)
square kilometer (km^2)	0.3861	square mile (mi^2)
	Flow rate	
millimeter per year (mm/yr)	0.03937	inch per year (in/yr)
	Density	
kilogram per cubic meter (kg/m^3)	0.06242	pound per cubic foot (lb/ft^3)

Temperature in degrees Celsius (°C) may be converted to degrees Fahrenheit (°F) as follows:
°F=(1.8×°C)+32

Temperature in degrees Fahrenheit (°F) may be converted to degrees Celsius (°C) as follows:
°C=(°F-32)/1.8

Datum

Vertical coordinate information is referenced to the North American Vertical Datum of 1988 (NAVD 88).

Sea-Level Rise Modeling Handbook: Resource Guide for Coastal Land Managers, Engineers, and Scientists

By Thomas W. Doyle,[1] Bogdan Chivoiu,[2] and Nicholas M. Enwright[1]

Abstract

Global sea level is rising and may accelerate with continued fossil fuel consumption from industrial and population growth. In 2012, the U.S. Geological Survey conducted more than 30 training and feedback sessions with Federal, State, and nongovernmental organization (NGO) coastal managers and planners across the northern Gulf of Mexico coast to evaluate user needs, potential benefits, current scientific understanding, and utilization of resource aids and modeling tools focused on sea-level rise. In response to the findings from the sessions, this sea-level rise modeling handbook has been designed as a guide to the science and simulation models for understanding the dynamics and impacts of sea-level rise on coastal ecosystems. The review herein of decision-support tools and predictive models was compiled from the training sessions, from online research, and from publications. The purpose of this guide is to describe and categorize the suite of data, methods, and models and their design, structure, and application for hindcasting and forecasting the potential impacts of sea-level rise in coastal ecosystems. The data and models cover a broad spectrum of disciplines involving different designs and scales of spatial and temporal complexity for predicting environmental change and ecosystem response. These data and models have not heretofore been synthesized, nor have appraisals been made of their utility or limitations. Some models are demonstration tools for non-experts, whereas others require more expert capacity to apply for any given park, refuge, or regional application. A simplified tabular context has been developed to list and contrast a host of decision-support tools and models from the ecological, geological, and hydrological perspectives. Criteria were established to distinguish the source, scale, and quality of information input and geographic datasets; physical and biological constraints and relations; datum characteristics of water and land components; utility options for setting sea-level rise and climate change scenarios; and ease or difficulty of storing, displaying, or interpreting model output. Coastal land managers, engineers, and scientists can benefit from this synthesis of tools and models that have been developed for projecting causes and consequences of sea-level change on the landscape and seascape.

Introduction

One of the more direct and scientifically accepted effects of modern-day climate change is that of rising sea levels associated with a warming climate and melting of glaciers and polar ice sheets. Although the direction of sea level is upward and unequivocal, the causes, rate, and periodicity are under study and debate. Based on observations from a worldwide network of tide gages over many decades, eustatic sea level rose at least 1–2 millimeters per year (mm/yr) in the 20th century (Melillo and others, 2014). Within the last two decades, sea-surface heights, as determined from satellite altimetry, have confirmed a global eustatic rise exceeding 3 mm/yr (Melillo and others, 2014). It is yet unclear whether this near doubling rate change in recent years is related to natural decadal variability of solar, orbital, or climate systems or is indicative of a longer term trend sped by human activity. Whether mostly a human or natural consequence, rising sea level will affect our coastal ecosystems and infrastructure through the consequences of coastal flooding if no action is taken.

The purpose of this guide is to describe and categorize the suite of data, methods, and models and their design, structure, and application for hindcasting and forecasting the potential impacts of sea-level rise in coastal ecosystems. Various climate and coastal wetland models have been developed to address the interaction and impact of changing climate and land use from a sea-level rise perspective. Simple models using generic datasets and constructs of the behavior of natural systems may provide only limited confidence and certainty suitable for instructional or educational purposes, whereas more complex models require expert development and more site-specific parameterization and validation for aiding coastal planning and ecosystem management. In

[1]U.S. Geological Survey.

[2]University of Louisiana at Lafayette.

2012, the U.S. Geological Survey (USGS) conducted more than 30 training and feedback sessions with Federal, State, and nongovernmental organization (NGO) coastal managers and planners across the northern Gulf of Mexico coast to evaluate user needs, potential benefits, current scientific understanding, and utilization of resource aids and modeling tools focused on sea-level rise. In response to the findings of these sessions, this sea-level rise modeling handbook has been designed as a guide to the science and simulation models for understanding the dynamics and impacts of sea-level rise on coastal ecosystems. The handbook is organized into two major sections, the first describing factors, rates, and models of observed and projected sea-level change and the second categorizing the suite of simulation tools for forecasting potential impacts of sea-level rise on coastal ecosystems. First, we present the physical properties and forms of the water cycle of the Earth's hydrosphere to constrain the discussion of how sea levels change in relation to the forces, data, and models that have been developed to reconstruct historical sea levels and to predict future sea levels.

Earth's Hydrosphere

There is a finite supply of water on the Earth, of which ocean water and open seas make up the largest portion. Oceans cover nearly three-fourths of the Earth's surface (361 million square kilometers [km^2]) and hold 97 percent of the total water volume. The remaining 3 percent is freshwater that is mostly frozen water of different forms and permanency, referred to as the "cryosphere," and includes snow cover, freshwater ice in lakes and rivers, sea ice (from saltwater), glaciers, ice sheets, and permafrost (frozen ground). The residency times and coupling of the different forms and sources of water vary with the seasons, decades, and millennia in relation to a warmer or cooler planet and geological periods (fig. 1). Ice depth and volume are greater in Antarctica (about 77 percent of the cryosphere), but more exposed areal extent and ice surface (about 23 percent of the cryosphere) lie in the Northern Hemisphere as snow, glaciers, frozen tundra, and polar ice.

Sea ice, snow cover, and freshwater ice fluctuate seasonally or over years between solid and liquid forms but affect sea level only marginally and temporarily by volume and cyclic behavior. A large or small block of floating sea ice does not affect sea level relative to equivalent weight displacement. Snow cover in the Northern Hemisphere fluctuates annually from highs of 46.5 million km^2 in winter to lows of 3.8 million km^2 in summer. Long-term observations and more current satellite imaging of snow cover over North America and Eurasia show little variability of areal cover change between years but more change with timing (for example, earlier melt) in recent decades. Freshwater frozen in glaciers, ice sheets, or ground ice has much longer melt periodicities, from 10 to 100,000 years or longer, and for deep polar ice the melt periodicity may exceed millions of years. Permafrost and seasonally frozen ground occupy the

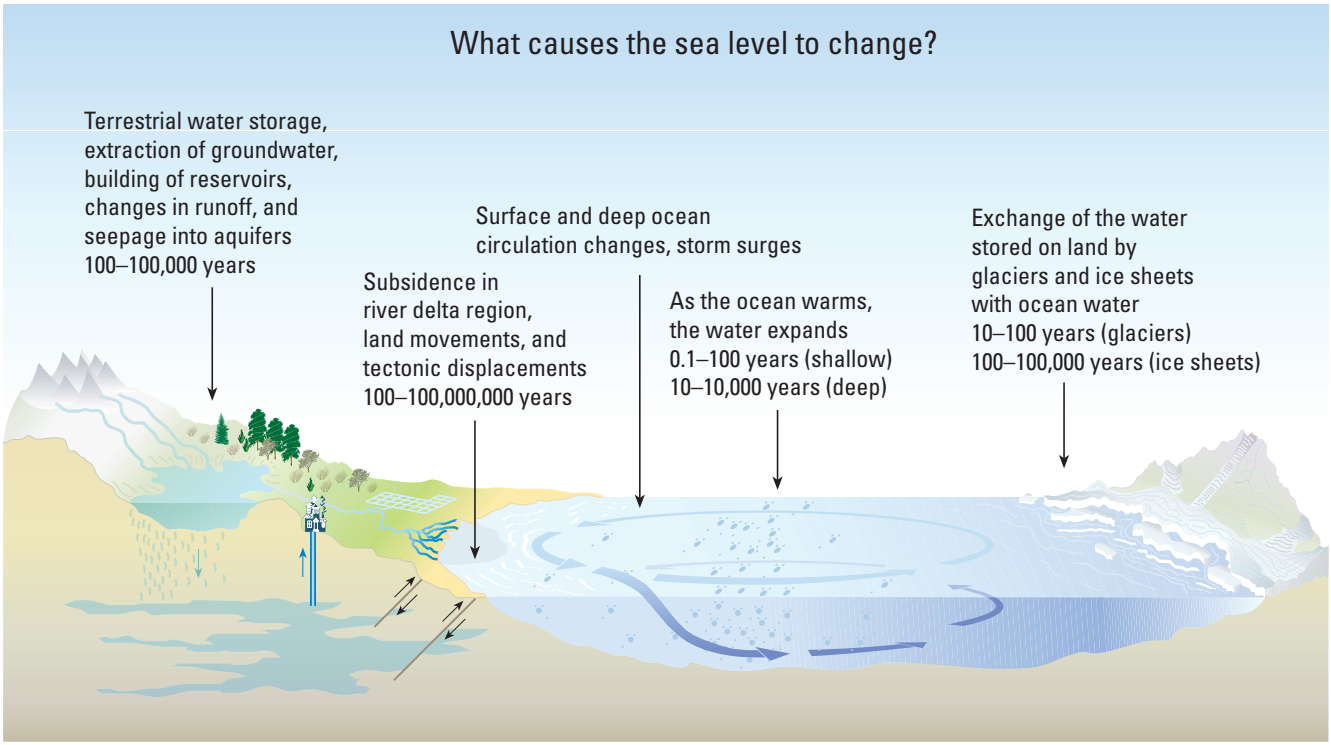

Figure 1. Forms, reservoirs, and residency times of the Earth's hydrosphere including atmospheric moisture (snow, rain, and clouds), oceans, rivers, lakes, groundwater, subterranean aquifers, polar icecaps, and saturated soil (Intergovernmental Panel on Climate Change, 2001).

largest areal extent of any component in the cryosphere, with approximately 54 million km^2. Permafrost thickness can extend 500 meters (m) below surface and varies by location, prevailing temperatures, and surficial factors of ground moisture content, vegetation cover, winter snow depth, and aspect. Thawing and freezing of permafrost, and advances and retreat of glaciers, have been monitored directly over decades and centuries, as well as on millennial time scales based on carbon dating of organic debris and tree ring analysis.

Deglaciation, or "icemelt," accounts for most of the sea-level change and cycles of recent Earth history, which amount to about 120 m or more every 100,000 years. As recently as about 20,000 years ago, the Earth was undergoing the Last Glacial Maximum of covered ice across North America and Europe, during which sea level was approximately 120 m lower than current levels and shorelines. In the last 8,000 years, sea-level rise has slowed and reached an expected maximum extent, having risen 4 m above current levels and fallen 4 m below current levels multiple times. Glacier and ice sheet melting alters sea levels on decadal and centennial cycles, thereby representing variation that is of most concern and potential impact to coasts today. Sea level rises or falls in concert with glacial retreat and advances at rates that vary by hemisphere and region and are not necessarily uniform. Of most concern to climate change scientists is the potential rise of sea level of 1–60 m based on the available mass balance of freshwater in vulnerable glaciers and polar ice if warming and icemelt continue.

A relatively minor storage of the Earth's hydrosphere is on or under the land surface in the form of surface water and groundwater. While these water sources have little to do with historical changes in sea levels comparable to glaciers and other ice forms, they have become a valuable resource and commodity for drinking supply, industrial use, and agricultural irrigation. In addition to natural lakes and rivers, the area of surface water exposed to evaporation has increased with the advent of dams and reservoirs built for hydropower, recreation, and water supply. The associated effects of regulated streamflow have changed the storage, routing, timing, and quality of water resources. The withdrawal of surface water from rivers and of groundwater and other fluids from aquifers for societal needs and consumption has altered the timing and magnitude of flow to downstream ecosystems and organisms dependent on or adapted to premodern flood frequencies. Withdrawal of surface water and groundwater has also increased the rate of natural geological subsidence of deep sedimentary formations. The connection of sea level to freshwater withdrawal is most apparent in receiving estuaries that become more saline with less freshwater flow over time and in locations where land subsidence from subsurface fluid withdrawal accelerates saltwater intrusion.

The atmospheric portion of the water cycle in liquid form is precipitation. The interannual and multidecadal variabilities of precipitation are evident in wet and dry years or arid versus mesic landscapes. Gradients of hydrological, geological, and biological significance controlled by precipitation rates, forms, patterns, and periodicity exist globally and across single continents. The withdrawal of surface water from rivers and the creation of man-made reservoirs have effectively mimicked a climate change effect equivalent to drought, or reduced freshwater flow to coastal estuaries. Although climate models agree on increased warming in the future, there is less certainty or agreement concerning amounts of precipitation in the future. In general, future projections of climate models account for less precipitation on the basis of warmer air holding more water, delivered in punctuated rain events with greater intensity, and longer periods between such events. It is important to consider that any climate model projections of less precipitation across a given region should account for an increase elsewhere because of the mass balance of water in the hydrosphere, which only changes in form and distribution rather than in overall quantity.

Factors, Rates, and Models of Sea-Level Change

In this section, we outline the various factors, processes, and evidence of sea-level change over the centuries and cycles of Earth's climate system. First, we explore long-term changes in eustatic sea level from geological evidence and models that allow reconstructions of ancient sea level related to plate tectonics, sediment geology, and glaciation. We then progressively review the rates and models of sea-level change of the modern era of deglaciation and contemporary records of tide gage and satellite observation. Lastly, we address future projections of sea-level rise from predictive climate models to understand the probabilities and timing of accelerated sea-level rise of the next century.

Ancient Sea-Level Reconstructions

Sea-level changes over the short and long terms of geological periods have been recorded and show in many mutually corroborating ways that in deep sediments there is a sequenced coastal overlap profile, indicating a globally consistent and repetitive pattern of sea-level change over time and space. The various disciplines have developed suites of models for reconstructing sea-level history that are beneficial for forecasting climate change direction and impacts for natural and cultural resource assessments. In most cases, we are primarily concerned for societal and conservation planning to know how and when current shorelines will flood with increasing sea level under warming climate. A review of the factors and rates of sea-level change over the course of the Earth's history expands the different types and disciplines of sea-level rise models.

Sediment Stratigraphy Geology Models

Deep beneath the ocean floor and land surface are the different layers of rock and sediment from terrigenous and marine sources that chronicle the interchange of terrestrial weathering of the exposed landform at low sea levels and aquatic life forms of a submerged condition during high sea levels. Together they tell the story of ancient sea levels before and since the age of dinosaurs. It was only decades ago that an understanding of the Earth's crustal movement was proposed and that the process of plate tectonics, in which continents and oceans reside on moving plates crashing into or sliding under or spreading from each other, was accepted. Geologists have since refined their understanding and constructed tectonic models to reconstruct the placement, movement, emergence, and submergence of land and sea over geological time. It was discovered that the order of geological formations and sedimentary layers is shared worldwide by fossil association, thereby representing progressive and subsequent time periods of varying sea level. Interpretation of these layers of associated fossil organisms and their isotopic composition has further shown that the Earth has been warmer and cooler than at present, with and without glaciation as a contributing factor.

As the Earth has cycled through cooling and warming periods, so has sea level cycled between minimum limits or levels, called lowstands, and maximum extents, known as highstands. Highstands occur during warming and icemelt periods when sea levels reach a high plateau before eventually reversing direction and falling again to another lowstand during cooling periods. Different geological methods and models of stratigraphic sequencing have been developed to interpret this pattern and history of sea-level change; these methods and models agree on concept and direction but differ with respect to magnitude, timing, and accuracy. Stratigraphic sequencing of common layers of rock type, fossil associations, marine terraces, alternating depositional sources (marine and terrigenous), and magnetic patterning, among other types of evidence, provides an analog of land-sea highstand and lowstand extents and periods. What can be determined from the various models is the direction of change, which indicates the process or contributions of plate tectonics on sea-level variation. The long view of hundreds of millions of years is that the spread and movement of continental plates have been increasing ocean basin volume since the sea-level highstand of the Late Cretaceous period, during which time sea level was nearly 120 m higher than present day. Two different methods for interpreting the stratigraphy of deep sedimentary layers largely agree on the long view of increasing and decreasing ocean basin volume and continental plate dynamics (fig. 2). Plate tectonics constantly changes the number, shape, geographic position, and shoreline relations of continents. When the continents are more consolidated, the lower extent of shoreline contributes to decreasing sea level. When the continents are breaking up and adding shoreline margins and land area, sea level subsequently rises. Related rifts or spreading of the ocean floor below the waterline can cause

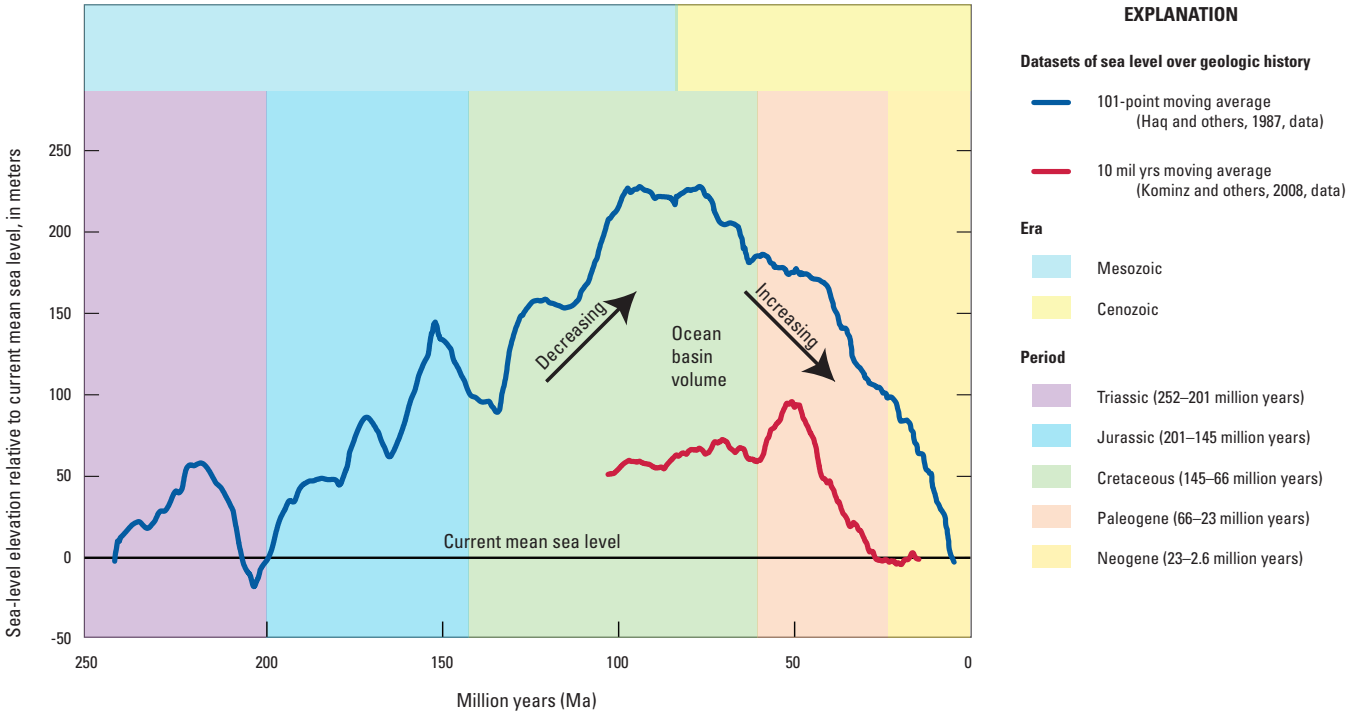

Figure 2. Sea-level reconstruction from sediment stratigraphy dating over geological time (modified from Haq and others, 1987; Kominz and others, 2008; used with permission).

similar effects on sea-level rise or fall. When spreading rates for deep ocean ridges collectively decrease, basin volume effectively increases and results in sea-level fall. In the case where there is net ridge subduction, a major loss of ocean floor features will precipitate a drop in sea level. For hundreds of millions of years, tectonic forces have controlled ocean basin volumes and long-term sea-level change by accommodation or displacement. These stratigraphic models of sea-level change show that ocean basin volumes are still increasing after the last major highstand more than 90 million years ago.

Glaciation and Sea-Level Cycles

Global sea level is controlled by geological and climatological processes of different scales and timing. In the last million years of Pleistocene history, glaciation acted as a prominent factor in cycles of sea-level rise and fall of 100 m or more over roughly 100,000-year cycles. The regulation of these highstand and lowstand sea levels is the result of greater or lesser glaciation that has been linked to the eccentricity of the Earth's orbit over a 96,000-year cycle known as the Milankovitch theory. Other prominent cycles in sea-level fluctuation of 41,000 and 21,000 years are tied to the periodicity of the Earth's tilt and the precession (wobble) of its axis, respectively. Acting in concert, these cycles interact in complicated phase relations of solar proximity and seasonal variance, both regionally and globally, driving differential icemelt and freeze, glacial advance and retreat, and consequentially, sea level.

Reconstructions of ancient sea level have been generated from multiple data sources, including oxygen isotope ratios of Foraminifera (a single-celled protist) deposition in ocean sediments, permanent ice core thickness, gas and particulate concentrations, sediment stratigraphy and fossil grouping, carbon dating, and others. The different methods of reconstruction capture similar timing and magnitude of major cycle inflections and only vary on fine resolution aspects on the basis of robustness of technique. Multiple oxygen-18 (^{18}O) reconstructions have been completed worldwide involving independent collections, analyses, and publications with repeatable results of sea levels, timing, and magnitude. These reconstructions demonstrate high rates of sea-level rise from lowstand to highstand and relatively low rates of sea-level fall over the longer period of the cycle with intermittent cycles of lesser magnitude (fig. 3). This pattern implies that orbital eccentricity and solar proximity drive a constant warmup that more effectively melts extended ice forms readily, whereas ice accumulation is a much slower and prolonged process. During glaciation periods of regular cyclic sea-level rise, the highest eustatic rates were more than an order of magnitude higher than current rates of sea-level rise (more than 20 mm/yr). If the pattern of past highstand and lowstand periods of glaciation repeats as expected, notwithstanding overriding greenhouse effect projections, sea levels would be subject to a cyclic fall for the next 90,000 years.

Holocene Sea-Level Rise

The recent history of sea-level rise begins less than 20,000 years ago at the end of the Last Glacial Maximum, when a vast ice sheet covered the Northern Hemisphere and sea level was about 120 m below present. The evidence of this period includes various biological data (for example, tree rings, coral remnants and growth rates, marsh and mangrove peat age, fossil associations), datable carbon and oxygen isotopes, and structural features of past shorelines and marine terraces. The numerous biological indicators provide an array and history of sea-level effects and conditions reported by many authors for many species and sites and include evidence from above and below present-day shorelines and ocean surface. A composite of calculated dates and heights of sea level during the Holocene epoch taken from various techniques and oceans shows a general sea-level curve with a slope and shape that is universally accepted and applicable worldwide (fig. 4). Since the Last Glacial Maximum, sea level has risen at an average rate of nearly 8 mm/yr, comparable to some of the highest current rates, such as those in high subsidence zones of delta systems worldwide. This rate is not uniform over the Holocene epoch; the highest rates approached or exceeded 20 mm/yr. For the past thousand years or more, sea level has been at a relative standstill subject to further icemelt and thermosteric effects of an extended warming climate or an eventual cyclic fall in the next few thousand years.

Contemporary Sea-Level Rates

Relative Sea and Land Motion

Globally, sea level is relative spatially and temporally until referenced by some fixed point, commonly referred to as a "datum" or "plane of reference." Datums are mathematical expressions or models of the Earth's surface and sphere (geoid) for aiding navigation and referencing horizontal distance and direction and vertical depth or height. Many horizontal and vertical datums have been established to approximate flat and curved land surfaces; they are not necessarily universal but are generally defined by political and geographic boundaries of parochial significance. Datums are based on unique empirical and theoretical models of the Earth's shape, size, and density. As such, a conversion (or rectification) is required to calculate and to compare distance and elevation differences between two or more points (or measurements) referenced to different datums. Referenced datums have known mathematical properties and are adopted into a geodetic control network. Over time, new or revised datums have been created for greater accuracy and utility. In the United States, horizontal datums, such as the North American Datum of 1927 (NAD 27) and the North American Datum of 1983 (NAD 83), and vertical datums, such as the National Geodetic Vertical Datum of 1929 (NGVD 29) and the North American Vertical Datum of 1988 (NAVD

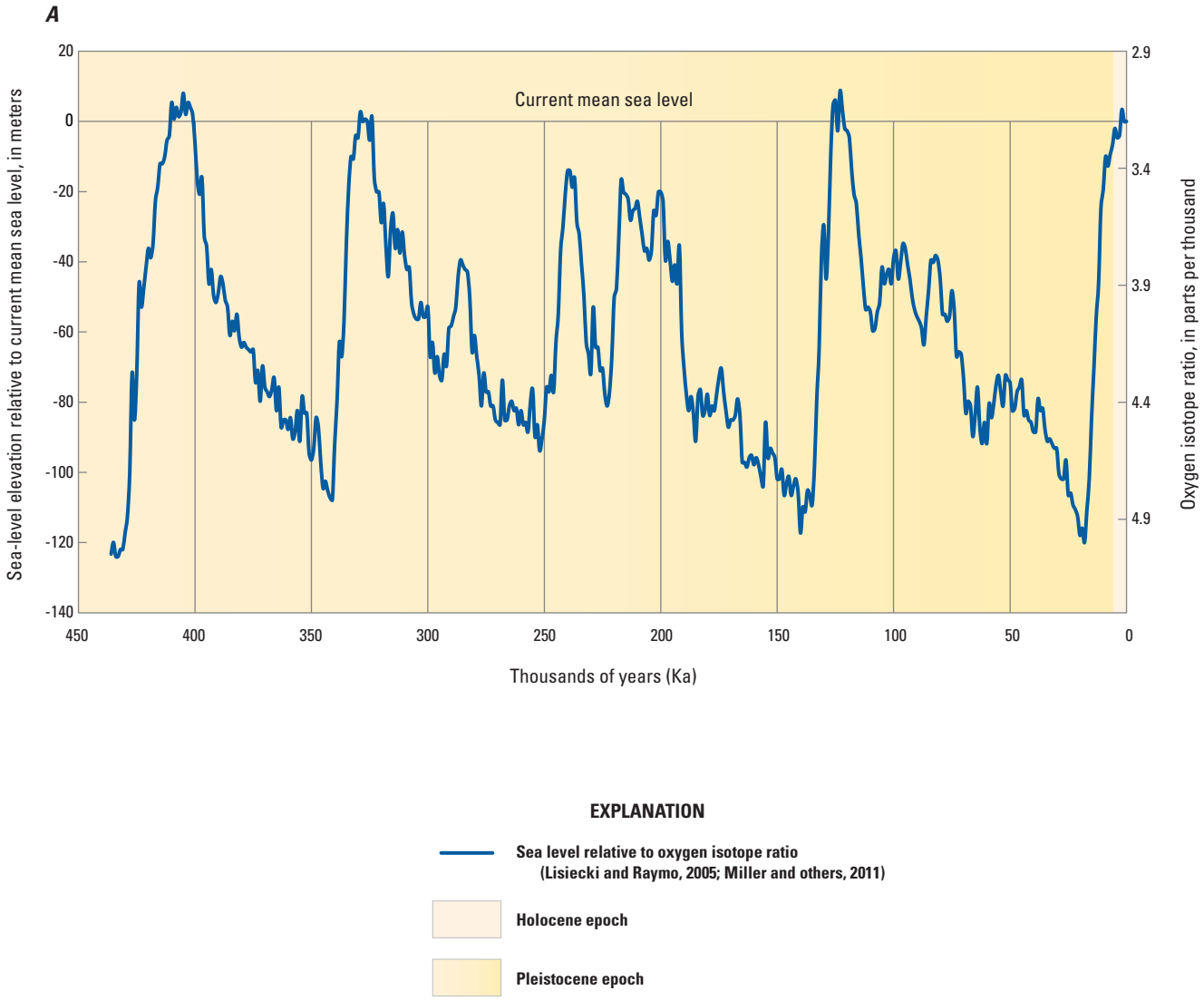

Figure 3. Sea-level reconstruction of late Quaternary, illustrating glaciation cycles determined from oxygen-18 (^{18}O) temperature correlated with sea level, Vostok ice core age and thickness, and carbon dioxide (CO_2) gas concentrations (modified from Petit and others, 1999; Lisiecki and Raymo, 2005; Imbrie and others, 2011; Miller and others, 2011; used with permission). *A*, Oxygen isotope ratio relative to sea level. *B*, Modeled ice volume and Vostok carbon dioxide data.

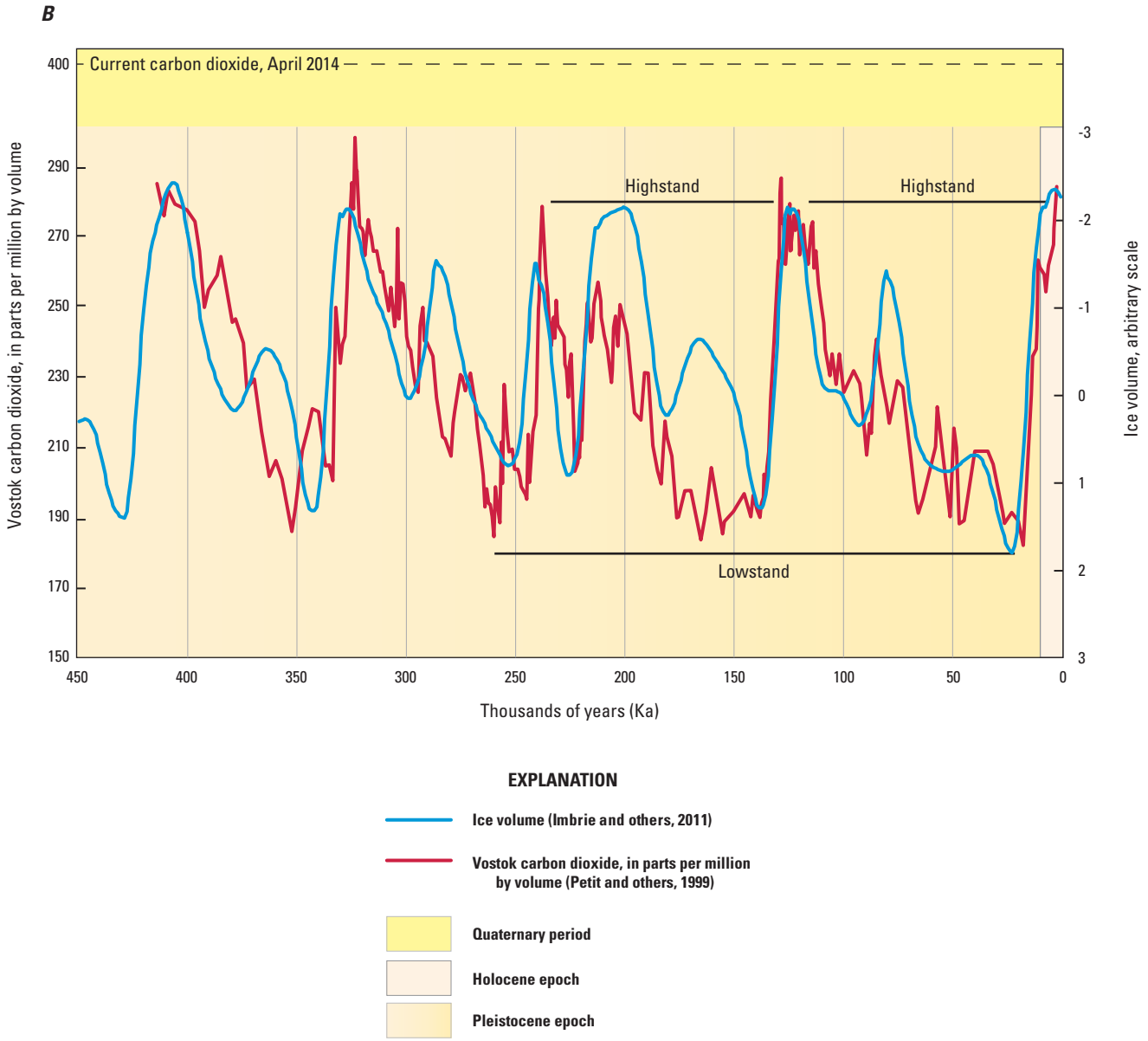

Figure 3. Sea-level reconstruction of late Quaternary, illustrating glaciation cycles determined from oxygen-18 (^{18}O) temperature correlated with sea level, Vostok ice core age and thickness, and carbon dioxide (CO_2) gas concentrations (modified from Petit and others, 1999; Lisiecki and Raymo, 2005; Imbrie and others, 2011; Miller and others, 2011; used with permission). *A*, Oxygen isotope ratio relative to sea level. *B*, Modeled ice volume and Vostok carbon dioxide data.—Continued

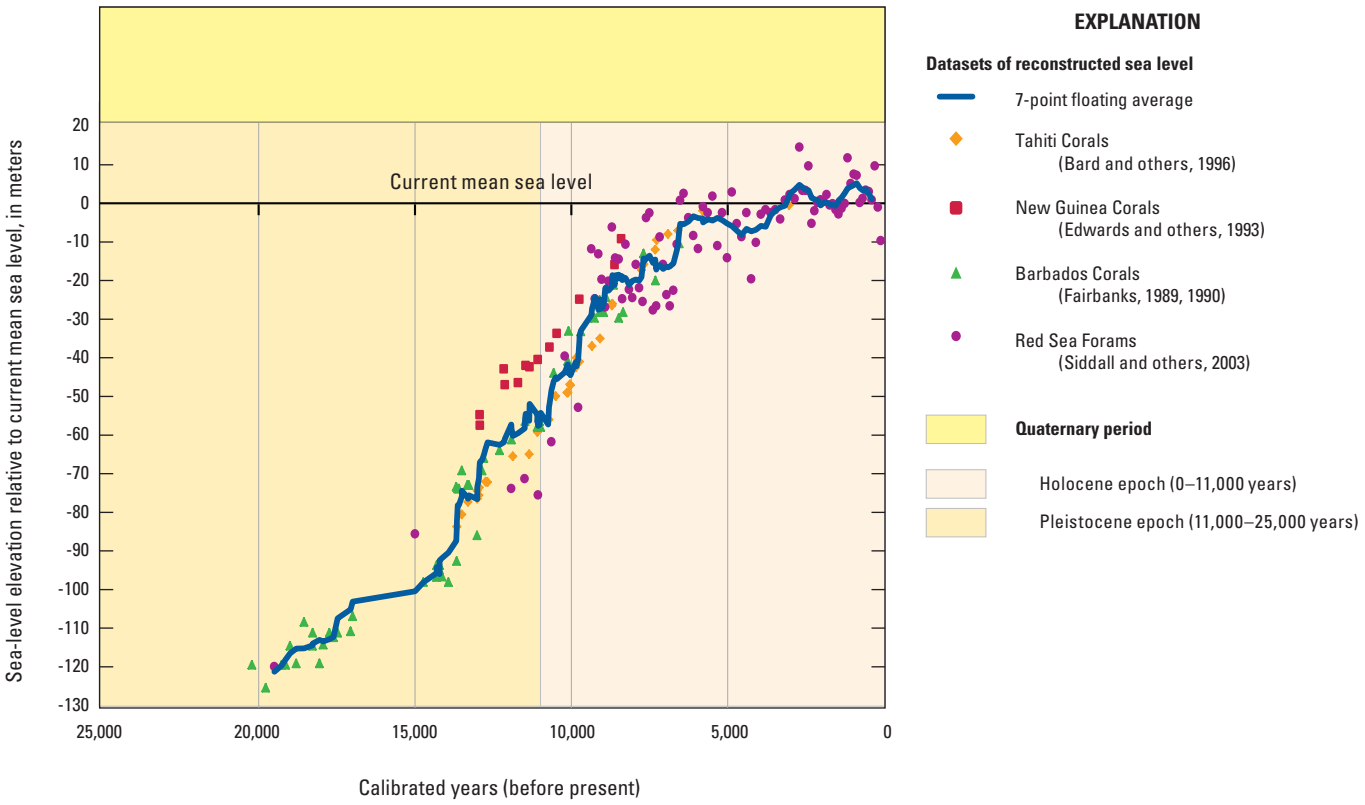

Figure 4. Holocene and Pleistocene sea-level reconstruction from composite studies and fossil dates illustrating a general sea-level curve that is more or less universally accepted and applicable worldwide (modified from Balsillie and Donoghue, 2004; used with permission).

88), are commonly used and referenced to assign a location and elevation, respectively, that are not interchangeable but can be easily rectified to one or the other by use of conversion software. Satellite navigation systems are likewise based on geoid and ellipsoid models of space that can be expressed or converted to a specified datum. The distinction of datums is an important aspect of all of the different kinds of models of land and water that will be discussed hereafter in this handbook.

Modeling sea-level rise is a challenge because both the land and sea are moving vertically and differentially by location, spatially and temporally. We easily envision how the ocean moves with the ebb and flow of tides, but it is more difficult to observe how the ground beneath our feet moves on a daily or seasonal basis or laterally in geological time. Land and sea motion together account for the relative sea-level rate at a given coastal location. While ocean volume (eustasy) is currently increasing and sea level is rising on a global scale, some coastal environments and communities are actually experiencing uplift of land surface (for example, in the Pacific Northwest) and drop in sea level both locally and regionally.

To effectively model the process and impacts of sea-level rise, models of both land surface and sea surface are required. Land surface and sea floors are measured and referenced differently, but all are part of the same landform that is covered or exposed with rising and falling sea levels spatially and temporally. The use of geodetic networks and tidal benchmarks provides a basis for referencing height or depth in relation to the sea surface. The intersection of land and sea may appear obvious (such as a beach), but it is much more difficult to ascertain when, where, and how much flooding occurs in and across the intertidal zone with the changing tide. This intertidal zone is where tide gages are so important and why the data are so valuable. Tide gage observations are used to predict tide behavior, to establish tidal datums of the different tide phases, and to determine mean sea level for a period of record. Predictive tide models require this information to reliably predict the astronomical timing and height of low and high tides. Tidal datums are also important for boundary determinations of private and public land, navigational aids and infrastructure, coastal development ordinances, and other political and economic uses.

A number of factors control the types and range of tides for a given coastal reach, and these factors are important for sea-level rise models and applications. First and foremost, every coastal reach has a unique tidal behavior and magnitude that are taken into account in more robust sea-level rise

models. Although the general characteristics of sea and tide motion are shared for proximal coastal reaches and tide gages, the bathymetric shape of bay and harbor bottoms and the coupling to open seas can produce unique tidal dynamics locally. The nature, direction, and circulation of nearshore currents and the geological properties of the underlying sediments also interact to account for higher or lower sea levels and the need for more frequent tidal analysis and datum updates.

Thermal Expansion of Seawater

From a global perspective, there are two main factors that control sea-level change, icemelt balance and ocean temperature, usually concomitant with respect to whether the global average or eustasy is relatively static or dynamic (rising or falling, slow or fast). Warmer climate periods of higher solar insolation and insulation melt the collective ice forms, glaciers, ice sheets, permafrost, and snow, effectively transferring a balance of icebound water in high latitudes and altitudes (that is, mountains) into the seas and oceans. At the same time, higher temperatures of air and surface waters over the Earth's hydrosphere cause thermal expansion of ocean waters and thus higher sea level. Effectively, a kilogram of warmwater displaces more volume than would a kilogram of coldwater. The volume (or height) for a given water mass and density increases under warmer temperatures (fig. 5). To illustrate further, a 1-degree Celsius (°C) change in ocean temperature over a depth of 1,000 m equals an expansion effect of 23.03 centimeters (cm). Although the properties of water have long been known with regard to density and mass relations of freshwater and seawater, a complex mathematical model is required to calculate and integrate the nonlinear response for the range of ocean conditions (app. 1).

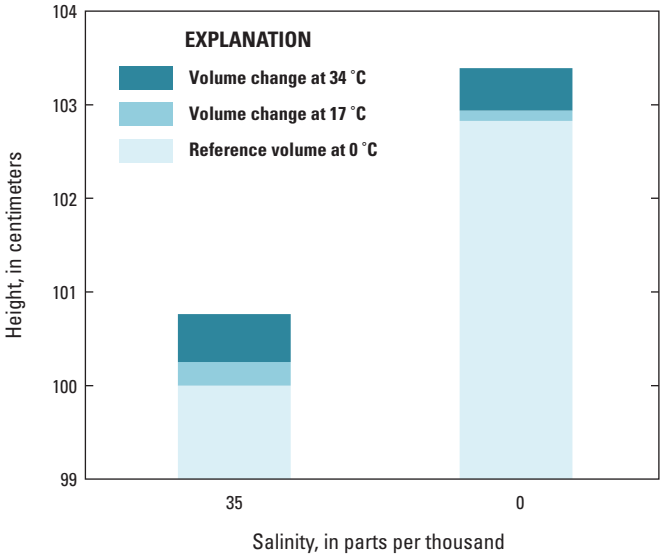

Note: °C, degrees Celsius

Figure 5. Change in height (or volume) for the same water mass at different temperatures and salinities.

Tide Gage Records and Relative Sea-Level Trends

Linear regression models are commonly applied to tide gage records to calculate relative sea-level trends based on long-term monthly or annual means of observed water level. A comparison of select tide gage records from the more geologically stable eastern Gulf Coast in Florida (Key West, Pensacola) with those from river deltas of the western Gulf Coast in Louisiana (Grand Isle) and Texas (Galveston) illustrates the extreme slope differences attributed to sustained low and high land subsidence, respectively (fig. 6). Tide gage records are readily available from two principal sources that can now be accessed via the Internet. The National Oceanic and Atmospheric Administration (NOAA) National Ocean Service maintains a user-friendly data portal of tide gage data and utility programs for public access, Tides Online (http://tidesonline.noaa.gov). Permanent Service for Mean Sea Level (http://www.psmsl.org) is another organization that maintains global tide gage records from contributors and cooperating government sources. Detailed descriptions of tide station history, datums, benchmarks, and semiprocessed data, such as long-term trend rates and seasonal variation, are often available.

Published sea-level trends are also readily available from government documents and peer-reviewed journal outlets but may be somewhat dated by time of publication. This report includes a record of published trends over the decades from NOAA tide specialists and sources (Flick and others, 2003; Hicks and Crosby, 1974; Lyles and others, 1988; Zervas 2001, 2009) for the larger set of U.S. tide gages (app. 2). These trends are derived from available records for each gage, some older and more continuous than others. Although current or past rates of sea-level rise by reach or region can be used for hindcasting and forecasting purposes, the differences in rate change from period to period demonstrate the dynamic nature of tides and sea level that warrants careful choice of record gap interpolation and trending method. Missing records are especially problematic if not rectified or interpolated prior to applying any trending process or calculation. Often the missing record is related to extreme low and high events or tide gage function critical for a representative sea-level trend calculation and appropriate gage-to-gage comparisons.

The choice of start and end dates alone can influence the slope or trend calculation when using least squares regression or quadratic models for fitting purposes. Failing to balance the start and end dates by equal months is enough to introduce undue weight and error of a disproportional high or low seasonal effect on either end of the period of record. This issue is more evident for seasonally driven and high-latitude locations with greater tidal variance. Removal of seasonal and storm effects (for example, hurricanes, cyclones, tsunamis, and extratropical fronts) will inherently generate more conservative

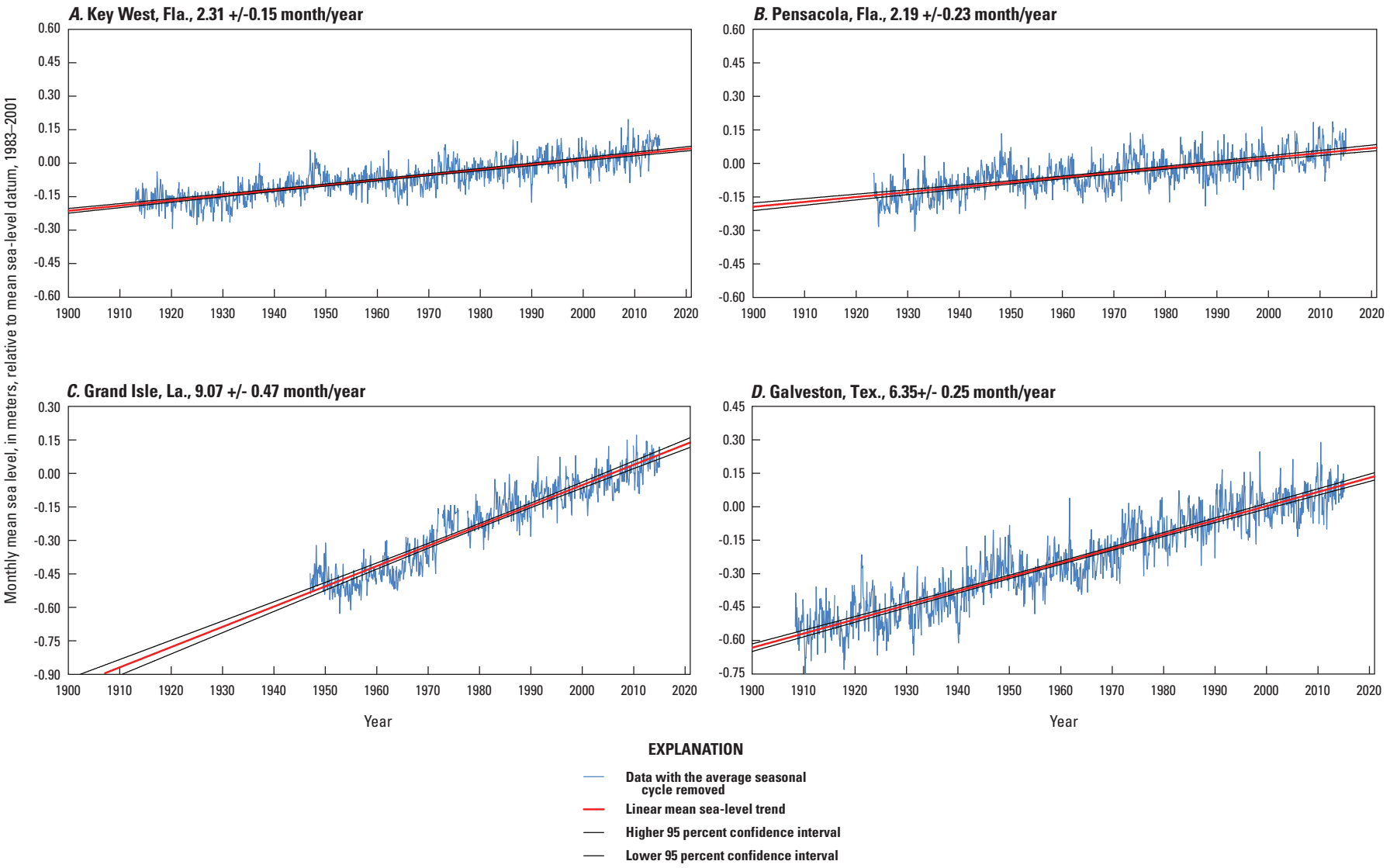

Figure 6. Relative sea-level records from select tide gages from the more stable eastern Gulf of Mexico coast in Florida and from river deltas of the western Gulf Coast in Louisiana and Texas illustrating land motion differences (National Oceanic and Atmospheric Administration, 2014). *A*, Key West, Florida, tide gage record, 1912–2014. *B*, Pensacola, Florida, tide gage record, 1922–2014. *C*, Grand Isle, Louisiana, tide gage record, 1946–2014. *D*, Galveston Pier 21, Texas, tide gage record, 1908–2014.

estimates of true slope or trend; this practice is rarely applied but is herein recommended. The position of these events in the record, earlier or later, and near the start and end dates, can add bias of inflated or deflated trending depending on overall record length. Longer records with fewer such events will tend to mediate the positional bias with nominal effect on rate change or magnitude.

There is currently much interest and debate regarding whether short-term satellite and long-term tide gage records can be used reliably for detecting accelerating and (or) decelerating sea-level change. Relatively few tide gages have been in operation with maintained continuous readings longer than a century. Short gaging records are problematic for trend analysis and accounting for confounding factors of eustatic and land motion influences that contribute to the actual (secular) change over time. The cycles of influence—climate, subsidence, fault movement, and crustal reaction—may be longer term than the records themselves, or there may be acute events not easily distinguished from seasonal variation or storm occurrences. There are, nevertheless, long and reliable gage records that provide trends of relevant influences (for example, subsidence) and expectations of future direction; however, to compare tide gage records with more recent satellite observations, it is necessary to compare complete records for each tide gage and for the same period of record. Considering the sea-level rate for the current tidal epoch (1994–2012) with appropriate overlap with satellite observations, we provide the range of relative sea-level rates for the different coastal reaches of the United States, thereby illustrating both high and low rates of sea-level rise and fall (fig. 7).

Satellite Altimetry and Eustatic Sea-Level Rise

The advent of satellites with sensors of different types and levels of accuracy has provided means to measure changes in the Earth's land cover, ocean levels, ice layers, and other surface characteristics useful for climate and sea-level assessment. A specific series of satellites similar to those of the Global Positioning System have been launched since 1992 to monitor global sea-surface height change over time. These satellites orbit the Earth many times in a single day on tracks that vary to capture a record of sea level and variation across the world's oceans and seas every 10 days. Although tide gages are useful for calibrating and validating satellite observations of sea-surface height, the gages are not evenly distributed across the globe and are subject to shoreline effects and tidal variance from differential bathymetric configuration, ocean currents, wave lapping, upland runoff, and land motion effects that confound determination of a definitive global mean sea level. Satellites provide a reference perspective that is independent of the Earth's surface above or below the dynamic water line that is commonly referred to as "local mean sea level." Because these satellites have gathered sea-surface height data since 1992, affording calibration checks and sustained observations for more than 20 years, the record length exceeds an entire tidal epoch (18.6 years), the astronomical cycle of gravitational tides of planetary and lunar orbits.

A major question with sea-level data from satellites concerns how they compare to longstanding, reliable tide gage records. Because the first reports of satellite-derived sea-level trends were published in the mid-1990s, the higher sea-level rate, above 3 mm/yr, supposedly verified acceleration in global mean sea level above tide gage rates of geologically stable coasts at 1–2 mm/yr over the last century (Melillo and others, 2014). Rate comparisons for different periods of record, short and long, are problematic, however, and warrant an understanding of the differences in sea-level measurements and rate calculations from satellite and tide gage data. The first difference is that the gage and the satellite are observing the water surface but one oriented upward from beneath sea surface and the other oriented downward from a geocentric orbit, respectively, with different measurement intervals and accuracy. Tide gages typically record sea-surface height at 6-minute (min) intervals at one location on the coast; these single locations are influenced by local factors of tidal behavior, upland runoff, and land subsidence or uplift. Satellites measure a series of single returns of an electromagnetic pulse to the sea surface and back, calculating an altimeter height of sea surface on the basis of signal time lapse. Both measures are then rectified to a common geoid or datum, which involves referencing the height of tidal benchmarks on land and satellite orbit in space. The geodetic rectification of observations from both tide gages and satellites is complex and beyond the scope of this handbook, but measurements should be expressed in the same datum and for the same period of record for direct comparison.

Although it is challenging to match a single sea-surface observation from an instantaneous satellite reading and a simultaneous 6-min reading of an associated tide gage, an average of measurements over weeks, months, and years is comparable. Satellite observations are not as exact or repetitive for a given location as are measurements from a tide gage, but instead, satellite observations are area specific and offer a wide distribution of locations, which is advantageous for continuous global monitoring. Satellite observations near coastlines are often not available or usable because of the proportion of altimeter readings that are on land rather than open water; however, satellite observations of sea-surface height provide a comprehensive regional and global measurement of absolute sea-level change that is independent of local land motion (subsidence or uplift). The difference in sea-level rate between satellite-derived records and tide gage records for the same observation period provides the degree and direction of land motion at that location. In effect, we therefore need both satellite observations and tide gage records for different purposes that are complementary.

For illustrative purposes, we analyzed satellite data from U.S. and European satellite services monitoring sea-surface heights for the Gulf of Mexico for comparison with select Gulf Coast tide gages. Water-level records for northern Gulf

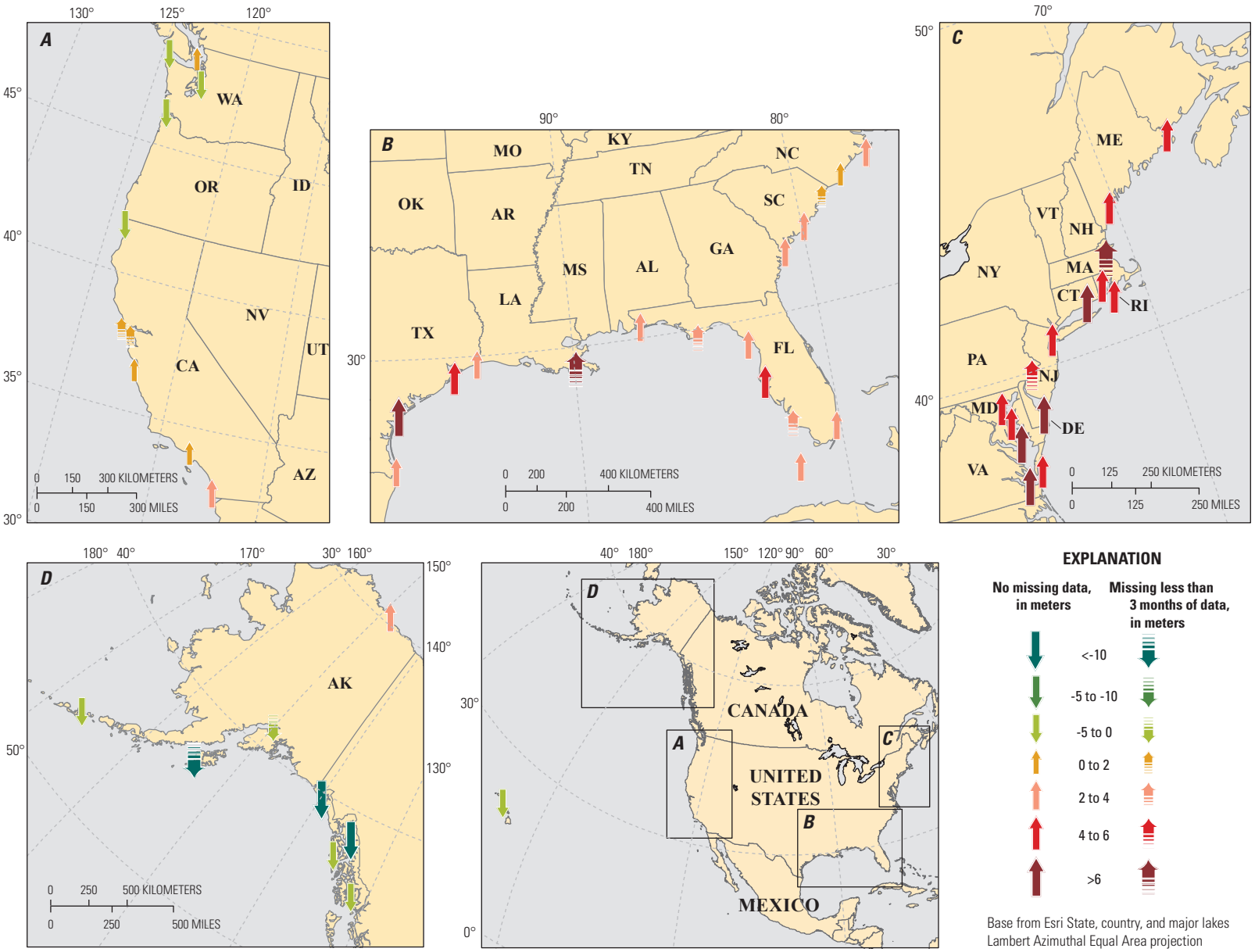

Figure 7. Range of relative sea-level rates for select tide gages of the United States, comparable with satellite altimetry period, illustrating both high and low sea-level change (rise and fall) for the same tidal epoch (1994–2012). *A*, Pacific coast. *B*, Gulf of Mexico and southern Atlantic coasts. *C*, Northern Atlantic coast. *D*, Alaskan coast.

Coast tide stations can be used to contrast relative sea-level rates of high-subsidence zones in deltaic settings of Louisiana and Texas to that in geologically stable coasts of western Florida to the concurrent satellite-observed rate for the Gulf of Mexico. The rate of sea-level rise for the period 1994–2012 for the select tide gages exceeded the eustatic sea-level rise trend of 3.32 mm/yr for satellite altimetry; both the U.S. (Topex/Poseidon/Jason) satellite dataset (National Aeronautics and Space Administration Goddard Space Flight Center [NASA GSFC], 2013) and the U.S. plus European satellite dataset (AVISO+ Satellite Altimetry Data, 2013) provided the same estimated rate of eustatic sea-level rise for this tidal epoch (1994–2012) (table 1). The residual of the difference between the higher sea-level rise rates for each gage and the eustatic sea-level rise rate for the satellite observations for this tidal epoch shows the degree to which the tide gage and landform are sinking (subsiding). In this case, the lower rates of subsidence for the eastern Gulf of Mexico gages at Key West and Pensacola demonstrate a fairly stable landform. In contrast, the higher rate of sea-level rise of the Grand Isle gage illustrates the rapid subsidence expected of a relatively new and thick deltaic platform undergoing compaction and perhaps affected by subsurface oil and gas withdrawal. The rate of subsidence along the Texas coast is comparatively moderate but shows signs of slowing from historical rates related to groundwater withdrawal and regulation. The spread and slope of monthly values and residual differences from these gages and satellite sea-surface heights for the tidal epoch 1994–2012 are shown in figure 8. In some cases, quadratic fits match the curvilinear trends and residuals better than linear regression models (fig. 8).

Table 1. Sea-level rise trends for select Gulf of Mexico satellite and tide gage data and the residual land motion for tidal epoch 1994–2012.

[SLR, sea-level rise; mm/yr, millimeters per year; -, not applicable. Data sources: AVISO+, 2013; National Aeronautics and Space Administration Goddard Space Flight Center, 2013; National Oceanic and Atmospheric Administration, 2014]

Location	SLR trend (1994–2012) (mm/yr)	Residual land motion (mm/yr)
Satellite		
U.S. Topex/Poseidon/Jason	3.32	-
AVISO dataset	3.32	-
Gage		
Key West, Fla., gage	3.45	0.13
Pensacola, Fla., gage	3.47	0.14
Grand Isle, La., gage	7.34	4.01
Galveston, Tex., gage	4.85	1.52

To determine whether the rate of sea-level rise during the most recent tidal epoch (1994–2012) is higher than in earlier tidal epochs, it is necessary to calculate the rates of sea-level rise for each tidal epoch similarly for equal 19-year segments. Table 2 shows the different sea-level rise trends by tidal epoch for each tide gage over their respective periods of record. The Key West and Pensacola tide gages show similar rates, ranging from about 1 to nearly 4 mm/yr for preceding tidal epochs. Slope calculations for the Galveston tide gage show higher rates, up to 10 mm/yr, corresponding with periods of high groundwater withdrawal associated with high industrial and population growth. Groundwater regulation and aquifer monitoring have reduced the effective withdrawal rates and related subsidence over the past few decades (Kasmarek and others, 2014). Although it is acceptable to compare rates of sea-level change over periods no less than 19 years, considering the length and effect of an astronomical cycle, it is best to calculate trends on even longer time periods or as long as possible for use in sea-level rise modeling applications.

Future Sea-Level Rise Projections

The IPCC has relied on general circulation models (GCMs) as the most advanced tools available for simulating the response of the Earth-climate system to increasing greenhouse gas concentrations. These models represent advanced knowledge of the coupled hydrological processes in the atmosphere, ocean, and land surface to provide projections of future climate change. There are dozens of GCMs from different research laboratories, universities, and government agencies worldwide. These GCMs similarly simulate the Earth-climate dynamics and processes but differ mostly in spatial and temporal resolution. The more complex GCMs depict the climate system by using a three-dimensional grid over the Earth, typically having a horizontal resolution between 250 and 600 kilometers (km), 10–20 vertical layers in the atmosphere, and sometimes as many as 30 layers in the oceans. Model-to-model differences translate into differences in the sensitivity to changes in greenhouse gas emission scenarios and in their predicted results.

Predicting future sea-level change from GCM simulations is based on a set of likely scenarios of greenhouse gas emissions depending on population growth and economic considerations of greenhouse gas controls and regulations. Emission scenarios are assumptions more than predictions or forecasts, and no probabilities are associated with them. Projections of future global mean sea level are based on thermal expansion of warmer oceans and the degree of melting glaciers and ice sheets as predicted from GCMs for different emission scenarios with greater or lesser greenhouse gas concentrations.

IPCC reports of climate change projections originally considered selected model output in the Third Assessment Report (2001) but have since reported composite findings for host institutions and countries providing GCM contributions.

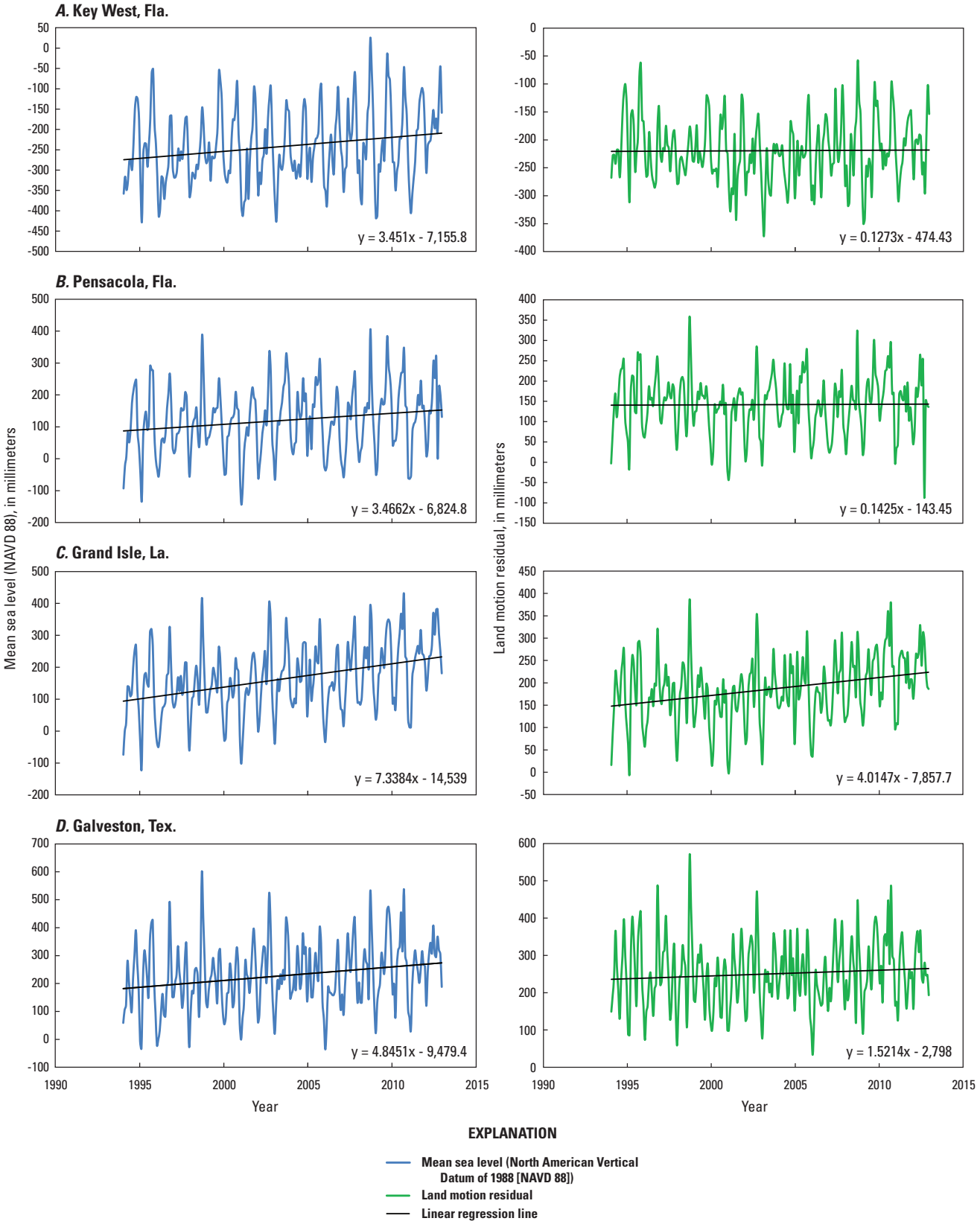

Figure 8. Slopes of mean monthly observations and residual differences from select Gulf of Mexico tide gages and corresponding satellite sea-surface heights for the tidal epoch 1994–2012 (data sources National Aeronautics and Space Administration Goddard Space Flight Center [NASA GSFC], 2013; National Oceanic and Atmospheric Administration [NOAA], 2014). *A*, Key West, Florida. *B*, Pensacola, Florida. *C*, Grand Isle, Louisiana. *D*, Galveston, Texas.

Table 2. Sea-level rise trends by tidal epoch during the period of record, 1918–2012, for select Gulf of Mexico tide gages.

[-, data not available]

Tide gage	Tidal epoch				
	1918–36	1937–55	1956–74	1975–93	1994–2012
Key West, Fla., gage	2.67	3.14	2.92	3.71	3.45
Pensacola, Fla., gage	-	2.62	3.01	0.81	3.47
Grand Isle, La., gage[1]	-	-	-	-	7.34
Galveston, Tex., gage	3.37	7.52	9.54	7.48	4.85

[1]Discontinuous record.

The IPCC Fourth Assessment Report (2007) resulted in a comparatively conservative projection for sea-level rise with likely low and high ranges of 18 and 59 cm, respectively, by 2100. The most recent National Climate Assessment report (Melillo and others, 2014) raised the upper estimate of sea-level projections from icemelt to 2 m (6.6 feet [ft]) by 2100 (fig. 9). The low projection of 20 cm (0.66 ft) by 2100 is an extension of the historical global mean sea-level rate of the last century without acceleration. The two intermediate forecasts between the low and high extremes indicate a likely sea-level rise of 0.3 m (1 ft) and 1.2 m (4 ft), respectively, by 2100. These and similar projections are commonly used in vulnerability assessments and as inputs to ecological and hydrological models to forecast the impact of sea-level rise on coastal infrastructure and habitat.

Predictive Models of Sea-Level Rise Impact and Coastal Vulnerability

In this section, we describe a host of simulation models, decision-support tools, and analytical techniques that have been applied to predict potential impacts of sea-level rise on coastal ecosystems and species, or related changes in the physical environment. We categorize the suite of data, methods, and models from a broad spectrum of disciplines involving different designs and scales of spatial and temporal complexity for predicting environmental change and ecosystem response. Model descriptions are given to highlight design type and features, functional attributes of input parameters and predictive variables, and characteristics of model utility or limitations. Criteria were established to distinguish the source, scale, and quality of information input and geographic datasets; physical and biological constraints and relations; datum characteristics of water and land components; utility options for setting sea-level rise and climate change scenarios; and ease or difficulty of storing, displaying, or interpreting model output.

Sea-Level Rise Simulation and Inundation Models

Some hydrological models have been developed to generate future sea-level projections for predicting inundation of shorelines or for use in other field and modeling studies. Model types range from arbitrary scenarios to derived projections based on tide gage records, glacial melt calculations, or climate change models designed to forecast probable increase of future sea level (table 3). Uncertainty in the extent of inundation for a particular sea-level rise scenario (such as 50 cm by 2100) is related to both the uncertainty in transformation of water-level datums (for example, orthometric to tidal) and the uncertainty in coastal elevation data. The combined amount of uncertainty from datum transformation and elevation sources can present critical limitations to sea-level rise applications. We exclude from this discussion tide simulation models or more sophisticated hydrodynamic models used for wave analyses, storm surge, or extreme flood forcing because these models are primarily used for engineering bridges and other coastal infrastructure.

CoastCLIM Sea-Level Simulator

CoastCLIM (Warrick, 2006; Warrick and Cox, 2007) is a database tool for generating predicted sea-level curves for any global coastal location. CoastCLIM uses a global database of regional grid cells to generate localized rates of sea-level change associated with downscaled GCM projections of future sea-level rise and CO_2 emission scenarios under climate change. A total of six emission scenarios are included in the package, and they can be queried for their associated changes in temperature, icemelt effects, and CO_2 concentration as produced for IPCC projections. CoastCLIM employs a user-friendly interface that allows users to select the region or coastal reach of interest from a global map. CoastCLIM associates selected locations with an overlapping GCM grid cell and extracts a normalized index of regional sea-level change relative to the global mean sea level. The normalized

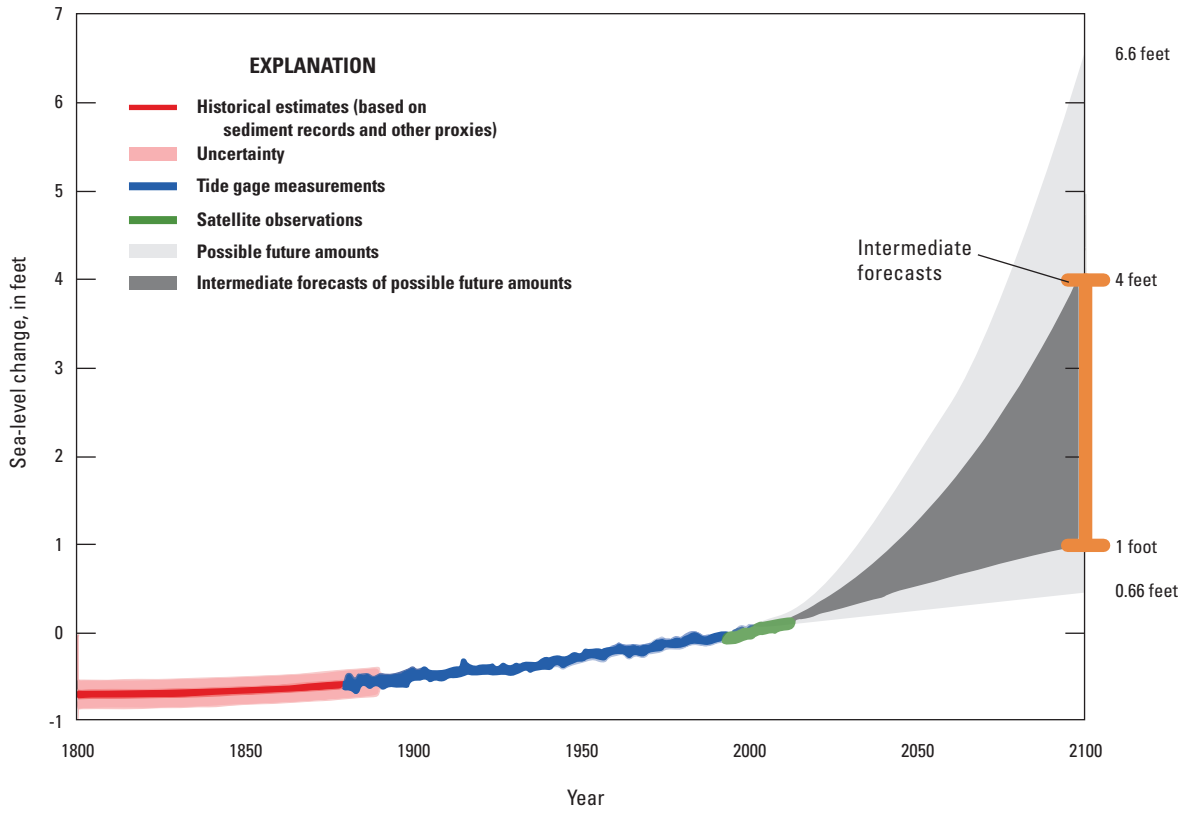

Figure 9. Historical, observed, and possible future amounts of global sea-level rise from 1800 to 2100 (from Melillo and others, 2014). Historical estimates (based on sediment records and other proxies) are shown in red (pink band shows uncertainty range), tide gage measurements in blue, and satellite observations in green.

index is derived as a ratio or scaling factor for the average pattern of sea-level change for the region of interest divided by the global mean sea-level change for the forecast period of 2071–2100. The user also selects which of six IPCC emission scenarios (A1B, A1F1, A1T, A2, B1, or B2) to correspond with downscaled GCM sea-level rise projections. CoastCLIM displays the predicted outcome in relative sea-level rise above zero in tabular and graphical format on an annual basis to 2100. CoastClim sea-level simulations show that sea-level rise can vary with both the selected model and scenario.

NOAA Inundation Frequency Analysis Program

An inundation frequency analysis program was developed by the NOAA National Ocean Service (http://tidesandcurrents.noaa.gov/inundation/) as a utility tool for coastal planners. The program uses observed 6-min water-level records of tide gages relating observed times and heights of high-water tides for a desired period of record as data input. The data output of this program is an Excel spreadsheet that takes each of the tabulated high tides in a specified time period relative to the user-specified reference datum or threshold elevations and calculates the elevations and durations of inundation above the reference datum. This inundation frequency analysis generates graphs and histograms of frequency occurrences by elevation and duration. For each threshold elevation, statistical summaries of flooding frequencies are generated for total number of high tides, hours inundated and number of days inundated, and the percentage of time inundated. For application of analyzing various sea-level rise scenarios, the reference datum is adjusted by the estimated amount of elevation change for a given sea-level rise scenario, and the aforementioned statistics are recalculated.

USGS Sea-Level Rise Rectification Program (SLRRP)

The Sea-Level Rise Rectification Program (SLRRP) (Keim and others, 2008) was developed by the USGS to generate future sea-level rise projections based on historical tide gage records and user-specified inputs or selections of IPCC (2001) GCMs and emission scenarios. SLRRP was designed to provide other USGS coastal ecosystem models with corresponding sea levels rectified to NAVD 88. SLRRP uses the mean monthly tide records of NOAA tide gages projected into the 21st century with the addition of curvilinear

Table 3. Attributes of select sea-level rise simulation and inundation models.

[GCM, general circulation model; NOAA, National Oceanic and Atmospheric Administration; SLRRP, Sea-Level Rise Rectification Program]

Model	Agency/ organization	Appropriate scale	Spatial resolution	Temporal scale	Input parameters	Output parameters	Citations
CoastCLIM Sea-Level Simulator (component of the SimCLIM system)	CLIMsystems	Local, regional, global	Varies; determined by data availability and computation demands	Variable depending on impact model being run	Elevation, climatologies, site time-series data, patterns of climate and sea-level changes from GCMs, impact models	Maps of areas/habitats potentially vulnerable to inundation. May estimate adaptation costs	Warrick (2006); Warrick and Cox (2007).
NOAA inundation frequency analysis program	NOAA	Local	Not applicable	1 month–5 years	Tide station, reference elevation, date range	Inundation duration, frequency of high water elevation or duration (tabular or graph format)	http://tidesandcurrents.noaa.gov/inundation/, Inundation Analysis Users' Guide.
Sea-Level Rise Rectification Program (SLRRP)	U.S. Geological Survey	Local, regional	Not applicable	Historical tide range plus projection to 2100, monthly to annual time step	Tide station, local subsidence rate (historical or custom), GCM sea-level rise rate	Cumulative sea-level rise, flood inundation potential for given elevation	Keim and others (2008).
Temperature-based sea-level rise model	Potsdam Institute for Climate Impact Research	Global	Not applicable	1990–2100	Global mean sea level, mean temperature, time	Future mean sea level	Rahmstorf (2007).

rates of eustatic sea level expected from climate change. The historical tide gage record is "wrapped" or extended into the future to mimic the natural cycle of high and low tidal variations attributed to astronomical and meteorological causes of seasonal and interannual variability including wind and storm tides. The mean monthly water levels capture both short-term seasonal variations and long-term trends of sea-level change for the respective gage and coastal reach selected. Projected data records are given in stage heights for different tidal datums such as mean low water, mean tide level, and mean high water, rectified to NAVD 88 to allow comparison with land-based elevations of tidal wetlands, roads, and other features of interest. The default tidal parameter simulated by SLRRP is the mean higher high water (MHHW), which corresponds with the upper boundary of the tidal-upland ecotone and higher flood extent to establish flooding potential of ecological and cultural importance.

SLRRP utilizes a graphic user interface of sequential pop-up windows to facilitate user selection of a desired tide station, GCM, emission scenario, or alternative customized inputs (fig. 10). The SLRRP customized mode allows users to manually enter a local subsidence rate and eustasy rate or elevation over a given time frame instead of using model defaults. The program gives the user options for saving graphical and digital formats of generated sea-level projections. SLRRP prompts the user to execute a seawater inundation option that builds a supplemental graph of the timing and rate of flooding for an elevation entry of a land surface or other feature (fig. 10). In effect, the model shows the prospective date and time period for which sea level may likely overtop and permanently submerge a given landscape feature under a future sea-level projection. Flooding potential is the percentage of months within a year when there is inundation by seawater for a given elevation determined by the user, assuming hydrological connectivity. SLRRP is used to generate projected sea-level rise curves for other USGS ecological models, such as SELVA-MANGRO, SLOPE, and WETLANDS, developed for assessing tidal wetland migration under sea-level changes for either a rise or a fall.

Temperature-Based Sea-Level Rise Model

A semi-empirical model of future sea-level rise was developed (Rahmstorf, 2007) to project possible changes in global sea-surface height from global near-surface air temperature. The model is based on the assumption that the rate of sea-level change is roughly proportional to the magnitude of relative warming above pre-industrial temperatures. A semi-empirical approach is a reasonable alternative to process-based GCMs given their accuracy limitations to reproduce historical sea-level trends of the 20th century. Modern climate records show a highly significant correlation of global temperature with sea-level change by rate and direction. It is expected that, with every 1 °C change in global air temperature, sea levels will rise or fall by 10–30 m. The linear approximation of sea-level change with this semi-empirical approach provides reproducible results of modern sea-level trends within centimeters. Future projections are based on the range of predicted temperature changes that will vary according to greenhouse gas controls and conservation measures. Projected rates for the 21st century from this model fall within the range of other global lows and highs from more complex models.

Soil Salinity Models

Salinity conditions within the estuarine gradient of tidal channels and wetland soils vary hourly and seasonally with changing tides, storms, and freshwater runoff (Morris, 1995; Teh and others, 2008; Wang and others, 2007). What wetland type and plant species may be found within the intertidal zone is controlled by persistent salinity concentrations. Saltmarsh and mangroves are known for their tolerance of high soil salinities that can well exceed the average or typical concentration of open seawater, 35 parts per thousand (ppt). As sea level rises, the circulation of seawater penetrates farther inland with each tidal cycle, as well as episodically by storm tides and waves from tsunamis and hurricanes. A major cause of coastal forest retreat is saltwater intrusion by way of major storm tides and surge events occurring during a local or regional drought. During times of low water, marshes dehydrate and compress below normal elevations such that refilling by seawater as opposed to rainfall or other freshwater input can elevate interstitial pore water salinities in the soil layer. Increases of 1 or 2 ppt of soil salinity concentrations are sufficient to cause plant mortality and shifts in vegetation dominance.

Expert Hydrodynamic Models for Engineering Applications

There are a host of expert hydrodynamic models for engineering applications that are used for coastal restoration purposes of different kinds that likewise have the capacity to evaluate future sea-level rise projections. These models generally require expert knowledge and costly data gathering and license agreements to execute hydrology applications for environmental impact assessment, construction design and planning, and other coastal engineering needs. These numerical models consist of empirically dependent two- and three-dimensional models used for comprehensive flood forcing, wave energy, nearshore circulation hydraulics, and storm-surge simulations such as Delft3D, MIKE 3FM, HECRas, MIKE 2, SLOSH, AdCirc, FV COM, and other associated sediment and water-quality transport models designed for complex engineering applications of oceanic, coastal, riverine, and estuarine environments. These model types are not necessarily appropriate or useful for generating future sea-level rise projections or impact assessments based on design or function but are relevant in other ways, such as for parallel efforts to better understand the effects of river and coastal management on coastal geomorphology and tidal change.

A

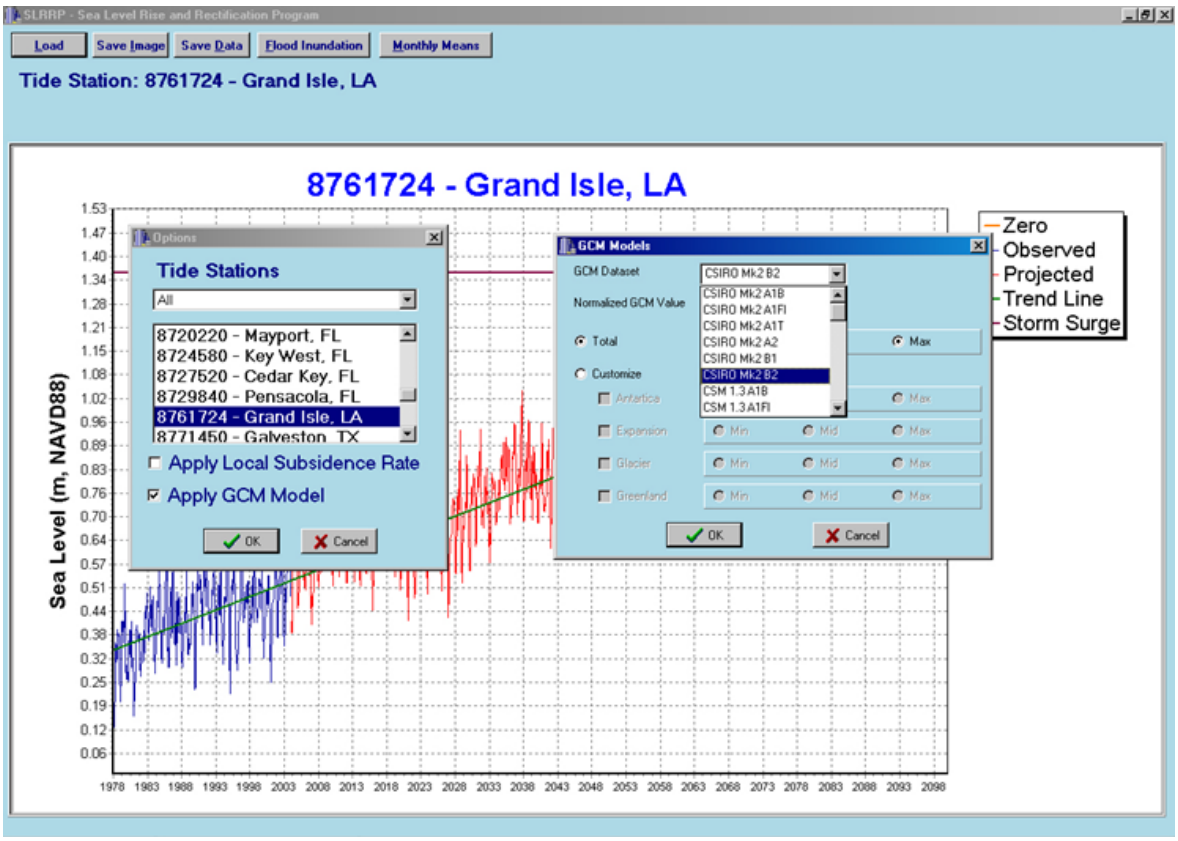

Figure 10. Screenshots showing Sea-Level Rise Rectification Program (SLRRP) graphic user interface (from Keim and others, 2008). *A*, User options for selecting the tide station and the GCM model parameters. *B*, Projected sea-level curve. *C*, Flood inundation chronograph.

B

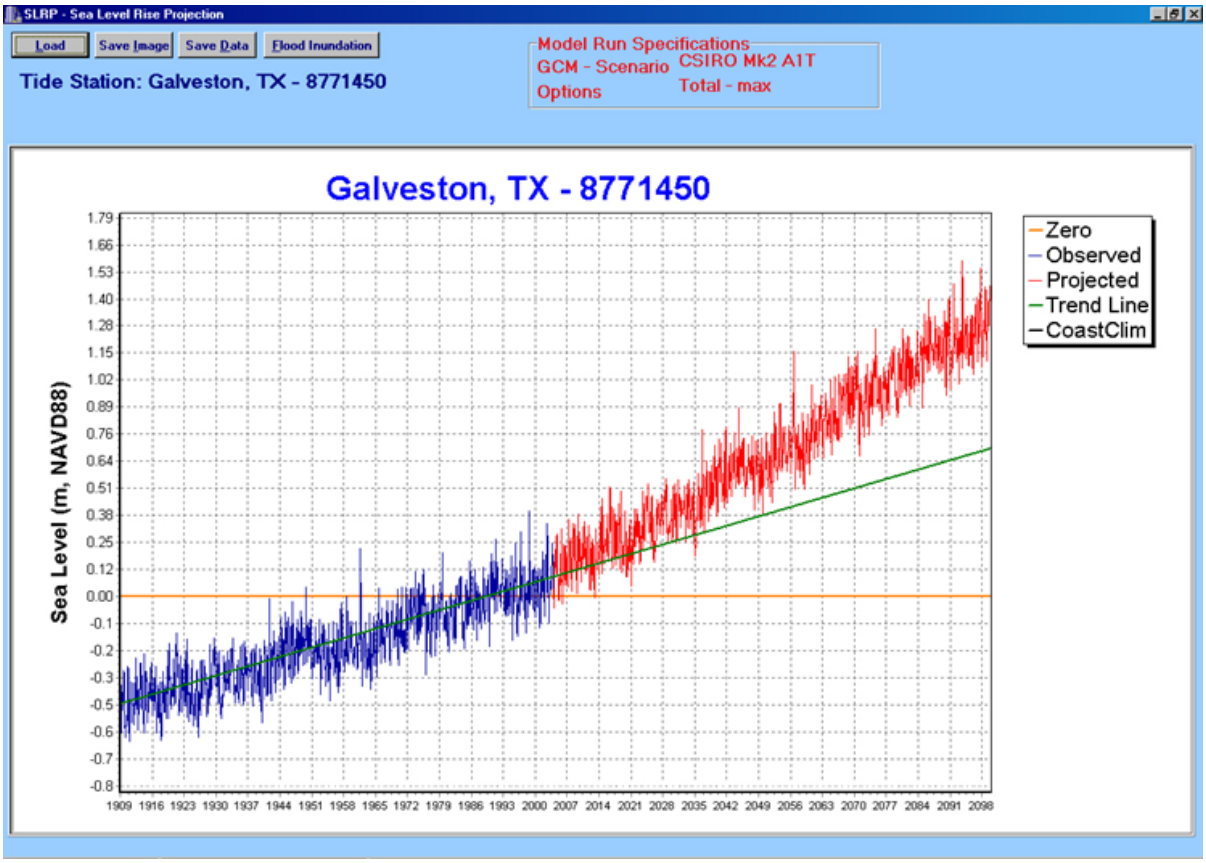

Figure 10. Screenshots showing Sea-Level Rise Rectification Program (SLRRP) graphic user interface (from Keim and others, 2008). *A*, User options for selecting the tide station and the GCM model parameters. *B*, Projected sea-level curve. *C*, Flood inundation chronograph.—Continued

C

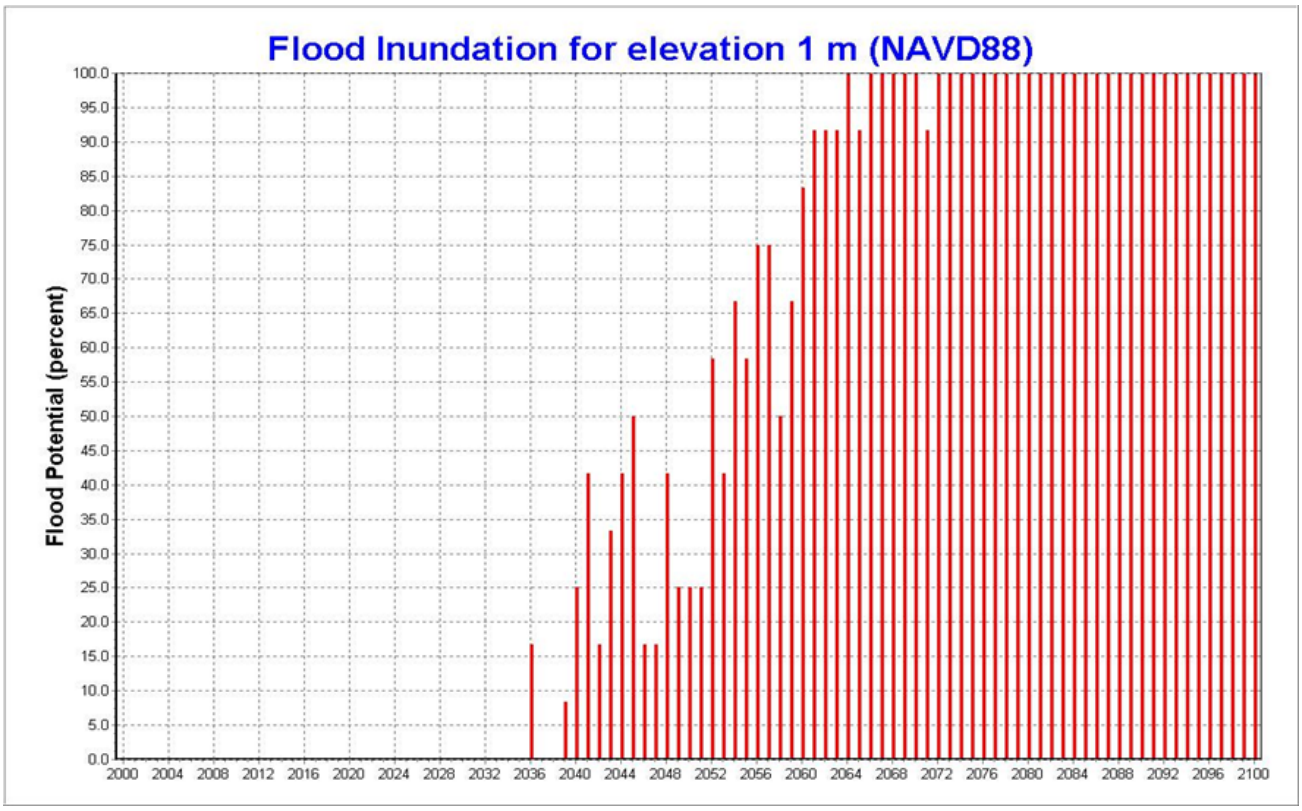

Figure 10. Screenshots showing Sea-Level Rise Rectification Program (SLRRP) graphic user interface (from Keim and others, 2008). *A*, User options for selecting the tide station and the GCM model parameters. *B*, Projected sea-level curve. *C*, Flood inundation chronograph.—Continued

Geographic Information System (GIS) Sea-Level Rise Mapping Tools

Geographic information system (GIS) sea-level rise mapping tools are abundant and popular for ease of construction and interactive graphical display. These tools are becoming commonly available online for public access as interactive maps. These tools allow Internet browsers to visualize the potential impact of future sea-level rise scenarios on land maps at local, regional, and global scales as determined by tool design and capability. Tool developers include Federal, State, university, and nongovernmental organizations utilizing GIS data, software, and graphic user interfaces to display developer-specified images or user-specified choices of geospatial extent and sea-level rise options (table 4). As a rule, these are non-expert tools lacking scientific credibility that display maps of potential coastal inundation based on public-domain digital elevation models (DEMs) (app. 3) and arbitrary sea-level projections. These mapping tools are often referred to as "bathtub" models for the overly simplified approach of water-over-land relations, an approach that disregards important biological, hydrological, physiographic, and geodetic considerations. At best, these mapping tools provide only a visualization of the future extent of tidal wetlands and shorelines suitable for facilitating discussion of coastal issues and, more importantly, highlighting the need for expert model application and accuracy.

Advantages of GIS sea-level rise mapping tools include their relative simplicity and ease of construction such that many organizations and individuals are able to produce their own versions by relying on the same or similar GIS mapping software and public-domain mapping sets of digital land elevation, vegetation, and land-use data. In this way, they are inexpensive and quick to build but also very limited functionally. Limitations of GIS sea-level rise mapping tools are numerous in places and situations where accuracy of coastal process, built features, differential land movement, ecosystem functions, and vertical rectification of water and land datums are lacking. Most importantly, these tools are almost exclusively unrectified and unverified for use or application as predictive models in the same context as more sophisticated ecological and engineering models (see following sections).

The more accurate predictive models for simulating sea-level change and coastal impacts require datum transformations of water and land sources that are rectified to the same units and reference plane to make legitimate comparison of flooded or unflooded land surface. Tidal datum and land datum are measured and reported differently and cannot be directly compared or analyzed without proper rectification to the same datum type and epoch. As discussed previously, there are many reference datums that have been established over the years of numerous local and regional origins that make rectification somewhat complex and subject to expert knowledge. In most cases, GIS sea-level rise mapping tools use arbitrary heights or rates of sea-level rise that are not based on any datum or measured local or global tide history. The more accurate sea-level rise applications by contrast consider the relative sea-level rate by coastal reach because of the variable conditions, causes, and directions of land movement and tidal behavior. In addition to not being rectified, GIS sea-level rise mapping tools are not verified (verification is the measure to which they have been tested for accuracy or function that adds to the sense of predictive reliability). Modeling that simply forecasts a predicted future condition without verification is akin to extrapolating beyond the boundary conditions and data of a statistical model. Although it may be useful to apply GIS sea-level rise mapping tools to consider "what if" scenarios for limited planning and educational purposes, these tools do not have any certainty bounds or other verification measures that ensure results, particularly given all of the limitations of data sources, design, and functionality.

GIS sea-level rise mapping tools may have an appearance of greater utility because of the busy display characteristics served from the quality and accuracy of DEMs incorporated (app. 3). The more detailed DEM sources of higher spatial resolution, however, have the advantage or disadvantage of being increasingly challenging to utilize because of file acquisition, size, and other factors that require greater computing skills and capacity to manage properly. Local features such as levees, dikes, revetments, and canals may not be included in associated public databases, which add to limitations of model application. A major assumption of GIS sea-level rise mapping tools is that there is uniform hydrological connectivity from open bays, oceans, estuaries, and rivers to adjacent or inland land units both in accessibility and in elevation. Water quality is also assumed to be uniform in that salinity or other nutrient constituents are not considered in these models. Table 4 identifies select publicly accessible, online GIS sea-level rise mapping tools with various characteristics and capabilities.

OzCoasts Sea-Level Rise Maps

The Australian Government has developed a series of sea-level rise maps (Australian Government, 2009) to illustrate the potential impacts of climate change for key urban areas. The online maps are activated by selecting among several regional map insets. The maps, prepared by combining a sea-level rise projection with a high tide value, illustrate an event that could be expected to occur at least once a year, but possibly more frequently, by 2100. This mapping tool provides an interactive display to visualize and realize the risks to the infrastructure and natural areas along the Australian coastal zone, where nearly 85 percent of the population resides.

Table 4. Attributes of select geographic information system (GIS) sea-level rise mapping tools.

[m, meter; IPCC, Intergovernmental Panel on Climate Change; DEM, digital elevation model; USGS, U.S. Geological Survey; km, kilometer; SRTM, Shuttle Radar Topography Mission; NED, National Elevation Dataset; NOAA, National Oceanic and Atmospheric Administration; ft, feet; VDatum, vertical datum transformation tool; MHHW, mean higher high water; C-CAP, NOAA Coastal Change Analysis Program; km^2, square kilometer; MHW, mean high water]

Model	Agency/ organization	Web page	Appropriate scale	Spatial resolution	Sea-level rise range options	Input parameters	Vegetation classification	Output parameters	Citations
OzCoasts sea-level rise maps	Australian Government	http://www.ozcoasts.gov.au/climate/sd_visual.jsp	Local, key urban areas (Australia)	Unknown	0.5, 0.8, and 1.1 m (IPCC projections)	DEM (lidar)	None	Inundation maps	Australian Government (2009).
USGS Sea Level Rise Animation	USGS	http://cegis.usgs.gov/sea_level_rise.html	Local, regional, national, global	30 m (U.S. coast), 90 m (regional), 1 km (global)	0–30 m (U.S. coast), 0–80 m (continetal, global)	DEM (GTOPO30, SRTM 90 m, NED 30 m), land cover, population	None	Inundation map, population affected	Usery and others (2010).
NOAA Digital Coast Sea-Level Viewer	NOAA	http://www.csc.noaa.gov/slr/viewer/#	Local, regional, national (U.S., territories)	Variable (3–30 m)	0–6 ft	DEM, vegetation, VDatum MHHW surface	C-CAP	Inundation map, socioeconomic vulnerability index	NOAA (2010); Marcy and others (2011).
University of Arizona Web Map Visualization Tool	University of Arizona	http://climategem.geo.arizona.edu/slr/us48prvi/index.html	Continental, global	1 km^2 (global), 30 m (U.S.)	0–6 m	DEM (GTOPO30, NED 30 m), land cover	None	Inundation map	Overpeck and Weiss (2009); Weiss and others (2011); Strauss and others (2012).
Surging Seas	Climate Central	http://sealevel.climatecentral.org/surgingseas/	City, county, State (lower 48 States)	10 m, 30 m	0–10 ft	DEM, VDatum MHW, tide gage data	None	Inundation map, population, housing and land affected, flooding risk (downloadable)	Tebaldi and others (2012); Strauss and others (2012).

NOAA Digital Coast Sea-Level Viewer

The NOAA Digital Coast Sea-Level Viewer (http://coast.noaa.gov/slr/; Marcy and others, 2011; National Oceanic and Atmospheric Administration National Ocean Service [NOAA NOS], 2010) was designed to be a teaching and planning tool for coastal land managers. The online user can slide a sea-level rise bar located left of the map to show the potential impact to locations where various sea levels may inundate coastal communities (fig. 11). The underlying digital elevation from the USGS National Elevation Dataset (NED) (1 arc-second) supplemented with available and accessible light detection and ranging (lidar) elevation data is converted to a vertical datum transformation tool (VDatum) surface or local tide station MHHW datum depending on location. The Digital Coast Sea-Level Viewer allows the user to select six static scenario heights of sea level rise by 1-ft increments up to 6 ft. Wetland data portrayed as the initial condition within the viewer are derived from the NOAA Coastal Change Analysis Program (C-CAP) (app. 3). The model allows marsh migration based on user-selected accretion rates such that, as sea level rises and higher elevations become more frequently inundated, marsh migrates landward. The user is allowed to select from four predetermined rates of accretion. These rates are presented as high (6 mm/yr), medium (4 mm/yr), low (2 mm/yr), and no (0 mm/yr) accretion. These rates were determined on the basis of observed rates from published field studies. The minimum mapping unit of the viewer was modified to remove features smaller than 0.202 hectares (0.5 acres) in size. Inclusion of additional coastal counties is planned for the near future so that all U.S. coastlines and coastal communities can be visualized with the tool.

The Nature Conservancy (TNC) Coastal Resilience Decision-Support Framework

The Nature Conservancy (TNC) Coastal Resilience Decision-Support Framework (http://maps.coastalresilience.org/network/) was developed as a Web-based mapping tool to assist decision makers with assessing alternative future scenarios that address sea-level rise, storm surge, and community vulnerability. TNC is using this tool to advance a global network for coastal resilience to support adaptation planning and post-storm redevelopment decisions, as well as to reduce the ecological and socioeconomic risks of coastal hazards. The framework includes local to global application for examining social, economic, and ecological priorities alongside data on coastal hazards. The interactive decision-support framework allows users to visualize future flood risks from sea-level rise and storm surge. The users can also identify areas and populations at risk and gain a better understanding of social, economic, and ecological impacts from coastal hazards. This information is particularly helpful for officials considering rising sea levels and increased storm intensity and frequency when making coastal management decisions, such as coastal planning, zoning, and land acquisition.

University of Arizona Web Map Visualization Tool

The University of Arizona Web Map Visualization Tool (Overpeck and Weiss, 2009; Weiss and others, 2011; Strauss and others, 2012) includes both global and conterminous U.S. map versions of different elevation data sources and scales of resolution. The global map, the Global Elevation Model (GEM), is composed of the GTOPO30 dataset at 1-km horizontal resolution, whereas the conterminous U.S. map is based on the USGS NED (1 arc-second) at 30-m horizontal resolution. The geoprocessing algorithm performs iterative cell-by-cell analysis of the selected DEM and highlights all land units (cells) with elevation values less than or equal to projected sea levels of 1–6 m above current sea level. The tool identifies low-lying coastal areas expected to be inundated by sea-level rise by 2100. The program is composed of ArcGIS Viewer software (Esri, Redlands, Calif.) with zoom capability to enlarge the map view (fig. 12). The map tool is based on modeled present-day elevations and does not predict future shorelines or include processes that may affect local elevation such as glacial isostatic adjustment, tectonics, subsidence, or erosion and accretion. The municipal boundaries are GIS shapefiles that are part of the U.S. Census Bureau Topologically Integrated Geographic Encoding and Referencing (TIGER) database. All maps are on an Albers Equal-Area Conic projection.

USGS Sea-Level Rise Animation

The online USGS Sea-Level Rise Animation (Usery and others, 2010) creates visualizations of seawater over land, illustrating vulnerability of low-elevation areas (rather than predictions of sea-level rise). The animated graphics are created by using raster elevation, land cover, and population data at 1-km (global), 90-m (regional), and 30-m (regional, specifically the U.S. areas) resolutions. Colors reflect land cover categories, and the counts are numbers of people living or impacted below specific elevations (fig. 13). The animated graphics are not meant to be site specific. They are based exclusively on elevation and do not attempt to account for tidal action, shoreline configuration, and other characteristics that might affect how the water would rise in a specific coastal zone. Data resolution and accuracy limit the ability to access a particular location and get an accurate measure of the exact inundation area and number of people. Any errors in the data affect the accuracy of the simulations. The limits of the rise in the global animated graphics are set to 80 m, the theoretical limit of sea-level rise if all glaciers and icecaps melt. For regional animated graphics, a limit of 30 m is used because this was the greatest rise resulting from the Indian Ocean tsunami in 2004.

A

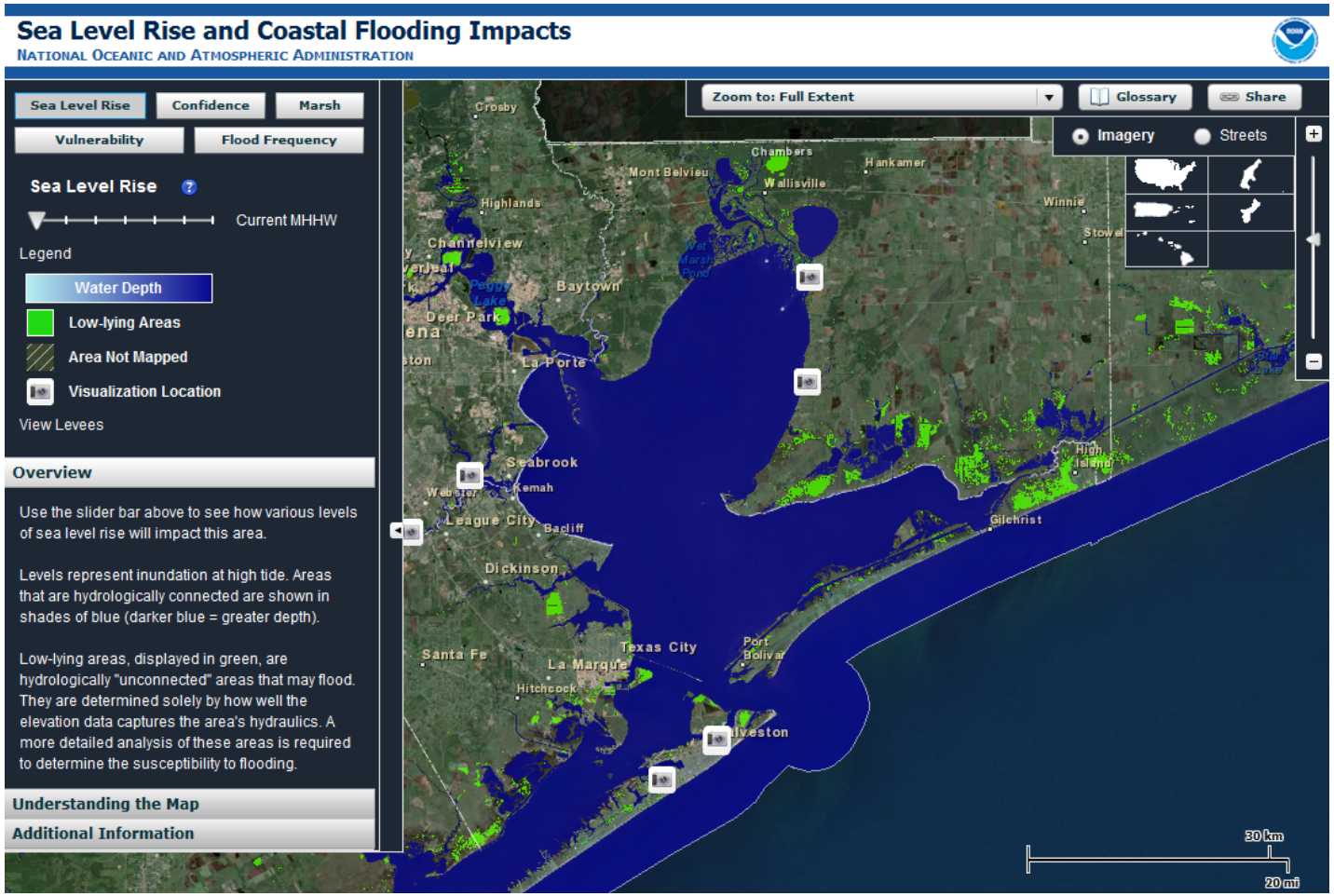

Figure 11. Screenshots showing National Oceanic and Atmospheric Administration (NOAA) Digital Coast Sea-Level Viewer graphic user interface for Galveston Bay, Texas (http://coast.noaa.gov/slr/). *A*, Inundation extent for current mean higher high water (MHHW). *B*, Inundation extent for 6-foot sea-level rise.

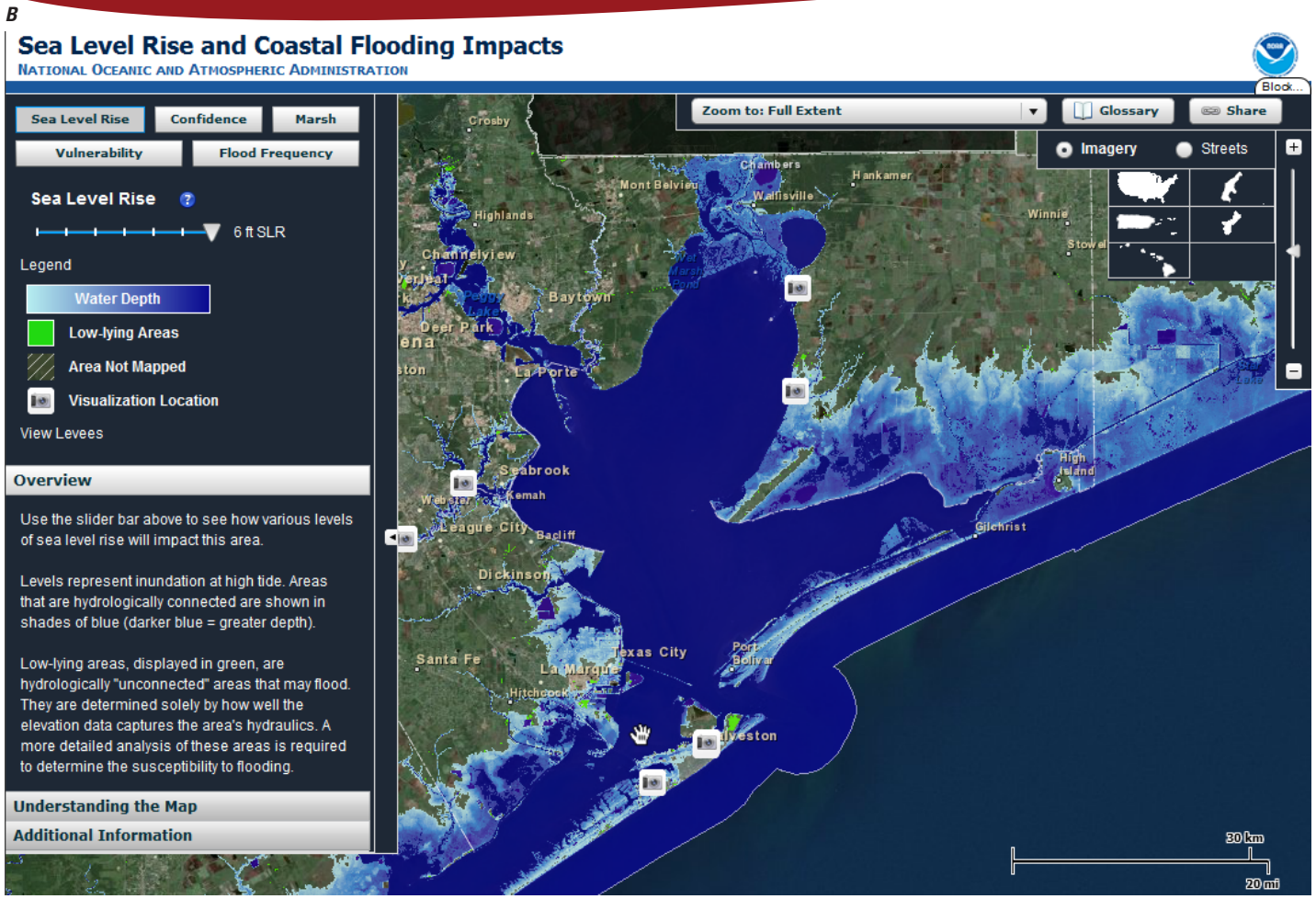

Figure 11. Screenshots showing National Oceanic and Atmospheric Administration (NOAA) Digital Coast Sea-Level Viewer graphic user interface for Galveston Bay, Texas (http://coast.noaa.gov/slr/). *A*, Inundation extent for current mean higher high water (MHHW). *B*, Inundation extent for 6-foot sea-level rise.—Continued

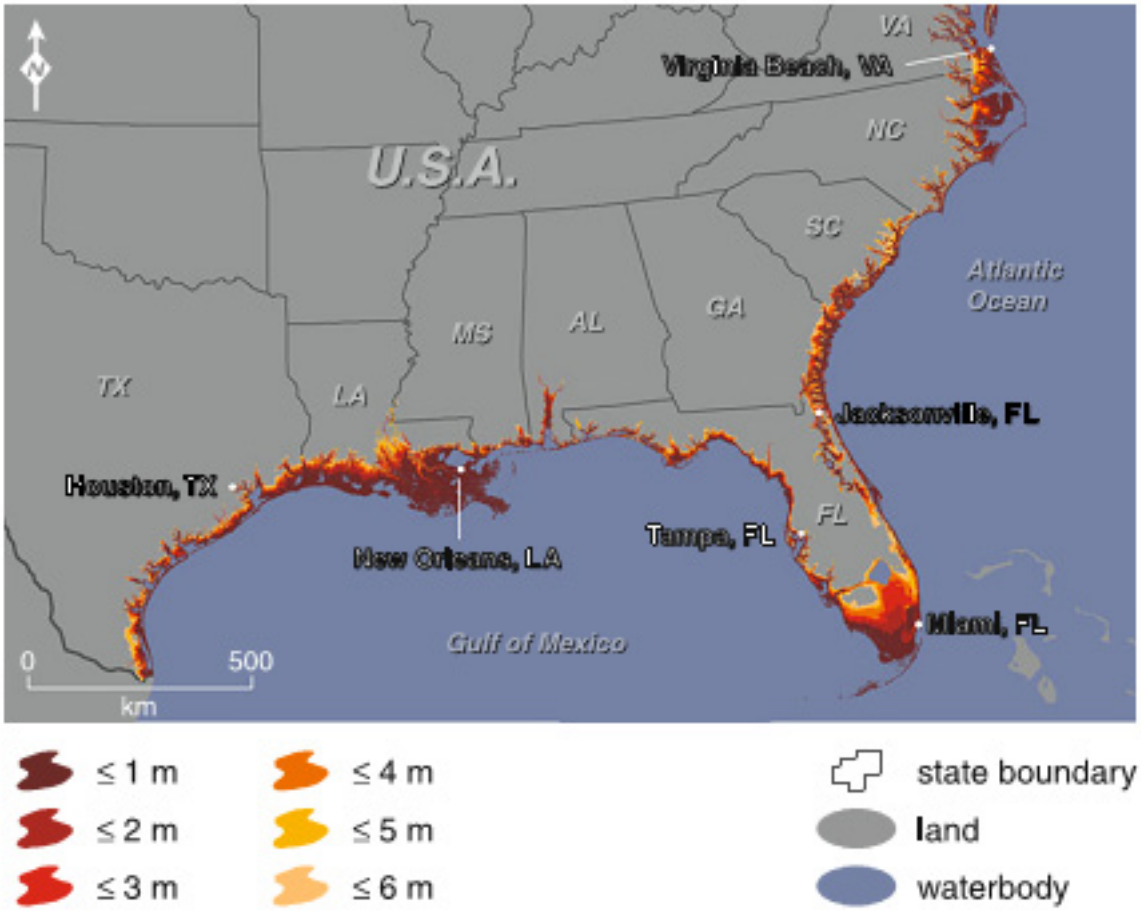

Figure 12. Screenshot showing University of Arizona Web Map Visualization Tool graphic user interface (from Strauss and others, 2012; used with permission).

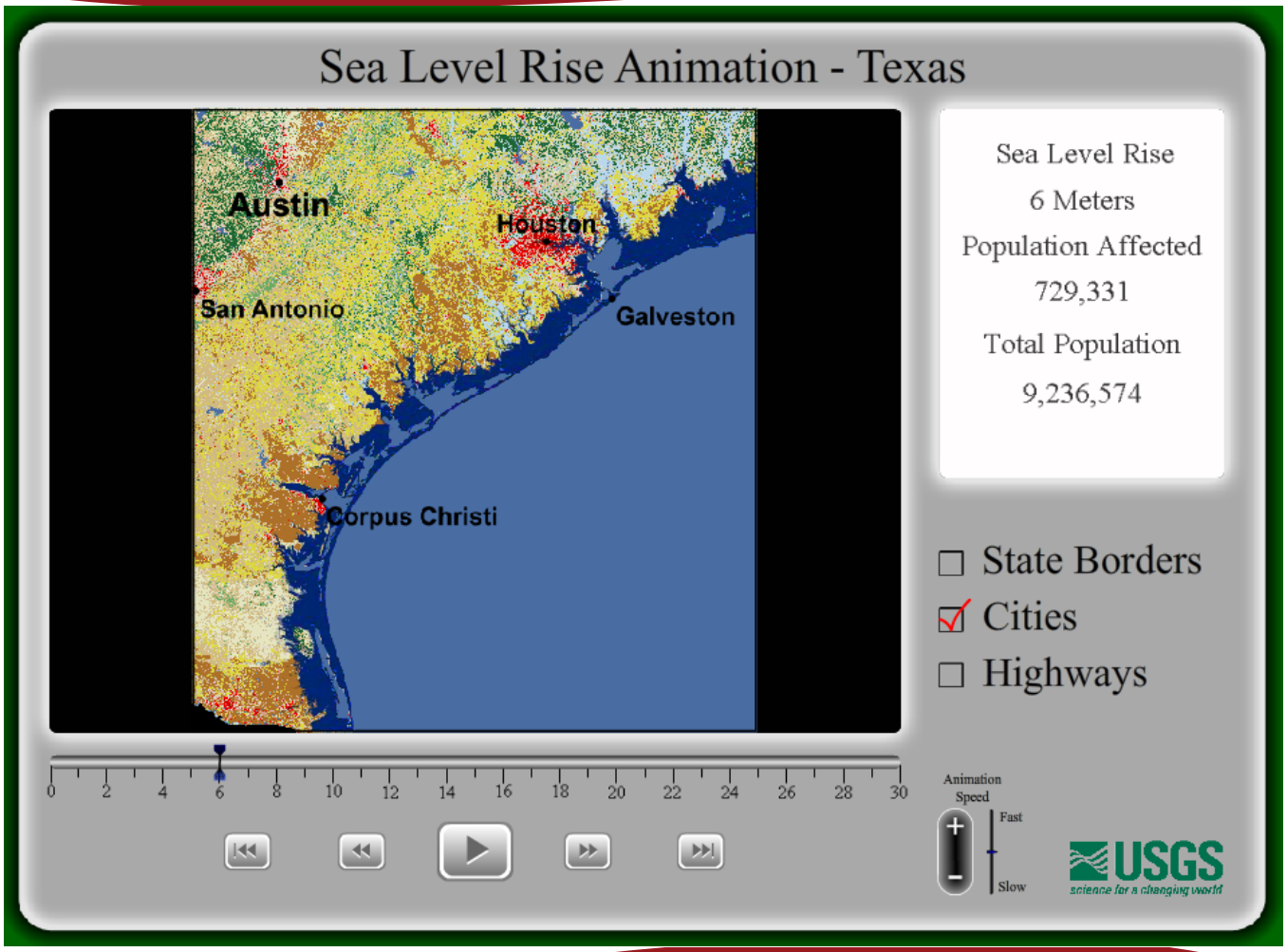

Figure 13. Screenshot showing U.S. Geological Survey Sea-Level Rise Animation graphic user interface (from Usery and others, 2010; used with permission).

Wetland Change Models

Ecological simulation models used for sea-level rise impact assessment vary fundamentally in design and function on the basis of the organizational unit, whether at ecosystem, species, or organism level. In this section, we describe the class of wetland change models designed to predict changes in land cover at the ecosystem (habitat) level in terms of presence or absence (table 5). In these models, there are no quantitative features or attributes applied to the cover type other than a descriptive classification. The wetland type or habitat cover descriptions vary in detail and discrimination from generic classification of terrestrial or aquatic forms to surficial qualifiers of tidal flat, beach, low marsh, high marsh, swamp, upland, or other cover type. These models are similar to GIS sea-level rise mapping tools ("bathtub" models; see section "Geographic Information System (GIS) Sea-Level Rise Mapping Tools") in that they predict change on the basis of the relation between land and water, but wetland change models assign a vegetative cover or habitat change effect. Further, whereas GIS sea-level rise mapping tools predict which and when land grid cells are overtaken by rising sea level to become open water, wetland change models generally have a simple rule set that assigns a given habitat type by degree of submergence. As the land grid cell becomes more inundated over time, these models account for the loss or gain of the different habitat types as a measure of impact from sea-level rise. Wetland change models differ largely on the delineation of habitat types or classification scheme used and the degree of inundation at which a habitat switches from one type to another. Predicted loss of habitat is generally a matter of erosion or submergence by surface inundation when a marsh, swamp, or mudflat eventually transitions to open water. As with GIS sea-level rise mapping tools, with wetland change models the sea-surface height is modeled as a static rise in adjoining water cells over annual or longer time steps assuming connectivity rather than any dynamic process. Most of these models have the capacity to parameterize the land elevation dataset with protective features of dikes, seawalls, or levees to mimic decoupling from adjacent water bodies, in which case the wetland type usually stays the same until the protective feature is overtopped by rising sea level.

Barataria-Terrebonne Ecological Landscape Spatial Simulation (BTELSS)

The Barataria-Terrebonne Ecological Landscape Spatial Simulation (BTELSS) (fig. 14) (Voinov and others, 1999, 2007; Martin and others, 2000; Reyes and others, 2000, 2004; Binder and others, 2003) and its predecessor, the Coastal Ecological Landscape Spatial Simulation (CELSS) (Constanza and others, 1990; Sklar and others, 1991), represent a process-based ecological model design of coastal wetland change and water constituents within a watershed context for evaluating potential impacts of restoration projects, river diversions, saltwater intrusion, climate change, and sea-level rise. The model framework is composed of raster cells representing interconnected 1-km^2 land units for a defined watershed. Each cell is connected to neighboring cells on all sides, involving a mass balance exchange of water volume and constituents of sediment, salt, and nutrients. The buildup of land or erosion to open water in a cell depends on the net balance of elevation gain by sedimentation and organic accretion or net loss from scour or subsidence. The effect of net surficial change is critical for predicting how marsh succession is affected by natural and human activities. Time-series data of Atchafalaya River and Mississippi River discharges, Gulf of Mexico salinity, river sediments and nutrients, rainfall, sea level, runoff, temperature, and winds are inputs to the model affecting water and constituent movement through the watershed. The location, dredging date, and characteristics of waterways, canals, and levees are also supplied as model inputs affecting historical conditions and effects on watershed hydrological dynamics. Land elevation in relation to flooding pattern determines succession of one habitat type to another by way of a simple switching algorithm. The model has been validated by hindcasting historical conditions and matching vegetation type and conversion with more contemporary vegetation maps.

Sea Level Affecting Marshes Model (SLAMM)

The Sea Level Affecting Marshes Model (SLAMM) (Park and others, 1989; Galbraith and others, 2002, 2003; National Wildlife Federation, 2006; Craft and others, 2009; Clough and others, 2010; Geselbracht and others, 2011) is a menu-driven, map-based simulation model using discrete time steps of 5–25 years. The different model versions reflect upgrades in software, data sources, and spatial resolution of subsequent site applications more than they reflect any substantial changes of functionality or design. Spatial resolution ranges from 500-m pixel size, for map areas confined to 7.5-min quadrangles prior to the advent of DEMs, to 10-m pixel dimensions of more recent versions. Orthometric land elevations are converted to tidal datum equivalents for selected regional tide gages. Sea-level rise is simulated as a static increase of projected eustatic sea-level rise for the proportion of years matching model time step. Earlier SLAMM versions did not account for marsh accretion, whereas version 6, the most updated version, assigns habitat-specific accretion rates that, if not exceeded by sea-level rise, allow for habitat migration or conversion. Model output consists of graphical displays of habitat change by color scheme (fig. 15) and tabular export files for calculating summary statistics of land loss and marsh migration with rising sea level. Model execution allows non-expert utility accomplished by command line and batch mode inputs of discrete user options for sea-level scenarios and map view based on a data matrix structure. Habitat data are based on classification of multispectral Landsat data of early versions

Table 5. Attributes of select wetland change models.

[<, less than; km², square kilometers; yr, year; NWI, National Wetlands Inventory; m, meter; lidar, light detection and ranging]

Model	Agency/ organization	Appropriate scale	Spatial resolution	Temporal scale	Input parameters	Vegetation classification	Output parameters	Validation	Citations
Barataria-Terrebonne Ecosystem Landscape Spatial Simulation (BTELSS)	Louisiana State University	Local, regional (such as <1 km²–100,000 km²)	1 km²	Variable time steps (daily, annual), simulation time up to 100 yr	Elevation and bathymetry, air temperature, wind speed and direction, precipitation, river discharge, sediment load, wetland land cover, regional salinity, plant growth and mortality rates, salinity and flooding tolerances of plants	NWI	Maps of land change (habitat switching), flooded and eroded areas, plant productivity, salinity, open-water circulation, and sediment transport	Hindcast	Reyes and others (2000, 2004); Martin and others (2000); Voinov and others (1999, 2007); Binder and others (2003).
Coastal Ecological Landscape Spatial Simulation (CELSS)	Louisiana State University	Local, regional (such as <1 km²–100,000 km²)	1 km²	Variable time steps (daily, annual), simulation time up to 100 yr	Elevation and bathymetry, air temperature, wind speed and direction, precipitation, river discharge, sediment load, wetland land cover, regional salinity, plant growth and mortality rates, salinity and flooding tolerances of plants	NWI	Maps of land change (habitat switching), flooded and eroded areas, plant productivity, salinity, open-water circulation, and sediment transport	Hindcast	Costanza and others (1990); Sklar and others (1991).
Sea Level Affecting Marshes Model (SLAMM 1–5)	Warren Pinnacle Consulting, Inc.	Local, regional (such as <1 km²–100,000 km²)	10–100 m	Time steps of 5–25 yr can be used on the basis of sea-level rise scenario, simulation time up to 100 yr	Elevation maps (lidar preferred), wetland land cover (such as NWI), development footprint, and dike location, sea-level rise projections	NWI	Maps of areas/ habitats potentially vulnerable to inundation (land cover and elevation maps)	None	Park and others (1989); Galbraith and others (2002, 2003); National Wildlife Federation (2006); Craft and others (2009).
Sea Level Affecting Marshes Model (SLAMM 6)	Warren Pinnacle Consulting, Inc.	Local, regional (such as <1 km²–100,000 km²)	10–100 m	Time steps of 5–25 yr can be used on the basis of sea-level rise scenario, simulation time up to 100 yr	Elevation maps (lidar preferred), wetland land cover (such as NWI), development footprint, dike location, sea-level rise projections	NWI	Maps of areas/ habitats potentially vulnerable to inundation (land cover and elevation maps)	Hindcast	Clough and others (2010); Geselbracht and others (2011).
Sea Level Over Proportional Elevation (SLOPE)	U.S. Geological Survey	Regional, national	County	Monthly or annual time step, simulation time up to 100 yr	Saltmarsh/mangrove area, monthly tide gage records, sea-level rise projections, tidal range by county	NWI	Maps of land change, habitat migration and displacement	Hindcast	Doyle and others (2010).

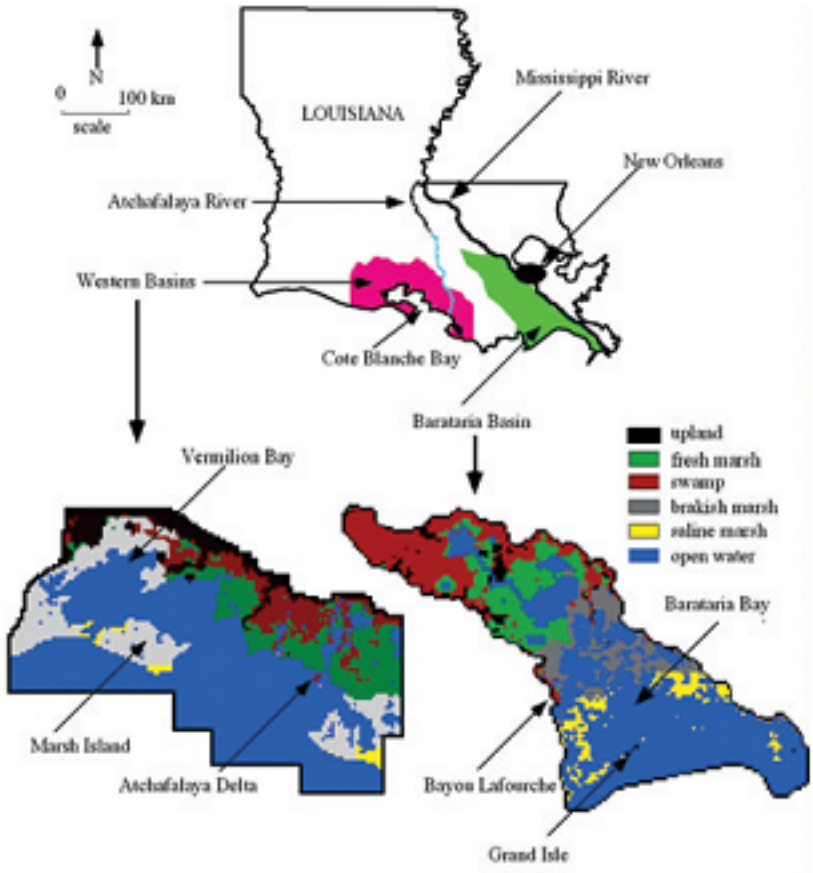

Figure 14. Screenshots showing Barataria-Terrebonne Ecosystems Landscape Spatial Simulation (BTELSS) model domain and sea-level change map for the Barataria and Terrebonne Basins, Louisiana (from Reyes and others, 2000; used with permission).

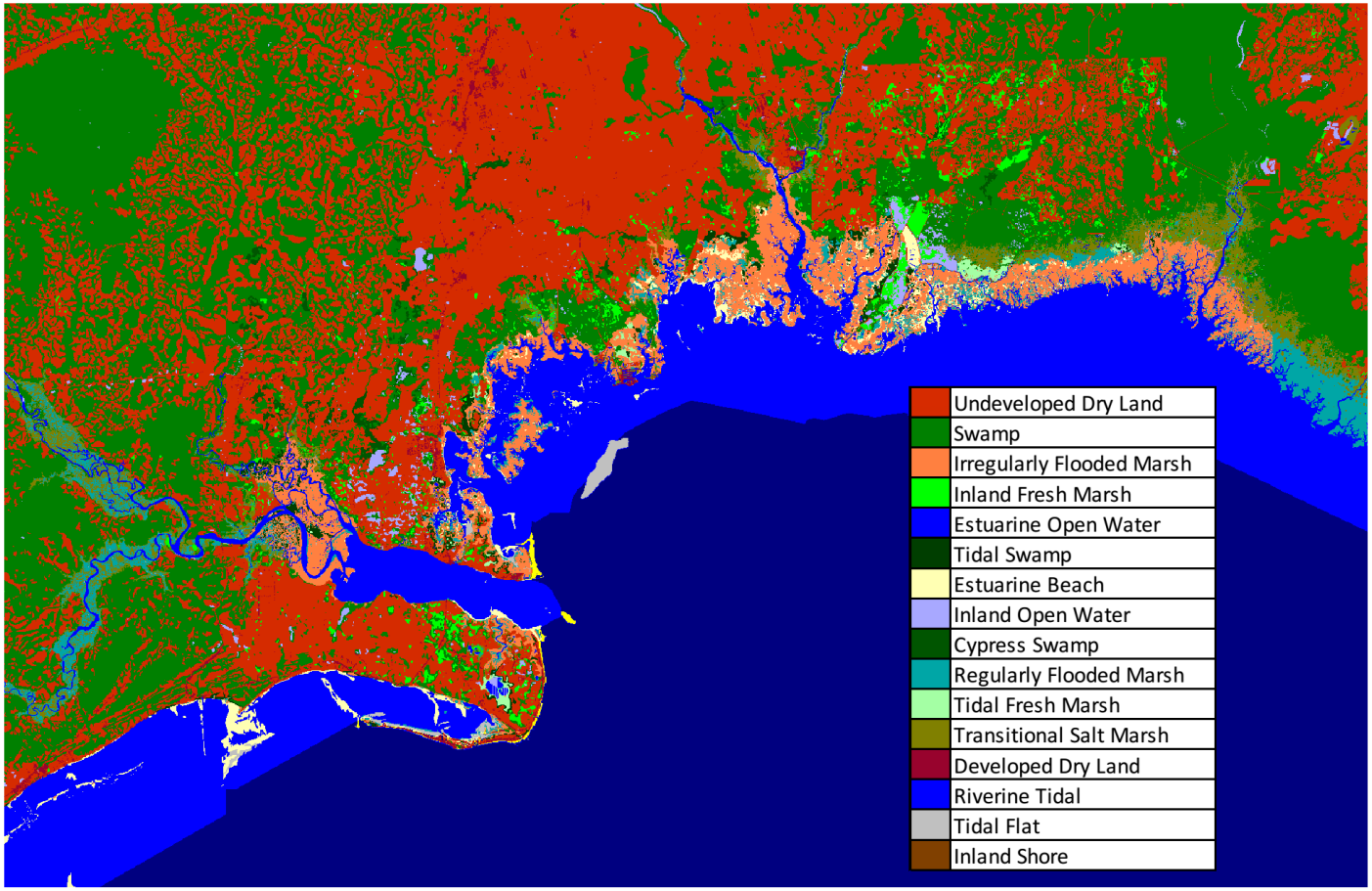

St. Marks NWR, 2100, Scenario A1B Mean, 0.39 m SLR by 2100.

Figure 15. Screenshot showing Sea Level Affecting Marshes Model 6 (SLAMM 6) display viewer for the St. Marks National Wildlife Refuge application (from U.S. Fish and Wildlife Service, 2012).

of SLAMM and U.S. Fish and Wildlife Service (FWS) National Wetland Inventory (NWI) habitat delineations of later versions of SLAMM, including aquatic systems, urban developed, terrestrial wetland, and upland forest classes (app. 3). NWI land cover classes describe generic habitat type more than they describe specific species or any metrics of habitat quality, density, height, or biomass. Elevations of the grid cells in SLAMM are based on interpolated topographic contour lines and slopes in early versions to DEMs based on USGS NED and supplementary lidar coverage in later versions (app. 3). Model predictions are based on rule sets of land loss/conversion relative to water-table inundation of the land surface and wave erosion on the edge of large water bodies, excepting protected land units behind dikes. Although the model predicts habitat loss/change on the basis of simple rule sets and Boolean decision trees, new site applications usually require expert knowledge to parameterize model drivers on the basis of tide range and datum relations.

Sea Level Over Proportional Elevation (SLOPE) Model

Tidal freshwater forests in coastal regions of the southeastern United States are undergoing dieback and retreat from increasing tidal inundation and saltwater intrusion attributed to climate variability and sea-level rise. In contrast, in many areas, tidal saltwater forests (mangroves) are expanding landward in subtropical coastal reaches, succeeding freshwater marsh and forest zones. Hydrological characteristics of these low-relief coastal forests in intertidal settings are dictated by the influence of tidal and freshwater forcing. The Sea Level Over Proportional Elevation (SLOPE) model (Doyle and others, 2010) is a USGS product that predicts coastal forest retreat and saltmarsh/mangrove migration from projected sea-level rise on the basis of a proxy relation of saltmarsh/mangrove area and tidal range (fig. 16). The model as applied to the Gulf Coast is subdivided into separate reaches defined by each of the 60 coastal counties from Texas to Florida. Summaries of saltmarsh/mangrove area for each coastal county were obtained from published sources on the basis of detailed grid sampling of the NWI database and habitat classification scheme. Tidal ranges were obtained from NOAA tide stations for more than 300 locations and filtered to assign corresponding maximum tide range for each coastal county. The SLOPE model assumes that the sum area of saltmarsh/mangrove habitat along any given coastal reach is determined by the slope of the landform and vertical tide forcing. The model assumes that area and boundary characteristics of saltmarsh/mangrove ecosystems have been defined by the local tidal prism in relation to ambient salinity concentrations and circulation suitable to support saltwater habitats in a given coastal reach.

Surface Elevation and Shoreline Erosion Models

Most predictive sea-level rise models previously discussed are GIS tools, not dynamic ecological models, and they lack any feedback relation of marsh accretion and elevation with sea-level change. More often the implicit assumption of GIS sea-level rise mapping tools is that, as sea level rises above surface elevation, marsh habitat succumbs to inundation and is consequently converted to open water. Wetland change models work similarly, but some assign fixed or static accretion rates by habitat type such that, as sea-level rise rate exceeds these values, the habitat type and land unit undergo inundation (that is, submersion, erosion), resulting in habitat loss and conversion to open seawater. Field studies of marsh soil stratigraphy and age demonstrate that saltmarsh and mangrove species can keep pace with sea-level change of past centuries and millennia even in delta settings subject to high rates of land subsidence, such as in the Mississippi River coastal platform. This long-term evidence of marsh resiliency indicates that we know less about under what conditions and for what reasons they erode and at what rates of sea-level rise they cannot keep pace. In this section, we describe process-based studies and models of marsh-elevation change, substrate biogeochemical state, and shoreline erosion that are complementary to predictive sea-level rise models, particularly species- and ecosystem-based simulation models to be discussed in later sections.

There are a number of empirical studies and observation systems for monitoring the process and rate of surface elevation change, substrate biogeochemical state, and shoreline erosion that are important to highlight. Geographic position of barrier island and mainland shorelines from maps dating to the European discovery of North America has been compared with more recent map sources to demonstrate shifts, erosion, and aggradation of coastal features linked to longshore currents and riverine influences. New observational tools and techniques to monitor surface elevation and soil salinity change within coastal wetlands have improved understanding of the dynamic nature of subsidence, accretion, sedimentation, eutrophication, and saltwater intrusion with changing hydrological forcing connected with hurricanes, sea level, streamflow, climate, and biotic factors. In this section, we describe different tools and techniques for monitoring and modeling surface elevation, shoreline change, and storm influences of coastal systems.

Figure 16. Screenshots showing Sea Level Over Proportional Elevation (SLOPE) model data layers for the northern Gulf of Mexico coast regional application (from Doyle and others, 2010; used with permission). *A*, Total saltmarsh and mangrove area (in hectares) extracted from the National Wetland Inventory (NWI) for coastal counties of the northern Gulf of Mexico. *B*, Relative sea-level rate (in millimeters per year) for National Oceanic and Atmospheric Administration (NOAA) tide stations. *C*, Predicted land loss or retreat of freshwater forest area (in hectares) for coastal counties under a 10-centimeter rise of sea level from accelerated global eustasy. *D*, Tidal range estimates (in centimeters) extracted from water level records for 300 NOAA coastal tide stations for coastal counties.

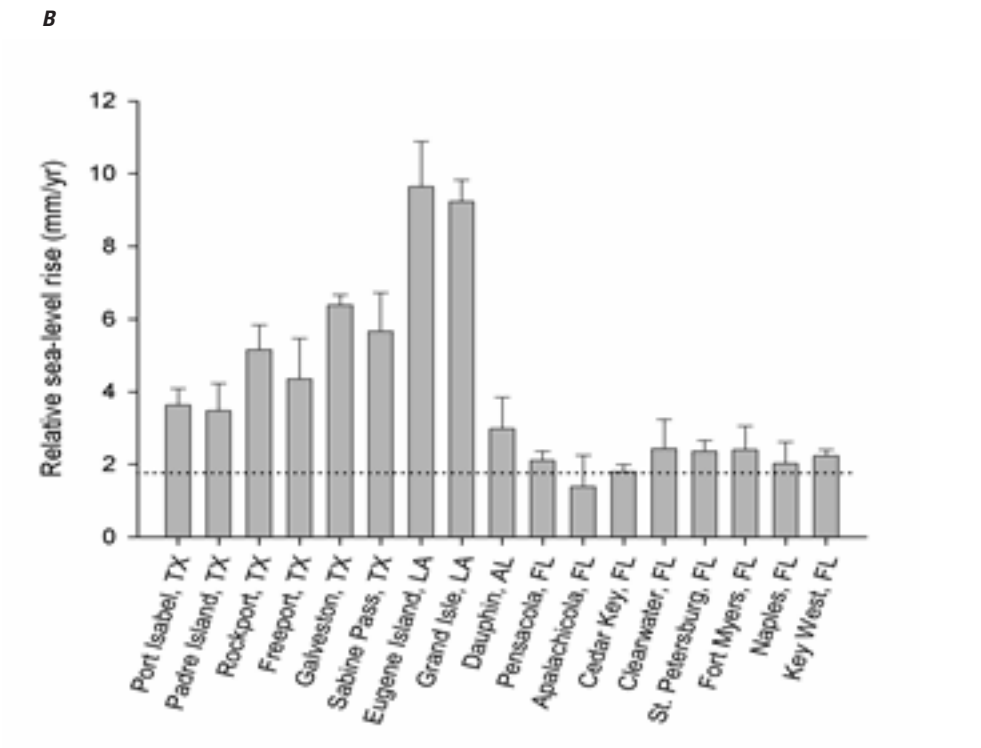

Figure 16. Screenshots showing Sea Level Over Proportional Elevation (SLOPE) model data layers for the northern Gulf of Mexico coast regional application (from Doyle and others, 2010; used with permission). *A*, Total saltmarsh and mangrove area (in hectares) extracted from the National Wetland Inventory (NWI) for coastal counties of the northern Gulf of Mexico. *B*, Relative sea-level rate (in millimeters per year) for National Oceanic and Atmospheric Administration (NOAA) tide stations. *C*, Predicted land loss or retreat of freshwater forest area (in hectares) for coastal counties under a 10-centimeter rise of sea level from accelerated global eustasy. *D*, Tidal range estimates (in centimeters) extracted from water level records for 300 NOAA coastal tide stations for coastal counties.—Continued

Figure 16. Screenshots showing Sea Level Over Proportional Elevation (SLOPE) model data layers for the northern Gulf of Mexico coast regional application (from Doyle and others, 2010; used with permission). *A*, Total saltmarsh and mangrove area (in hectares) extracted from the National Wetland Inventory (NWI) for coastal counties of the northern Gulf of Mexico. *B*, Relative sea-level rate (in millimeters per year) for National Oceanic and Atmospheric Administration (NOAA) tide stations. *C*, Predicted land loss or retreat of freshwater forest area (in hectares) for coastal counties under a 10-centimeter rise of sea level from accelerated global eustasy. *D*, Tidal range estimates (in centimeters) extracted from water level records for 300 NOAA coastal tide stations for coastal counties.—Continued

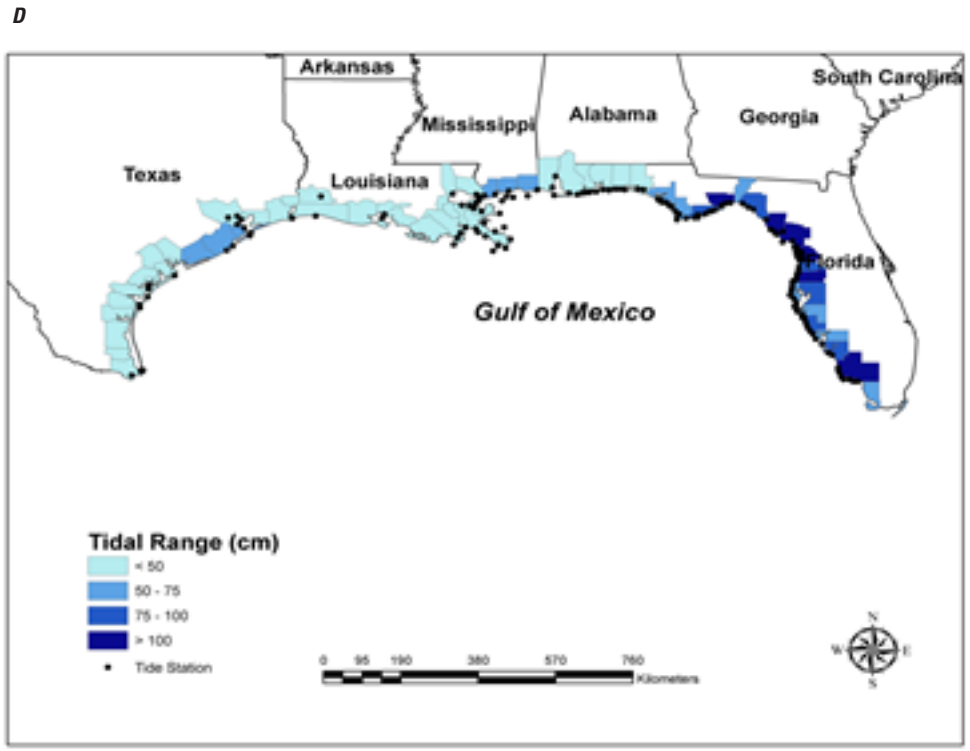

Figure 16. Screenshots showing Sea Level Over Proportional Elevation (SLOPE) model data layers for the northern Gulf of Mexico coast regional application (from Doyle and others, 2010; used with permission). *A*, Total saltmarsh and mangrove area (in hectares) extracted from the National Wetland Inventory (NWI) for coastal counties of the northern Gulf of Mexico. *B*, Relative sea-level rate (in millimeters per year) for National Oceanic and Atmospheric Administration (NOAA) tide stations. *C*, Predicted land loss or retreat of freshwater forest area (in hectares) for coastal counties under a 10-centimeter rise of sea level from accelerated global eustasy. *D*, Tidal range estimates (in centimeters) extracted from water level records for 300 NOAA coastal tide stations for coastal counties.—Continued

Coastal Vulnerability Index (CVI)

The Coastal Vulnerability Index (CVI) (Gutierrez and others, 2011) represents an objective (observed) measure of shoreline erodibility for the coastlines of the United States—Atlantic, Pacific, and Gulf of Mexico—on the basis of historical shoreline maps and geological studies. The CVI is a probability index designed to assign relative risk and future threat of shoreline change under rising sea level. The index is based primarily on empirical measures of physical changes determined from comparative shoreline surveys or maps related to physical forces and features of tidal range, wave height, coastal slope, geomorphology, and relative sea-level trend by coastal reach. This approach, using combinations of measured change, coastal attributes, and physical forcings, provides a relative vulnerability, or erodibility, measure for guiding coastal planning and research. Prediction of shoreline retreat and land loss rates is critical to planning future coastal development and management strategies. CVI provides a useful construct and decision-support tool on a national and regional basis for assessing economic risk and threats of coastal erosion, flooding, and storm damage. For example, along the U.S. Atlantic Coast, high-vulnerability areas are typically barrier islands having small tidal ranges, large waves, a low coastal slope, and high landform subsidence, such as in the Mid-Atlantic region (fig. 17). Coasts with rocky cliffs or steep slopes are generally associated with large tidal ranges and low subsidence rates, such as most of the coastline in the Northeast, and are represented as low vulnerability (that is, low CVI). A Bayesian Network (BN) analysis has been developed to complement the historical perspective of the CVI to predict long-term shoreline change for the different projections of sea-level rise. The BN analysis links the relations between driving forces, geological constraints, and coastal response for the U.S. Atlantic Coast that include observations of local rates of relative sea-level rise, wave height, tide range, geomorphic classification, coastal slope, and shoreline change rate. Probabilistic predictions of shoreline retreat can be generated in response to different sea-level rise projections, mostly demonstrating that shoreline retreat increases with higher rates of sea-level rise (fig. 17).

Marsh Substrate Geochronology Methods

A number of well-established methods are used to date peat and mineral layers of marsh substrates and biological deposits with different radioactive isotopes, mainly carbon-14 (^{14}C), lead-210 (^{210}Pb), cesium-137 (^{137}Cs), beryllium-7 (^{7}Be), oxygen-18 (^{18}O), and uranium-238 (^{238}U). The concentration and ratios of the different radioactive isotopes for each element have been used successfully to age the different depths of soil and fossil deposits for reconstructing ancient sea level, glacial advance and retreat, fossil age, and marsh accretion rates (DeLaune and others, 1989; Appleby and Oldfield, 1992; Turner and others, 2006; Mudd and others, 2009). The different radioactive isotopes are used for different purposes and time periods but provide similar results of identifying dates for organic debris, fossils, and mineral layers of marsh soils and bog peats. Geochronology is the science of aging (dating) rocks, fossils, peats, and sediments that is inherent to the accuracy and limitations of the isotope and properties of radioactive decay or half-life. A number of radioactive isotopes are used for this purpose and, depending on the rate of decay, are used for dating different geological periods. More slowly decaying radioactive isotopes are useful for dating longer periods of time but are less accurate in absolute years. Radiocarbon dating is well known and commonly used for reconstructing ancient sea level of the more recent Holocene epoch of the last 12,000 years. Cesium-137 dating of marsh substrate is a reliable method for estimating near-term sediment accretion rates as an artificial radionuclide product of bomb testing and peak fallout in 1963–64. Isotopic analysis, such as ^{18}O and ^{16}O ratios, is also used to relate the climate conditions under which fossils grew, which correlate with ocean temperature and salinity that can be further extrapolated to sea-level equivalents.

Saltmarsh Stratigraphy and Evolution Models

There are a number of field and modeling studies that have attempted to understand the process and feedback mechanisms of marsh accretion of different coastal settings and environmental drivers (Allen, 1990; French, 1993; Morris, 1995; Rybczyk and others, 1998; Fagherazzi and others, 2012; Kirwan and Mudd, 2012). Conceptual, analytical, and numerical models have been developed to predict the process and rate on the basis of the different biotic and abiotic factors that vary with coastal position and degree of marine influence. In most applications, vegetation health and productivity are important components controlled by degree of inundation and submergence by tidal influence relative to mean sea level. Model types vary with complexity of processes and parameters to predict the genesis of saltmarsh soils controlled by relative rates of nutrient mineralization and inputs of organic and inorganic matter. Processes include sedimentation of exogenous and endogenous organic and inorganic matter, decomposition, aboveground and belowground biomass and production, and nitrogen and phosphorus mineralization. Models vary with vegetation type, tidal relations, and deposition rates as a function of surface elevation and distance from a channel. Distinctions of refractory and labile forms of organic fractions, aboveground and belowground production models, and decay rates add to model detail and functionality (fig. 3).

Surface Elevation Tables (SETs)

The surface elevation table (SET) (Cahoon and others, 2002a, 2002b; Krauss and others, 2010; Rogers and others, 2012) is composed of a benchmark set in wetland soils and environments that is repeatedly resurveyed with a portable mechanical device for precise releveling of the soil surface.

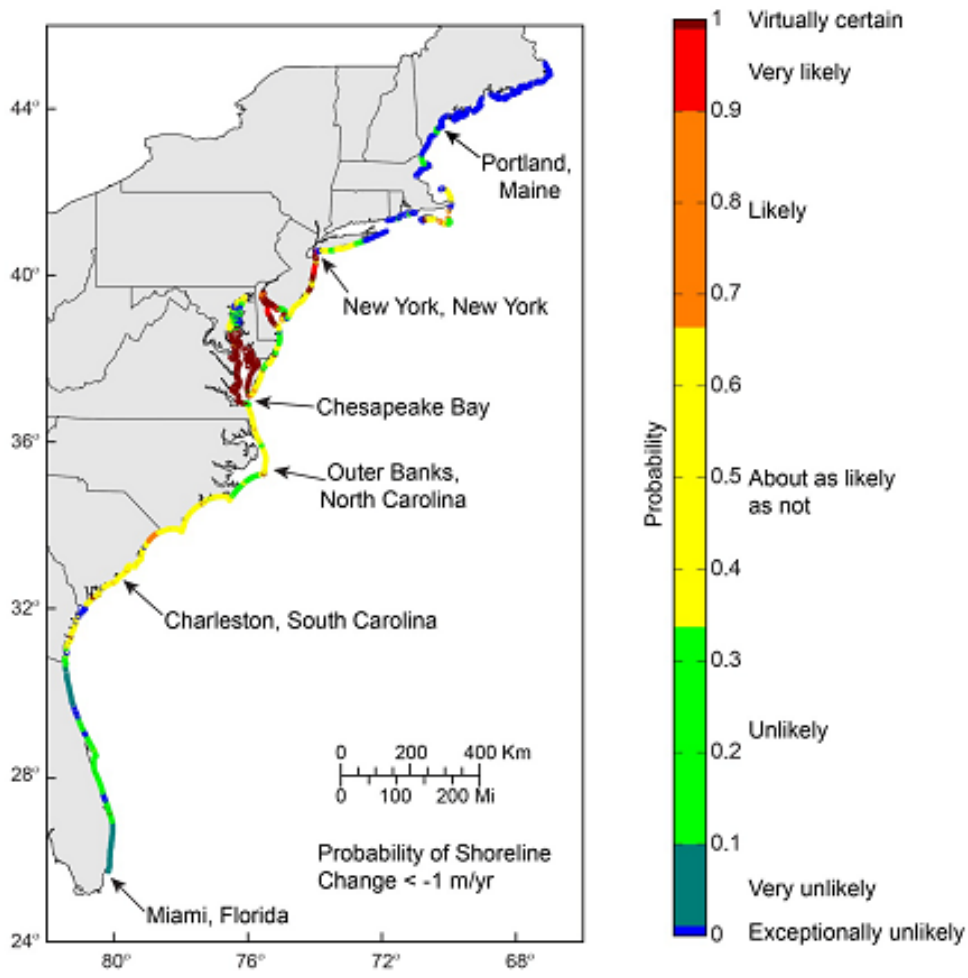

Figure 17. Screenshot showing Coastal Vulnerability Index (CVI) Bayesian Network application for the U.S. Atlantic Coast (from Gutierrez and others, 2011).

The SET provides a nondestructive method for making highly accurate and precise remeasurements of sediment elevation of intertidal and subtidal wetlands over long periods of time relative to a fixed benchmark attached to a subsurface rod usually deep and driven to refusal (fig. 18). This technique overcomes many of the limitations of methods currently used to estimate elevation, such as sedimentation pins and precision surveying. The rod SET can be attached to either deep or shallow rods driven to different depths below surface into stable geological formations (fig. 18*A*). This flexible design allows the rod SET to be used to monitor elevations across different depths of the soil profile. A number of SETs may be established in a network for a particular site along a landscape or geomorphic gradient or in different wetland types to determine rates and processes of elevation change in different settings relative to abiotic and biotic factors. SETs are typically revisited quarterly, annually, or after storm events to monitor change over time and to identify what sources, mechanisms, and factors are contributing to elevation loss or gain. Clay feldspar pads are used in conjunction with SETs to establish a marker horizon of a known date on the wetland surface (fig. 18*B*) from which organic and mineral deposition rates can be estimated from subsequent core sampling. A data record of SET readings over years provides a definitive picture of the various contributing factors of accretion, deposition, subsidence, and storms that determine whether a given soil surface is either increasing or decreasing in elevation and is either keeping pace with or falling behind relative sea-level change for a given coastal setting.

Tidal Channel Network Models (TIGER)

Beyond the coarse coastline-change measures on a national or regional scale are the local and more fractal changes of tidal creeks and river outlets that relate to the process of marine and riverine coupling with marsh platforms, which is important to hydrological exchange and biophysical controls of marsh evolution, species composition, and productivity. Various numerical models have recently been developed to describe the morphogenesis and long-term dynamics of saltmarsh channels and tidal creek networks during periods of rising sea levels (Fagherazzi and Sun, 2004; D'Alpaos and others, 2005; Kirwan and Murray, 2007). Current understanding of coastal landform evolution is still more conceptual than certain in ability to validate quantitative predictions of how, when, where, and whether saltwater and freshwater systems can or will keep pace with different rates of sea-level rise. Tidal channels are related conduits that shape the marsh landscape and are in turn affected by the marsh landscape. The composition and constituency of marsh substrate and its exposure to tidal forcing and storm surge flooding dictate the proximity and dendritic patterns of tidal creeks, as do human influences of coastal modifications, dredging, and channelization. Where static models are simple to apply and to simulate flooding of marsh surfaces, they assume that surface water is delivered instantaneously rather than with temporal and spatial variability across the marsh platform. More advanced hydrodynamic models consider the time-dependent processes of flooding path, depth, and duration on the basis of distance, shape, and function of associated tidal creeks and marsh platforms. The rate of flooding and draining varies sharply at the highest and lowest elevations of the tidal range more than around the mean condition because of the different astronomical tide types and meteorological extremes. Sea-level rise models should be improved or more accurate as more realistic tidal hydrodynamics are incorporated rather than static "bathtub" treatment.

Niche-Based Species Distribution Models

Niche-based species distribution models describe the interrelation of environmental factors or conditions thought to define or limit species range on the basis of geographic extent. These models assume that modern distribution of species is controlled by associated climate and edaphic factors that can be quantified and expressed as favored and adapted ecological space. Fundamental niche space is theoretically all sets of factors controlling species presence, colonization, and persistence, whereas realized niche space (actual species range) is a limited expression of full ecological potential. Commonly, the overlap of precipitation and temperature datasets coincident with species range is used to construct niche space and project potential spread with changing climate. This approach assumes that environment solely controls species spread and success apart from event-driven causes or other physiographic, hydrological, or biotic factors.

A prime example of how niche-based modeling may be deficient for some plant species is the range extent of *Taxodium distichum* (baldcypress) across the Eastern United States. The range boundary is not uniform with latitude or longitude, including disjunct distribution and populations. One biological attribute of baldcypress is its modest but comparatively elevated salt tolerance among freshwater tree species. Baldcypress is more readily known for its site preference and dominance in flood zones and growth production under high-precipitation conditions. Its interrupted range extent in the western Gulf Coastal Plain of Texas is indicative of arid conditions less suitable for baldcypress sustainability. Studies of tidal freshwater forests along coastal margins of the Southeastern United States indicate that, as residual soil salinities of these systems become elevated above 3 ppt from storm tides, prolonged drought, and saltwater intrusion, baldcypress persists in degraded, monospecific stands along the marsh-estuarine ecotone. The distribution and range of baldcypress correspond with the elevation of ancient sea level (about 120 m above current sea level) dating back to highstand shorelines of the Late Cretaceous epoch around 65 million years ago (fig. 19). State records of champion baldcypress trees provide evidence that planted baldcypress persists to mature age and size in nearly every northern State and Canada, beyond its natural range, suggesting that colder climate is not a limitation to growth.

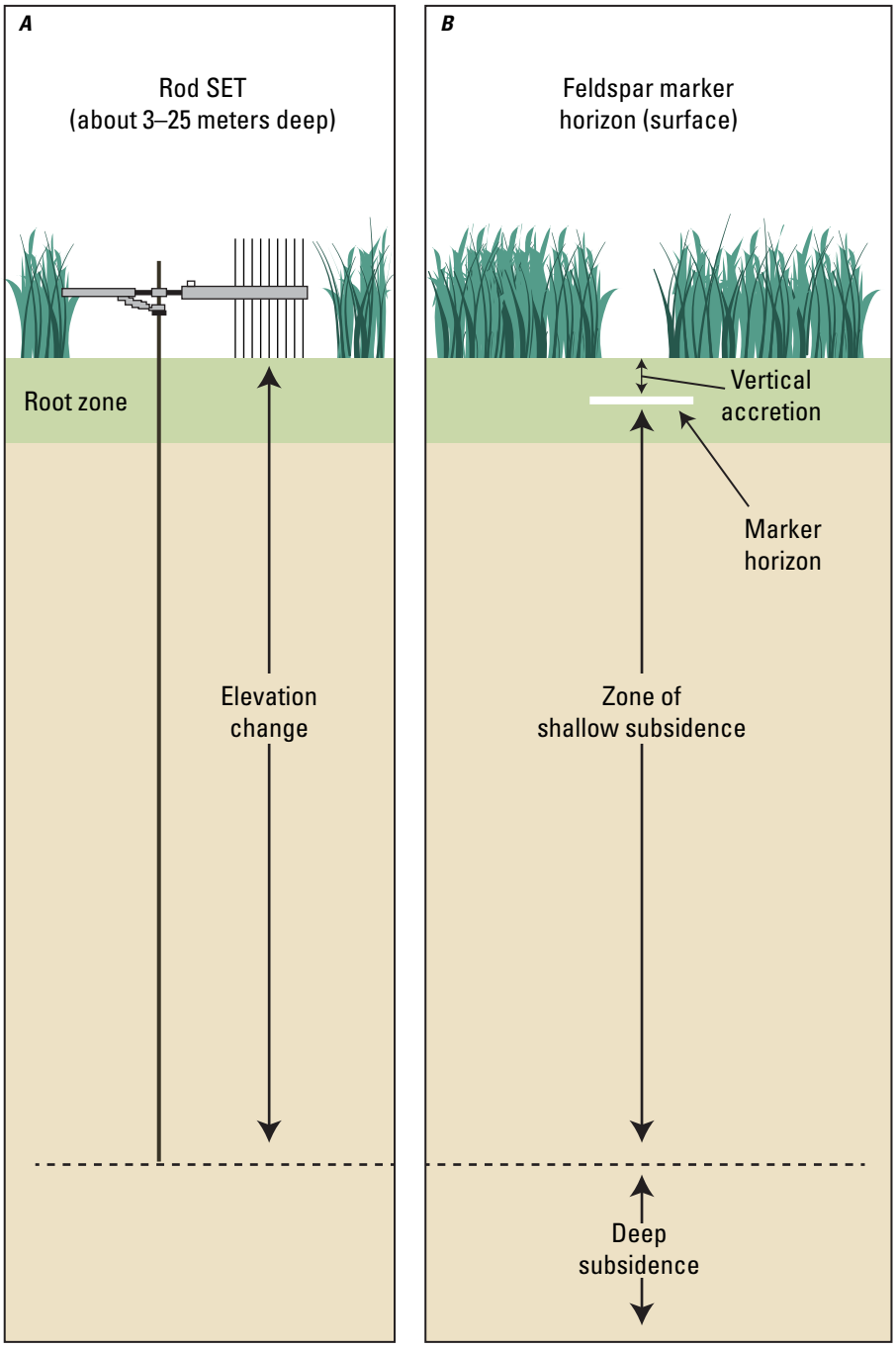

Figure 18. Surface elevation tables (SETs) (from Cahoon and others, 2002b; used with permission). *A*, Rod SET. *B*, Feldspar marker horizon.

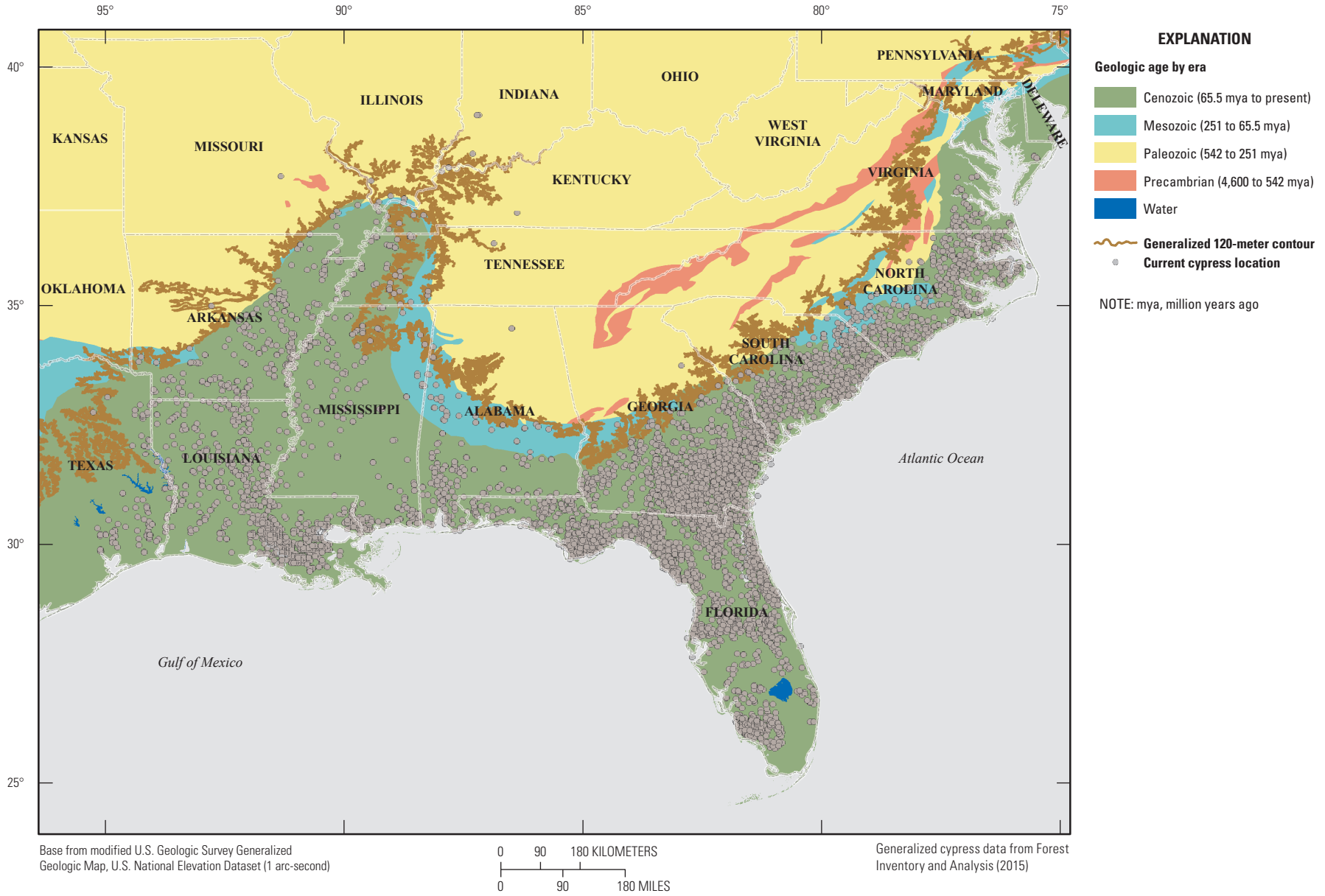

Figure 19. *Taxodium distichum* (baldcypress) distribution in relation to elevation of ancient sea level (about 120 meters above current sea level) dating back to highstand shorelines of Late Cretaceous epoch.

Mangroves are another group of wetland species whose range is related to sea level by adaptation to saltwater conditions and propagule spread by ocean tides and currents. As tropical plant species that dominate coastal areas in tropical zones worldwide, mangroves also delineate intertidal zones of higher latitudes over geological periods under favorably warm climates with an absence of freeze events and of lower, equatorial latitudes during cooling periods (fig. 20). A weakness, therefore, of many sea-level models is the singular factor approach, in which only sea level by submergence controls loss or gain of coastal habitat with its projected rise or fall, and there is a lack of an interactive or integrated approach of allowing mangroves to supersede saltmarsh under warmer, frost-free, climate.

A niche-based species distribution model with sea-level controls does not exist, but the related Climate-Envelope Mangrove Model (Osland and others, 2013), developed by the USGS, demonstrates how projected climate warming allows for mangrove expansion to higher latitudes. This species distribution model was developed to predict potential mangrove expansion latitudinally with rising temperatures and lower freeze probabilities under a future climate scenario. By using existing mangrove distribution across the northern Gulf of Mexico, an empirical relation was derived to explain mangrove presence and abundance with a host of multidecadal winter climate parameters, and the niche-based modeling approach was applied by using current mangrove distributions for the five Gulf Coast States—Texas, Louisiana, Mississippi, Alabama, and Florida—to determine whether and where mangroves might expand in the absence of freeze events for different emission scenarios. The resulting Climate-Envelope Mangrove Model is based on winter severity climate parameters to predict either potential loss or injury from freeze or population spread and abundance with warming climate. Mean annual minimum temperature (MAMT) was identified as the winter climate variable that best explained mangrove presence and abundance. Model simulations were applied to predict where mangrove colonizers can establish and spread under different cases of future temperature regimes under climate change. The northern Gulf of Mexico represents a broad longitudinal expanse within a narrow latitudinal band within a subtropical zone where only slight changes in rising temperatures will favor spread of tropical species (fig. 21). In this case, sea-level rise alone is not sufficient to predict the fate of mangrove spread but requires additional predictors such as favorable temperature regimes.

Leaf to Landscape (L2L) Ecosystem Models

Leaf to landscape (L2L) ecosystem models are the most sophisticated ecological models developed for sea-level rise application. These models predict ecosystem change at the species and organism level on the basis of the physiological tolerances and ecological requirements of a species and specific environmental conditions of an organism or individual plant (table 6). L2L ecosystem models incorporate a hierarchical integration of ecological processes and response from the leaf level, where photosynthesis, water exchange, and carbon allocation take place on an individual tree or plant basis, to the stand level, where interplant competition, biomass, and diversity are measured, to the landscape level, where physical factors of soil, watershed, climate, and disturbance differences affect system-level response.

Coupled Saltmarsh Biogeochemical and Demographic Model

A coupled biogeochemical and demographic model (Simas and others, 2001) was developed for saltmarsh in the Tagus estuary in Portugal to predict potential effects of sea-level rise on distribution of C_3 and C_4 plant species (plants that use a carbon fixation pathway with 3- and 4-carbon molecules, respectively, in the first stable photosynthetic product). Saltmarsh processes are simulated as a function of C_3 and C_4 species carbon production from light- and temperature-dependent functions of growth, respiration, and leaf mortality. A class transition model simulated the demographics of plant population density per unit area. A GIS tool was used to track changes in elevation with constant sedimentation inputs over time and the various production attributes of lower marsh (C_4) and upper marsh (C_3) with sea-level rise of 95 cm by 2100. The model does not simulate marsh migration upslope but rather simulates the loss of marsh habitat cover and production over time.

Hammock-Mangrove Vadose Zone Model

The ecotone of vegetation boundaries between tidal freshwater and saltwater wetlands is often fairly discrete but can be overlapping and intermingled. In The Everglades, mangroves have expanded upslope into zones once dominated by freshwater wetlands over the past century concomitant with sea-level rise and freshwater drainage effects. Mangrove propagule transport by landward wind and storm tides pushing up tidal creeks and drainage canals allows for regeneration opportunities far inland. Saltwater intrusion simultaneously occurs with redirected freshwater drainage and increasing sea level. The Hammock-Mangrove Vadose Zone Model (Teh and others, 2008) was developed by the USGS to investigate the process of species distribution and productivity response of changing salinity concentrations with sea-level rise. The simulation model is of hypothetical design for a 1-hectare landscape (made of 100-by-100 1-m grid cells) at the ecotone of hardwood hammock and mangrove vegetation with an assumed elevation gradient of 10 cm/km.

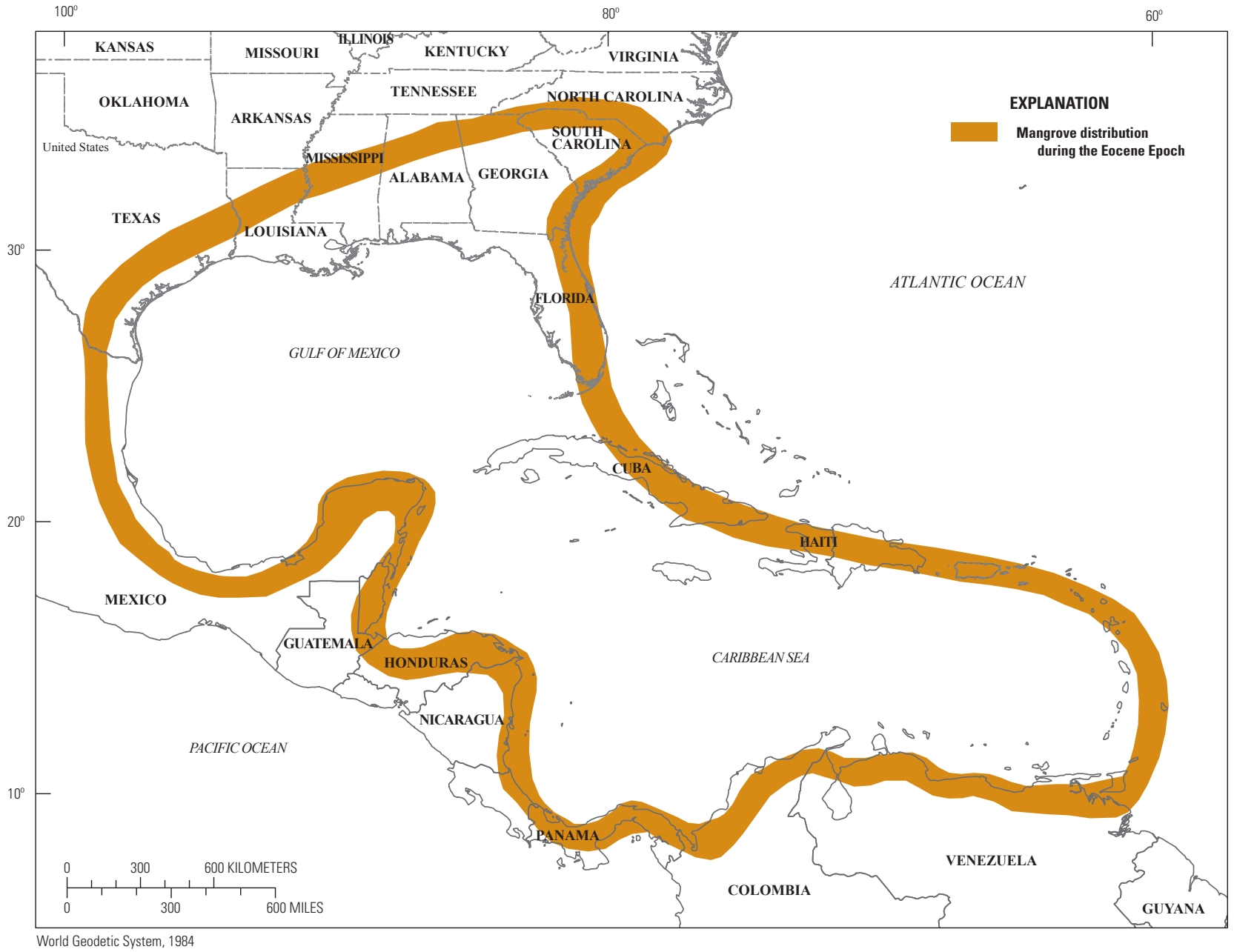

Figure 20. Eocene distribution limits of mangrove (modified from Sherrod and McMillan, 1985; used with permission).

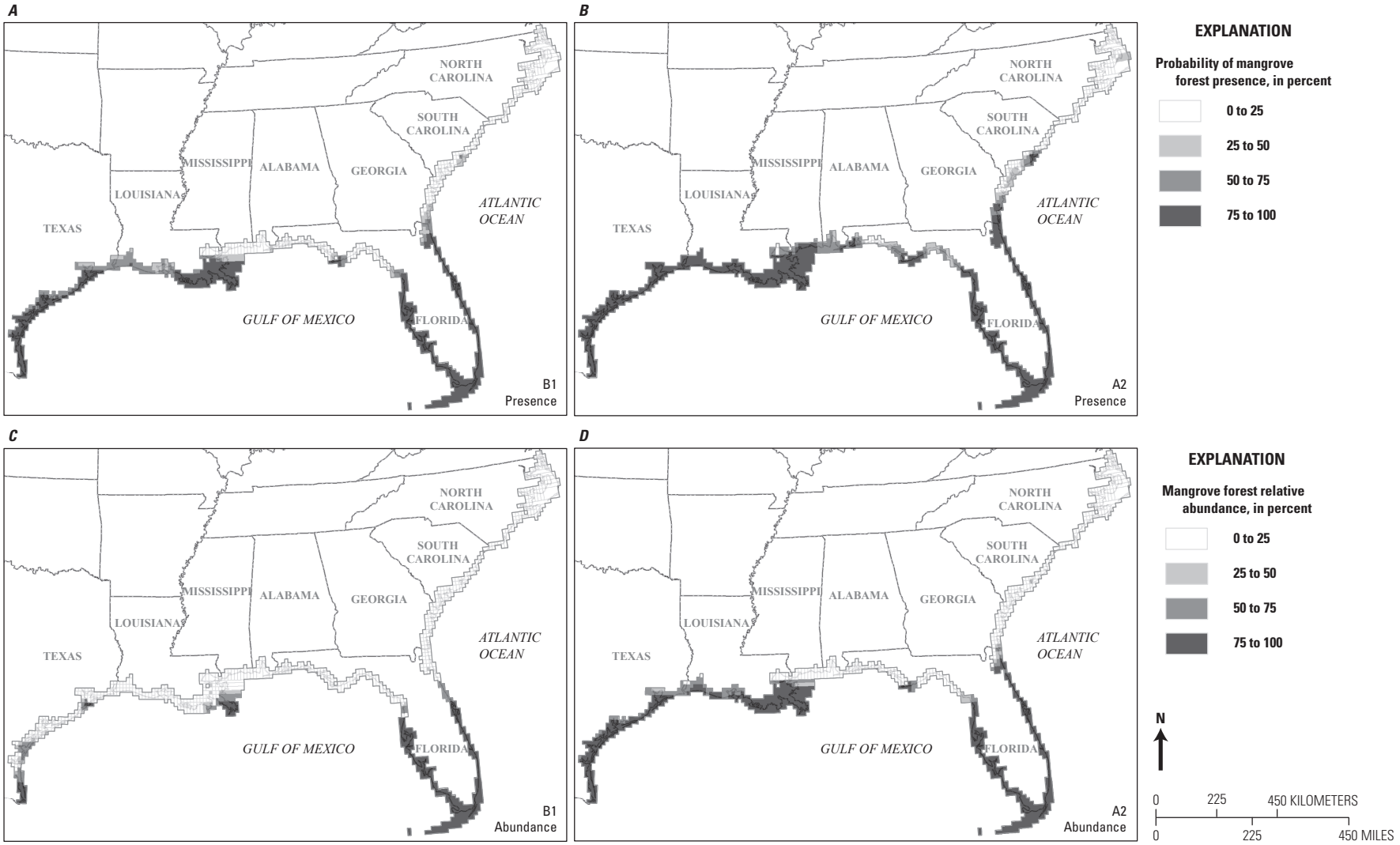

Figure 21. Climate-Envelope Mangrove Model predictions of mangrove forest presence and relative abundance under future climate scenarios (from Osland and others, 2013; used with permission). *A*, Probability of mangrove forest presence with an ensemble B1 scenario climate. *B*, Probability of mangrove forest presence with an ensemble A2 scenario climate. *C*, Mangrove forest relative abundance with an ensemble B1 scenario climate. *D*, Mangrove forest relative abundance with an ensemble A2 scenario climate.

Table 6. Attributes of select leaf to landscape ecosystem models.

[m, meter; yr, year; TM, Landsat Thematic Mapper; NWI, National Wetlands Inventory; <, less than; m^2, square meter; km^2, square kilometer; lidar, light detection and ranging; cm, centimeter]

Model	Agency/ organization	Appropriate scale	Spatial resolution	Temporal scale	Input parameters	Vegetation classification	Output parameters	Validation	Citations
Coupled Saltmarsh Biogeochemical and Demographic Model	Universidade Nova de Lisboa-Quinta Da Torre, Portugal	Local	30–300 m	Hourly time step, simulation time up to 110 yr	Elevation and bathymetry, air temperature, physiological parameters for marsh plants, TM imagery	NWI	Maps of land change, flooded areas, biomass and plant density	None	Simas and others (2001).
Hammock-Mangrove Vadose Zone Model	U.S. Geological Survey	Hypothetical landscape 100 by 100 m	1 m	Daily time step, simulation time 50 yr	Precipitation, tidal height, species-specific physiological parameters, storm surge data, hypothetical elevation	Hammock mangrove	Maps of vegetation change, salinity, vegetation density, gross productivity	Sensitivity analysis	Teh and others (2008).
Spatially Explicit Landscape Vegetation Analysis Model (SELVA)	U.S. Geological Survey, National Wetlands Research Center	Local, regional (such as <1 m^2–100,000 km^2)	100–10,000 m	Time step of 1 yr, simulation time up to 1,000 yr	Elevation maps (lidar preferred), wetland land cover (such as NWI), development footprint, sea-level rise projections, monthly tide gage records	Gap Analysis, Landsat TM imagery, NWI	Maps of areas/habitats/ forest structure/ biodiversity potentially vulnerable to inundation, hurricanes, lightning strikes, drought, hydrology (land cover and elevation maps)	Hindcast	Doyle and others (2003b); Berger and others (2008).
Mangrove Forest Growth and Succession Model (MANGRO)	U.S. Geological Survey, National Wetlands Research Center	Tree and stand level, local (such as <1 cm–100 m)	1 cm–100 m	Time step of 1 yr can be used on the basis of the sea-level rise scenario, simulation time up to 1,000 yr	Elevation maps (lidar preferred), wetland land cover (such as NWI), development footprint, climate data, hydrology, sea-level rise projections	Mangrove species, *Avicennia germinans*, *Laguncularia racemosa*, *Rhizophora mangle*	Forest composition, biomass, density and individual tree height, diameter, growth, and mortality metrics by species	Hindcast	Doyle and Girod (1997); Doyle and others (2003b); Berger and others (2008).
Spatial Relative Elevation Model (SREM)	Skagit River System cooperative, Western Washington University	Local (70 km^2)	50 m	Time step of 0.25 weeks, simulation time 400 years	Bathymetry grid, subsidence rate from SET, sea-level rise rate, net primary production and biomass functions, sediment dynamics model parameters	Eelgrass species, *Zostera marina*, *Zostera japonica*	Bathymetry, annual net aboveground primary productivity, standing stock	Hindcast	Kairis and Rybczyk (2010).
WETLANDS	U.S. Geological Survey	Local, regional, national	10–30 m	Monthly or annual time step, simulation time up to 100 yr	Monthly tide gage records, sea-level rise projections, climate data, hydrology	Landsat TM imagery, NWI	Maps of land change, habitat migration and displacement	Hindcast	Doyle and others (2003a).

The Hammock-Mangrove Vadose Zone Model simulates daily changes and diffusion of saltwater intrusion on the basis of difference calculations or infiltration rates of precipitation, evaporation, and transpiration distinguished by wetland type. Daily tide values are compared with cell elevation to determine flux additions of salinity that is subsequently diffused among neighboring cells and with soil depth based on salinity concentrations. A single 1-m grid cell can contain both hammock and mangrove species. Physiological parameters are species specific to account for species growth rates and litter production. The model was developed principally to evaluate the process of self-organization under chronic sea-level changes and acute impacts of storm surge synoptics. The model predicts species biomass and distribution spatially and temporally for exploring the process of regime shifts of species dominance.

SELVA-MANGRO Model

The near-sea-level elevation and flat slope of the protected ecosystem of The Everglades account for one of the largest contiguous tracts of mangrove forests found anywhere in the world and emphasize the potential vulnerability of coastal wetlands to rising sea level and changes in freshwater management. An L2L ecosystem model known as SELVA-MANGRO (Doyle and Girod, 1997; Doyle and others, 2003b; Berger and others, 2008) was developed for Neotropical mangrove forests by the USGS to investigate the potential impacts of climate change on the quality and distribution of future coastal wetland habitat of The Everglades. SELVA-MANGRO predicts mangrove displacement of freshwater marsh and swamp habitat with increasing tidal inundation in proportion to the rate of sea-level rise. SELVA-MANGRO represents a hierarchically integrated landscape-scale vegetation model (SELVA) spatially linked to an individual-based stand simulation model (MANGRO) (table 6) for predicting change in the structure and distribution of mangrove forests at a park, a refuge, or regional scale. Both models are spatially explicit, thereby accounting for arrangement of trees within a forest stand and stand distribution within a landscape. SELVA-MANGRO comprises multiple linked hierarchical relations at the leaf, tree, species, stand, ecosystem, and landscape level. The location of each individual tree and stand is explicitly mapped within the same coordinate system, akin to a GIS. SELVA and MANGRO represent trees and space in three-dimensional architecture of horizontal and vertical articulation. SELVA contains a regionally interpolated DEM of south Florida based on a 1-ft contour survey conducted in the 1950s (fig. 22).

SELVA tracks predicted changes in the biotic and abiotic conditions of distributed land units, including forcing functions and environmental conditions on an annual time step for the entire simulated landscape. SELVA passes necessary information of environmental change to the MANGRO model at the stand level for each and all land units in the landscape profile. MANGRO returns a system condition of stand structure and composition to SELVA as predicted for each growth season or calendar year. Composite maps are produced that exhibit the predicted changes in species composition and forest migration, loss, or gain as influenced by changes in climate, sea level, hurricane disturbance, and freshwater flow (fig. 22).

SELVA is composed of several primary data layers delineating ecosystem boundaries, land elevation, tidal range, sea level, river stage, and disturbance conditions. Classified vegetation maps of the study area are imported into SELVA from all available sources to distinguish ecosystem distribution across the simulated landscape including mangrove and non-mangrove vegetation of other habitat types, such as saltmarsh, freshmarsh, swamp forest, and upland forest. Tidal inundation and circulation are key factors controlling marsh and forest distribution. Subsidence and accretion rates are user-specified inputs that SELVA accepts to affect annual elevation change. Boundary zones of major habitat classes are used to delineate the lower and upper elevations of the intertidal zone as defined by mangrove extent relating to mean low tide and mean high tide by coastal reach. Tide gage records are used to interpolate tidal range across the land-sea interface of the study region and to define the intertidal plane.

MANGRO is an individual-based model composed of a species-specific set of biological functions predicting the growth, establishment, and death of individual trees. Species selection and function include mangrove species common to Florida and the Neotropics: *Avicennia germinans* (black mangrove), *Laguncularia racemosa* (white mangrove), and *Rhizophora mangle* (red mangrove). MANGRO includes empirically based algorithms for tolerance of each species to shade on the basis of light-response experiments and the ability of each species to regenerate and grow under flooded conditions. MANGRO predicts the tree and gap replacement process of natural forest succession as influenced by stand structure and prevailing environmental conditions (fig. 22*B*). MANGRO assigns attributes to each tree including latitude, longitude, species, stem diameter, height, crown dimensions, leaf area, and spatial position relative to neighbors (distance and azimuth). Growth of individual trees is dependent on species, stem diameter, crown size, leaf area, light availability, flooding, salinity, and competition from neighboring trees. Crown growth and structure are explicitly modeled as a function of crown space and preeminence as to which tree fills space first for a given crown height and class. Canopy structure is modeled as a three-dimensional process of crown height, width, and depth in relation to sun angle and shading by neighboring trees. Tree growth is modeled as a function of growth potential for a given tree size reduced by derived crown volume, light availability to the individual tree, and species response to shade. Tree death results from prolonged growth suppression, senescence, or disturbance by hurricane, logging, or lightning strike.

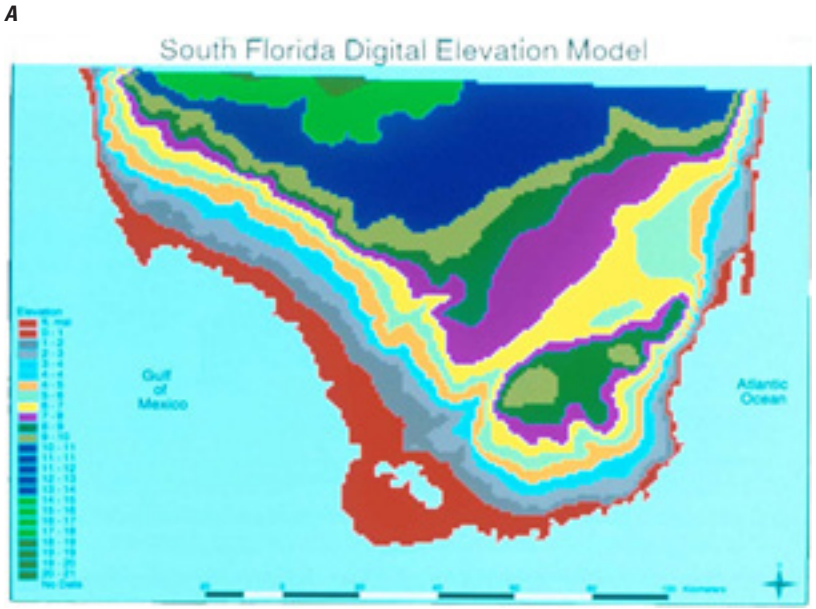

Figure 22. Screenshots showing SELVA-MANGRO model application in south Florida (from Doyle and others, 2003b; used with permission). *A*, South Florida digital elevation model. *B*, MANGRO stand simulation model. *C*, Historical mangrove distribution circa 1940. *D*, Predicted mangrove distribution under sea-level rise by 2100.

B

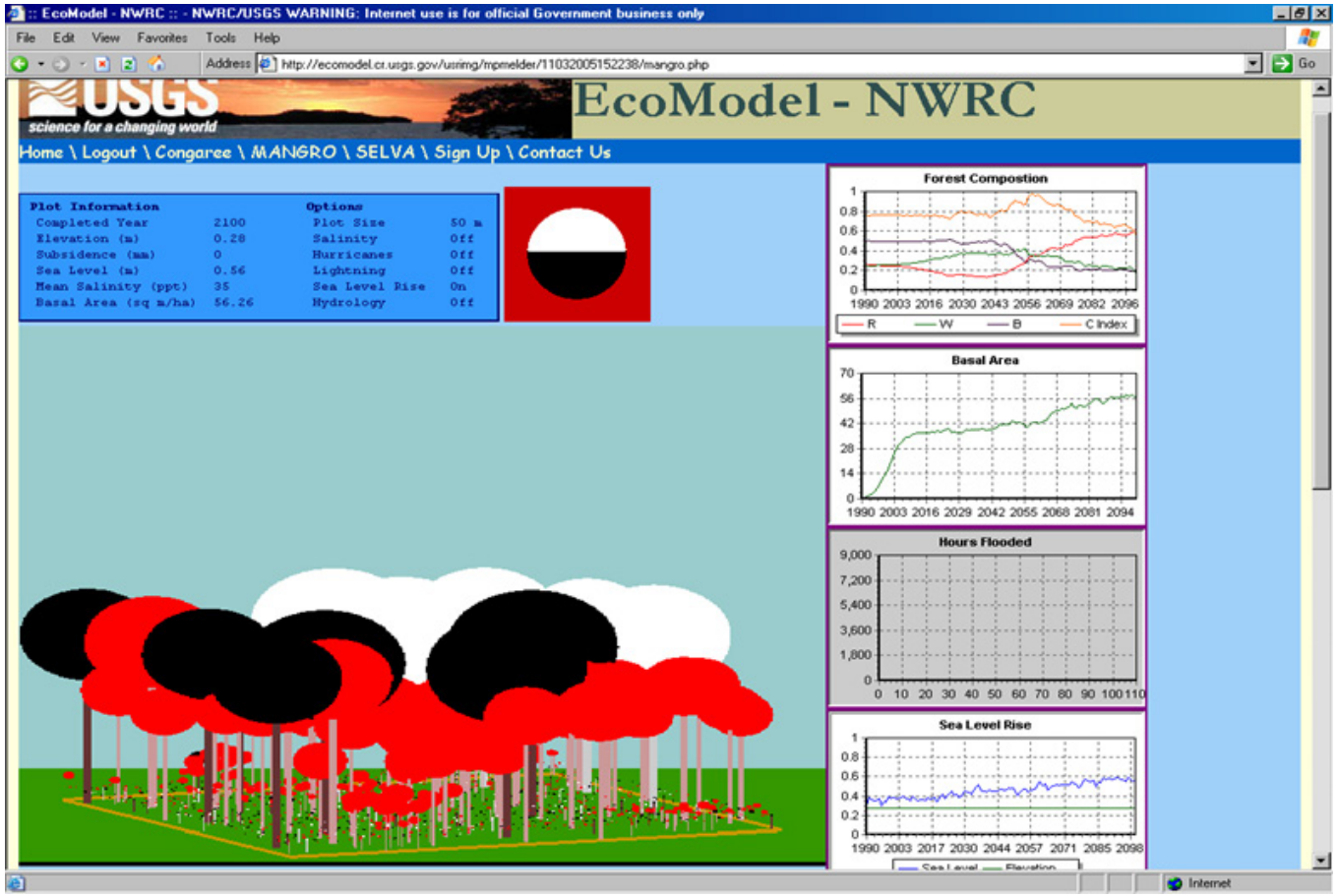

Figure 22. Screenshots showing SELVA-MANGRO model application in south Florida (from Doyle and others, 2003b; used with permission). *A*, South Florida digital elevation model. *B*, MANGRO stand simulation model. *C*, Historical mangrove distribution circa 1940. *D*, Predicted mangrove distribution under sea-level rise by 2100.—Continued

C

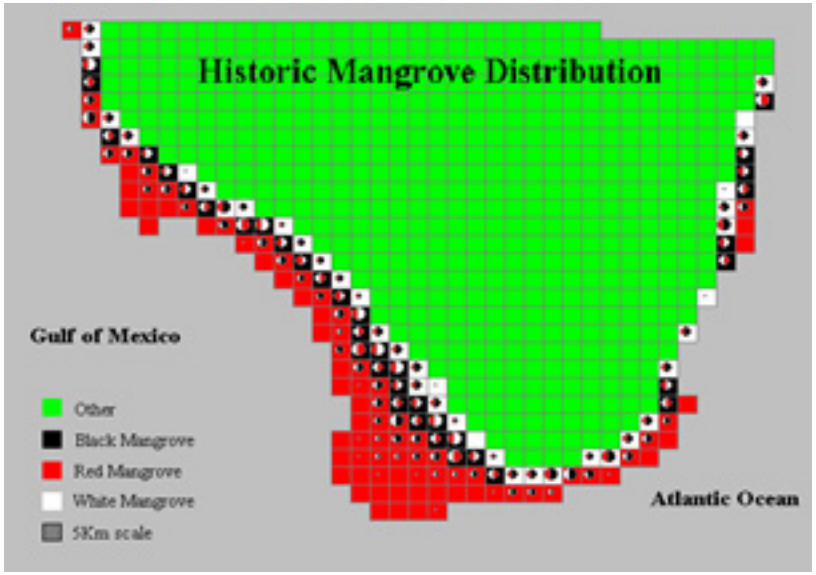

Figure 22. Screenshots showing SELVA-MANGRO model application in south Florida (from Doyle and others, 2003b; used with permission). *A*, South Florida digital elevation model. *B*, MANGRO stand simulation model. *C*, Historical mangrove distribution circa 1940. *D*, Predicted mangrove distribution under sea-level rise by 2100.—Continued

D

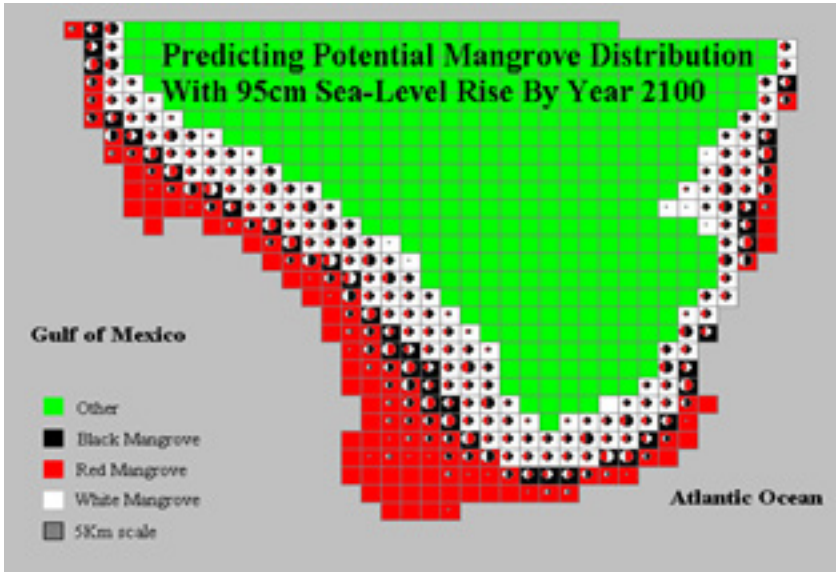

Figure 22. Screenshots showing SELVA-MANGRO model application in south Florida (from Doyle and others, 2003b; used with permission). *A*, South Florida digital elevation model. *B*, MANGRO stand simulation model. *C*, Historical mangrove distribution circa 1940. *D*, Predicted mangrove distribution under sea-level rise by 2100.—Continued

Spatial Relative Elevation Model (SREM)

Seagrass meadows are important habitats for a number of fisheries and wildlife taxa. Although aquatic, these meadows are also at risk under rising sea levels. Seagrasses exist within a restricted depth range as influenced by substrate, water quality, and most importantly, turbidity, which can limit light penetration and growth. A change in sea level, whether rise or fall, affects their distribution and survival in nearshore waters. The ability of certain species to persist or migrate with rising sea level depends on how and where sediment deposition occurs as sea level changes over time. The Spatial Relative Elevation Model (SREM) (Kairis and Rybczyk, 2010) was developed for Padilla Bay, Washington, to predict changes in bathymetry on the basis of distribution and productivity of seagrass meadows dominated by *Zostera marina* (eelgrass). SREM is a modified version of a marsh soils cohort model for coastal Louisiana adapted to consider the processes of sediment deposition affecting bathymetry of an aquatic bay system. SREM is a spatial model of Padilla Bay at a 50-m grid resolution with no interaction between neighboring cells. Each cell simulates processes of seagrass productivity, aboveground and belowground, and standing stock resulting in net changes in bay-bottom elevation. Survival is determined by discrete depth ranges, taking into account that water can be too shallow or too deep. A number of sea-level rise scenarios were applied to forecast bathymetric changes of Padilla Bay and the threat to eelgrass communities. Results show that, except for the most extreme sea-level rise projections, eelgrass communities will not diminish and may even flourish because of the proportion of shallow mud flats that will become favorable colonization sites.

WETLANDS

The WETLANDS L2L ecosystem model (Doyle and others, 2003a) predicts plant-species distribution and migration with changing land-water relations. The WETLANDS model is a USGS product that uses empirical relations of species occurrence by elevation within the tidal plane to project marsh regression or transgression with sea-level fall or rise, respectively. The model uses data from a field study that was conducted to relate plant-species distribution and ecotones to surface elevation and tidal inundation by using differential leveling surveys (fig. 23). The WETLANDS model contains functional probabilities of species tolerance to flooding conditions that dictate the rate and process of ecological succession and coastal retreat

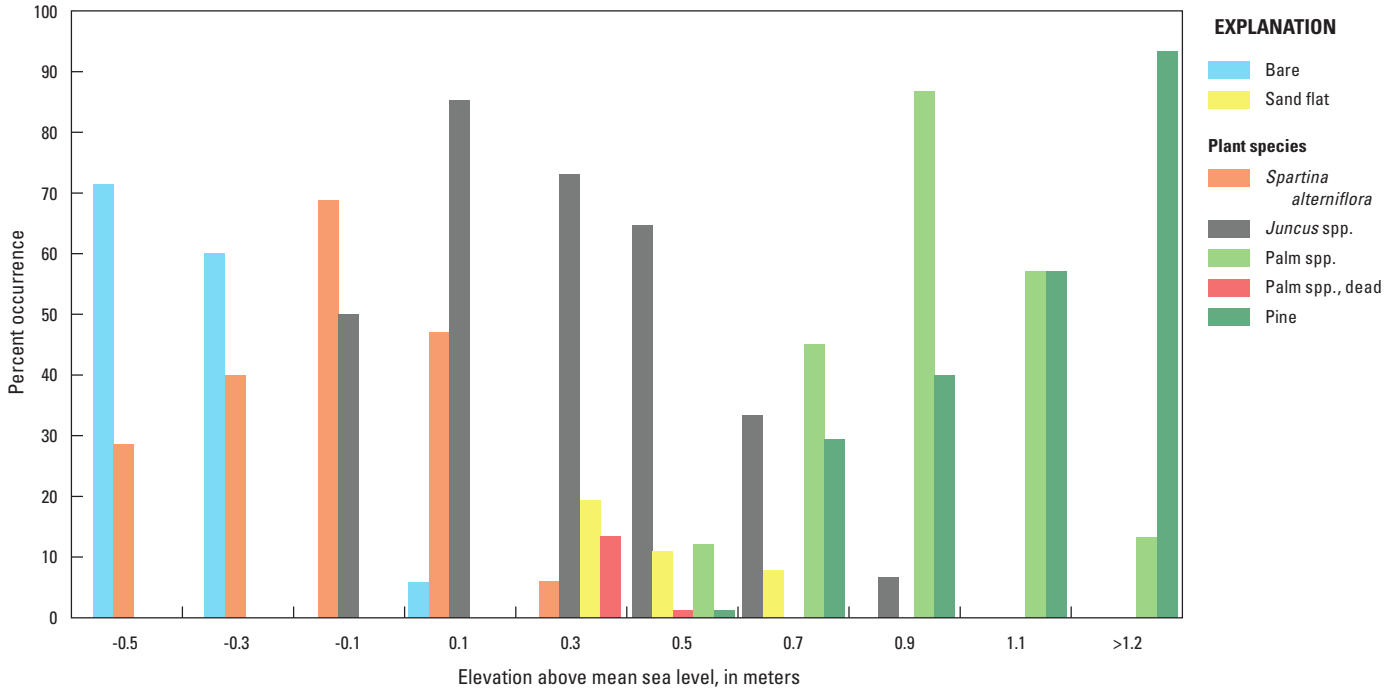

Figure 23. WETLANDS species distribution by elevation (from Doyle and others, 2003a; used with permission).

with sea-level rise. Map information of hypsography and bathymetry of the coastal zone was digitized and interpolated to construct a regional-scale DEM prior to the availability of NED and lidar datasets. Classified Landsat Thematic Mapper imagery of aquatic and terrestrial habitat at a community level was used to initialize model simulation by species and vegetation type. The WETLANDS model, assuming hydrological connectivity of adjacent open water cells, tracks the process and pattern of coastal inundation spatially and temporally. The model predicts migration of marsh habitat and transgression of coastal forest habitat as sea level moves upslope. Simulated forecasts of the tidal regime are based on mean monthly sea-level projections from regionally relevant tide gage records. The model contrasts the predicted mean sea-surface height with surface elevations of each land unit (that is, 30-m pixel) to determine flood height. Flood height is then used to predict favored habitat condition on the basis of probability functions of species and community tolerance to coastal inundation and elevation calibrated from field surveys. In years in which flood height exceeds tolerance for the prevailing species complement or habitat condition, new or updated species cover and community type are assigned to the habitat array to reflect a change in ecological succession. Model output consists of pixel counts and hectares of converted habitat (loss and gain) by calendar year.

Summary

Changes in climate during past ice ages and warming periods have affected sea levels and coastal extent as evidenced from ice, sediment, peat, and fossil records. Ancient sea-level reconstructions from multiple disciplines and techniques demonstrate worldwide consistency of high and low sea-level cycles of 120 meters (m) or more for long glaciation periods and higher and lower rates during the rise and fall segments. Current sea-level rates of more than 3 millimeters per year (mm/yr) in global ocean volume (eustasy) are moderate by historical calculations but when amplified by high rates of land subsidence may prove consequential to wetland stability and persistence on a local or regional basis. Tide gage records show that some coastal reaches are undergoing uplift from glacial rebound that accounts for an effective sea-level fall counter to the prevailing global rise of sea level elsewhere. Satellite altimetry provides a more accurate rate of global ocean volume (eustasy) exceeding 3 mm/yr for the most recent tidal epoch (1994–2012). Tide gages for the same time period generally show higher sea-level rise rates where there is active subsidence or crustal tilt. Sea-level rise rates for U.S. tide gages along the Gulf of Mexico coastline exhibit comparatively lower and higher rates in earlier tidal epochs of the 20th century, confounding any certainty of short- or long-term acceleration based on satellite observations.

In this handbook, we explain and illustrate proper evaluation of sea-level rates between satellite observations and tide gages, which requires observed records that are longer than a tidal epoch (greater than 19 years), have the same start and end dates, are seasonally balanced, have equal frequency modulation, and are complete (without data gaps). Otherwise, it is improper and problematic to contrast a sea-level rate from long-term tide gage trends with short-term satellite observations, as has been done in media and scientific reports. In effect, tide gage records and satellite observations are compatible and complementary, and there is value and need for both. Satellites account solely for the change in eustasy, whereas tide gages also capture the rate and direction of land motion (rise or fall).

No matter the degree of human or natural consequence, rising sea level is already affecting our coastal ecosystems and infrastructure to an extent that society must deal with the problems and setbacks of coastal flooding. Various Earth-climate and coastal wetland models have been developed to address the interaction and impact of changing climate and land-use from a sea-level rise perspective. Simple models utilizing coarse datasets and constructs of the behavior of natural systems may only provide limited utility and certainty suitable for instructional or educational purposes, whereas more complex models require expert development and more site-specific parameterization and validation for aiding management decisions. The dynamic nature of the components of the Earth's hydrosphere and climate that account for the net balance of ocean volumes combined with the interactive effects of rebound and tilting of continental plates, as well as differential local and regional subsidence, presents a complicated process to model easily or with certainty. Models help our understanding of these interacting processes and provide the basis for forecasting potential change useful for land management and conservation planning.

In 2012, the U.S. Geological Survey conducted more than 30 training and feedback sessions with Federal, State, and nongovernmental organization (NGO) coastal managers and planners across the northern Gulf of Mexico coast to educate and to evaluate user needs and their understanding of concepts, data, and modeling tools for projecting sea-level rise and its impact on coastal habitats and wildlife. It was our goal to introduce the non-expert to the broad spectrum of models and applications that have been used to predict or forecast environmental change and ecosystem response for sea-level rise assessments. We have compiled a fairly comprehensive treatise of the data, models, and methods from various related disciplines to offer a condensed synthesis of the science and simulation models of sea-level rise, past, present, and future. As demonstrated, the models vary greatly in design and detail, functionally and structurally, spatially and temporally, physical to biological, from leaf to landscape, and so on. It is our hope that coastal managers, engineers, and scientists will benefit from a greater understanding of the dynamics and models for projecting causes and consequences of sea-level change on the landscape and seascape.

References Cited

Allen, J.R.L., 1990, Salt-marsh growth and stratification—A numerical model with special reference to the Severn Estuary, southwest Britain: Marine Geology, v. 95, no. 2, p. 77–96.

Appleby, P.G., and Oldfield, F., 1992, Applications of lead-210 to sedimentation studies, *in* Ivanovich, M., Harmon, R.S., eds., Uranium series disequilibrium: Oxford, Clarendon Press, Applications to Earth, Marine and Environmental Sciences.

Australian Government, 2009, Climate change risks to Australia's coast—A first pass national assessment: Australian Government, Department of Climate Change.

AVISO+ Satellite Altimetry Data, 2013, Dataset: Accessed April 2013 at http://www.aviso.oceanobs.com/en/data/products/sea-surfaceheight-products/global/index.html.

Balsillie, J.H., and Donoghue, J.F., 2004, High resolution sea-level history for the Gulf of Mexico since the last glacial maximum: Tallahassee, Fla., Florida Geological Survey, Report of Investigations No. 103.

Bard, Édouard; Hamelin, Bruno; Arnold, Maurice; Montaggioni, Lucien; Cabloch, Guy; Faure, Gérard; and Rougerie, Francis, 1996, Deglacial sea-level record from Tahiti corals with the timing of global meltwater discharge: Nature, v. 382, p. 241–244.

Berger, Uta; Rivera-Monroy, V.H.; Doyle, T.W.; Dahdouh-Guebas, Farid; Duke, N.C.; Fontalvo-Herazo, M.L.; Hildenbrandth, Hanno; Koedame, Nico; Mehligi, Ulf; Pioua, Cyril; and Twilley, R.R., 2008, Advances and limitations of individual-based models to analyze and predict dynamics of mangrove forests—A review: Aquatic Botany, v. 89, no. 2, p. 260–274.

Binder, Claudia; Boumans, R.M.; and Costanza, Robert, 2003, Applying the Patuxent Landscape Unit Model to human dominated ecosystems—The case of agriculture: Ecological Modelling, v. 159, no. 2–3, p. 161–177.

Cahoon, D.R.; Lynch, J.C.; Hensel, Philippe; Boumans, Roelof; Perez, B.C.; Segura, Bradley; and Day, J.W., 2002a, High-precision measurements of wetland sediment elevation—I. Recent improvements to the sedimentation-erosion table: Journal of Sedimentary Research, v. 72, no. 5, p. 730–733.

Cahoon, D.R.; Lynch, J.C.; Perez, B.C.; Segura, Bradley; Holland, R.D.; Stelly, Carroll; Stephenson, Gary; and Hensel, Philippe, 2002b, High-precision measurements of wetland sediment elevation—II. The rod surface elevation table: Journal of Sedimentary Research, v. 72, no. 5, p. 734–739.

Clough, J.S., Park, R.A., and Fuller, Roger, 2010, SLAMM 6 beta technical documentation: Warren, Vt., Warren Pinnacle Consulting Inc.

Costanza, Robert, Sklar, F.H., and White, M.L., 1990, Modeling coastal landscape dynamics: BioScience, v. 40, no. 2, p. 91–107, doi:10.2307/1311342.

Craft, Christopher, Clough, Jonathan, Ehman, Jeff, Jove, Samantha, Park, Richard, Pennings, Steven, Guo, Hongyu, and Machmuller, Megan, 2009, Forecasting the effects of accelerated sea-level rise on tidal marsh ecosystem services: Frontiers in Ecology and the Environment, v. 7, p. 73–78.

D'Alpaos, A., Lanzoni, S., Marani, M., Fagherazzi, S., and Rinaldo, A., 2005, Tidal network ontogeny—Channel initiation and early development: Journal of Geophysical Research—Earth Surface, v. 110, no. F2, p. F02001.

DeLaune, R.D., Whitcomb, J.H., Patrick, W.H., Pardue, J.H., and Pezeshki, S.R., 1989, Accretion and canal impacts in a rapidly subsiding wetland. I.137Cs and210Pb techniques: Estuaries, v. 12, no. 4, p. 247–259.

Doyle, T.W., Day, R.H., and Biagas, J.M., 2003a, Predicting coastal retreat in the Florida Big Bend region of the Gulf Coast under climate change induced sea-level rise, *in* Ning, Z.H., Turner, R.E., Doyle, T.W., and Abdollahi, K., eds., Integrated assessment of the climate change impacts on the Gulf Coast region: Baton Rouge, La., GCRCC and LSU Graphic Services, p. 201–209.

Doyle, T.W., and Girod, G.F., 1997, The frequency and intensity of Atlantic hurricanes and their influence on the structure of south Florida mangrove communities, *in* Diaz, H.F., and Pulwarty, R.S., eds., Hurricanes: Climate and Socioeconomic Impacts—Springer Berlin Heidelberg, p. 109–120.

Doyle, T.W., Girod, G.F., and Books, M.A., 2003b, Modeling mangrove forest migration along the southwest coast of Florida under climate change, *in* Ning, Z.H., Turner, R.E., Doyle, T.W., and Abdollahi, K., eds., Integrated assessment of the climate change impacts on the Gulf Coast region: Baton Rouge, La., GCRCC and LSU Graphic Services, p. 211–222.

Doyle, T.W., Krauss, K.W., Conner, W.H., and From, A.S., 2010, Predicting the retreat and migration of tidal forests along the northern Gulf of Mexico under sea-level rise: Forest Ecology and Management, v. 259, no. 4, p. 770–777.

Edwards, R.L., Beck, J.W., Gurr, G.S., Donahue, D.J., Chappell, J.M.A., Bloom, A.L., Druffel, E.R.M., and Taylor, F.W., 1993, A large drop in atmospheric $^{14}C/^{12}C$ and reduced melting in the Younger Dryas documented ^{236}Th ages of corals: Science, v. 260, p. 962–968.

Fagherazzi, S., Kirwan, M.L., Mudd, S.M., Guntenspergen, G.R., Temmerman, S., D'Alpaos, A., van de Koppel, J., Rybczyk, J.M., Reyes, E., Craft, C., and Clough, J., 2012, Numerical models of salt marsh evolution: Ecological, geomorphic, and climatic factors—Reviews of Geophysics, v. 50, no. 1, p. RG1002.

Fagherazzi, S., and Sun, T., 2004, A stochastic model for the formation of channel networks in tidal marshes: Geophysical Research Letters, v. 31, no. 21, p. L21503.

Fairbanks, R.G., 1989, A 17,000-year glacio-eustatic sea-level record—Influence of glacial melting rates on the Younger Dryas event and deep-ocean circulation: Nature, v. 342, p. 637–642.

Fairbanks, R.G., 1990, The age and origin of the "Younger Dryas climate event" in Greenland ice cores: Paleoceanography, v. 5, p. 937–948.

Forest Inventory and Analysis, 2015, The Forest Inventory and Analysis Database—Database description and user guide version 6.0.1 for Phase 2: U.S. Department of Agriculture Forest Service, 748 p., accessed February 2015 at http://www.fia.fs.fed.us/library/database-documentation/.

French, J.R., 1993, Numerical simulation of vertical marsh growth and adjustment to accelerated sea-level rise, North Norfolk, U.K.: Earth Surface Processes and Landforms, v. 18, no. 1, p. 63–81.

Galbraith, Hector, Jones, Richard, Park, R.A., Clough, J.S., Herrod-Julius, Susan, Harrington, Brian, and Page, Gary, 2002, Global climate change and sea level rise—Potential losses of intertidal habitat for shorebirds: Waterbirds, v. 25, no. 2, p. 173–183.

Galbraith, Hector, Jones, Richard, Park, R.A., Clough, J.S., Herrod-Julius, Susan, Harrington, Brian, and Page, Gary, 2003, Global climate change and sea level rise—Potential losses of intertidal habitat for shorebirds, *in* Valette-Silver, N.J., Scavia, D., eds., Ecological forecasting—New tools for coastal and marine ecosystem management: Silver Spring, Md., National Oceanic and Atmospheric Administration, p. 19–22.

Geselbracht, Laura, Freeman, Kathleen, Kelly, Eugene, Gordon, D.R., and Putz, F.E., 2011, Retrospective and prospective model simulations of sea level rise impacts on Gulf of Mexico coastal marshes and forests in Waccasassa Bay, Florida: Climatic Change, v. 107, p. 35–57.

Gutierrez, B.T., Plant, N.G., and Thieler, E.R., 2011, A Bayesian network to predict coastal vulnerability to sea level rise: Journal of Geophysical Research—Earth Surface, v. 116, no. F2, F02009.

Haq, Bilal, Hardenbol, U.J., and Vail, P.R., 1987, Chronology of fluctuating sea levels since the Triassic: Science, v. 235, p. 1156–1167.

Imbrie, J.Z., Imbrie-Moore, Annabel, and Lisiecki, L.E., 2011, A phase-space model for Pleistocene ice volume: Earth and Planetary Science Letters, v. 307, p. 94–102.

Intergovernmental Panel on Climate Change (IPCC), 2001, Climate change 2001—Synthesis report, a contribution of working groups I, II, and III to the third assessment report of the Intergovernmental Panel on Climate Change [Watson, R.T., and the Core Writing Team, eds.]: Cambridge, United Kingdom, and New York, N.Y., Cambridge University Press, 398 p.

Intergovernmental Panel on Climate Change (IPCC), 2007, Climate change 2007—Synthesis report, contribution of working groups I, II and III, *in* Pachauri, R.K., and Reisinger, A., eds., Fourth assessment report of the Intergovernmental Panel on Climate Change Core Writing Team: Geneva, Switzerland, IPCC, 104 p.

Kairis, P.A., and Rybczyk, J.M., 2010, Sea level rise and eelgrass (*Zostera marina*) production—A spatially explicit relative elevation model for Padilla Bay, WA: Ecological Modelling, v. 221, no. 7, p. 1005–1016.

Kasmarek, M.C., Johnson, M.R., and Ramage, J.K., 2014, Water-level altitudes 2014 and water-level changes in the Chicot, Evangeline, and Jasper aquifers and compaction 1973–2013 in the Chicot and Evangeline aquifers, Houston-Galveston region, Texas: U.S. Geological Survey Scientific Investigations Map 3308, pamphlet, 16 sheets, scale 1:100,000, accessed October 2014 at http://dx.doi.org/10.3133/sim3308.

Keim, B.D., Doyle, T.W., Burkett, V.R., Van Heerden, Ivor, Binselam, S.A., Wehner, M.F., Tebaldi, Claudia, Houston, T.G., and Beagan, D.M., 2008, How is the Gulf Coast climate changing?, *in* Savonis, M.J., Burkett, V.R., and Potter, J.R., eds., Impacts of climate change and variability on transportation systems and infrastructure—Gulf Coast study, phase I.: A Report by the U.S. Climate Change Science Program and the Subcommittee on Global Change Research: Washington, D.C., Department of Transportation.

Kirwan, M.L., and Mudd, S.M., 2012, Response of salt-marsh carbon accumulation to climate change: Nature, v. 489, no. 7417, p. 550–553.

Kirwan, M.L., and Murray, A.B., 2007, A coupled geomorphic and ecological model of tidal marsh evolution: Proceedings of the National Academy of Sciences, v. 104, no. 15, p. 6118–6122.

Kominz, M.A., Browning, J.V., Miller, K.G., Sugarman, P.J., Mizintseva, Svetlana, and Scotese, C.R., 2008, Late Cretaceous to Miocene sea-level estimates from the New Jersey and Delaware coastal plain coreholes—An error analysis: Basin Research, v. 20, no. 2, p. 211–226.

Krauss, K.W., Cahoon, D.R., Allen, J.A., Ewel, K.C., Lynch, J.C., and Cormier, N., 2010, Surface elevation change and susceptibility of different mangrove zones to sea-level rise on Pacific high islands of Micronesia: Ecosystems, v. 13, no. 1, p. 129–143.

Lisiecki, L.E., and Raymo, M.E., 2005, A Pliocene-Pleistocene stack of 57 globally distributed benthic $\delta^{18}O$ records: Paleoceanography, v. 20, no. 1.

Marcy, Douglas; Brooks, William; Draganov, Kyle; Hadley, Brian; Haynes, Chris; Herold, Nate; McCombs, John; Pendleton, Matt; Ryan, Sean; Schmid, Keil; Sutherland, Mike; and Waters, Kirk, 2011, New mapping tool and techniques for visualizing sea level rise and coastal flooding impacts, *in* Wallendorf, L.A., Jones, Chris, Ewing, Lesley, and Battalio, Bob, eds., Proceedings of the 2011 solutions to coastal disasters conference, Anchorage, Alaska, June 26 to June 29, 2011: Reston, Va., American Society of Civil Engineers, p. 474–490.

Martin, J.F.; White, M.L.; Reyes, Enrique; Kemp, G.P.; Mashriqui, Hassan; and Day, J.W., Jr., 2000, Profile—Evaluation of coastal management plans with a spatial model—Mississippi Delta, Louisiana, USA: Environmental Management, v. 26, no. 2, p. 117–129.

Melillo, J.M., Richmond, T.C., and Yohe, G.W., eds., 2014, Climate change impacts in the United States—The Third National Climate Assessment: U.S. Global Change Research Program, 841 p., doi:10.7930/J0Z31WJ2.

Miller, K.G., Mountain, G.S., Wright, J.D., and Browning, J.V., 2011, A 180-million-year record of sea level and ice volume variations from continental margin and deep-sea isotopic records: Oceanography, v. 24, no. 2, p. 40–53, doi:10.5670/oceanog.2011.26.

Morris, J.T., 1995, The mass balance of salt and water in intertidal sediments—Results from North Inlet, South Carolina: Estuaries, v. 18, no. 4, p. 556–567.

Mudd, S.M., Howell, S.M., and Morris, J.T., 2009, Impact of dynamic feedbacks between sedimentation, sea-level rise, and biomass production on near-surface marsh stratigraphy and carbon accumulation: Estuarine, Coastal and Shelf Science, v. 82, no. 3, p. 377–389.

National Aeronautics and Space Administration (NASA) Goddard Space Flight Center (GSFC), 2013, Integrated multi-mission ocean altimeter data for climate research complete time series version 2: PO.DAAC, Calif., USA, dataset accessed November 18, 2013, at http://dx.doi.org/10.5067/ALTTS-TJ122.

National Oceanic and Atmospheric Administration (NOAA), 2013, Sea level trends: National Oceanic and Atmospheric Administration Tides and Currents dataset, accessed August 2013 at http://tidesandcurrents.noaa.gov/sltrends/sltrends.html.

National Oceanic and Atmospheric Administration (NOAA), 2014, Water levels: National Oceanic and Atmospheric Administration Tides and Currents dataset, accessed March 2014 at http://tidesandcurrents.noaa.gov/stations.html?type=Water+Levels.

National Oceanic and Atmospheric Administration (NOAA) National Ocean Service (NOS), 2010, Technical considerations for use of geospatial data in sea level change mapping and assessment: Silver Spring, Md., NOAA NOS Technical Report.

National Wildlife Federation (NWF), 2006, An unfavorable tide—Global warming, coastal habitats and sportfishing in Florida: Florida Wildlife Federation, National Wildlife Federation.

Osland, M.J., Enwright, Nicholas, Day, R.H., and Doyle, T.W., 2013, Winter climate change and coastal wetland foundation species—Salt marshes vs. mangrove forests in the southeastern United States: Global Change Biology, v. 19, no. 5, p. 1482–1494.

Overpeck, J.T., and Weiss, J.L., 2009, Projections of future sea level becoming more dire: Proceedings of the National Academy of Sciences of the United States of America, v. 106, p. 21461–21462.

Park, R.A., Treehan, M.S., Mausel, P.W., and Howe, R.C., 1989, The effects of sea level rise on U.S. coastal wetlands, *in* Smith, J.B., Tirpak, D.A., eds., The potential effects of global climate change on the United States: Washington, D.C., U.S. Environmental Protection Agency, p. 1–55.

Petit, Jean-Robert, Jouzel, Jean, Raynaud, Dominique, Barkov, N.I., Barnola, Jean-Marc, Basile, Isabelle, Bender, M.L., Chappellaz, J.A., Davis, M.D., Delaygue, Gilles, Delmotte, M.M., Kotiyakov, V.M., Legrand, M.R., Lipenkov, V.Y., Lorius, Claude, Pépin, Laurence, Ritz, Catherine, Saltzman, E.S., and Stievenard, Michel, 1999, Climate and atmospheric history of the past 420,000 years from the Vostok ice core, Antarctica: Nature, v. 399, no. 6735, p. 429–436.

Rahmstorf, Stefan, 2007, A semi-empirical approach to projecting future sea-level rise: Science, v. 315, no. 5810, p. 368–370.

Reyes, Enrique, Martin, J.F., Day, J.W., Kemp, G.P., and Mashriqui, Hassan, 2004, River forcing at work—Ecological modeling of prograding and regressive deltas: Wetlands Ecology and Management, v. 12, no. 2, p. 103–114.

Reyes, Enrique, White, M.L., Martin, J.F., Kemp, G.P., Day, J.W., and Aravamuthan, Vibhas, 2000, Landscape modeling of coastal habitat change in the Mississippi Delta: Ecology, v. 81, no. 8, p. 2331–2349.

Rogers, K., Saintilan, N., and Copeland, C., 2012, Modelling wetland surface elevation dynamics and its application to forecasting the effects of sea-level rise on estuarine wetlands: Ecological Modelling, v. 244, p. 148–157.

Rybczyk, J.M., Callaway, J.C., and Day, J.W., Jr., 1998, A relative elevation model for a subsiding coastal forested wetland receiving wastewater effluent: Ecological Modelling, v. 112, no. 1, p. 23–44.

Sherrod, C.L., and McMillan, C., 1985, The distributional history and ecology of mangrove vegetation along the northern Gulf of Mexico coastal region: Contributions in Marine Science, v. 28, p. 129–140.

Siddall, Mark, Rohling, E.J., Almogi-Labin, A., Hemleben, Christoph, Meischner, Dieter, Schmetzer, Ina, and Smeed, D.A., 2003, Sea-level fluctuations during the last glacial cycle: Nature, v. 423, p. 853–858.

Simas, T.C., Nunes, J.P., and Ferreira, J.G., 2001, Effects of global climate change on coastal salt marshes: Ecological Modelling, v. 139, no. 1, p. 1–15, doi:10.1016/S0304-3800(01)00226-5.

Sklar, F.H., White, M.L., and Costanza, Robert, 1991, The coastal ecological landscape spatial simulation (CELSS) model—Users' guide and results for the Atchafalaya-Terrebonne study area: U.S. Fish and Wildlife Service, National Wetlands Research Center.

Strauss, B.H., Ziemlinski, Remik, Weiss, J.L., and Overpeck, J.T., 2012, Tidally adjusted estimates of topographic vulnerability to sea level rise and flooding for the contiguous United States: Environmental Research Letters, v. 7, no. 1.

Tebaldi, Claudia, Strauss, B.H., and Zervas, C.E., 2012, Modelling sea level rise impacts on storm surges along U.S. coasts: Environmental Research Letters, v. 7, no. 1.

Teh, Su Yean, DeAngelis, D.L., da Silveira Lobo Sternberg, Leonel, Miralles-Wilhelm, F.R., Smith, T.J., and Koh, Hock-Lye, 2008, A simulation model for projecting changes in salinity concentrations and species dominance in the coastal margin habitats of the Everglades: Ecological Modelling, v. 213, no. 2, p. 245–256.

Turner, E.R., Milan, C.S., and Swenson, E.M., 2006, Recent volumetric changes in salt marsh soils: Estuarine, Coastal and Shelf Science, v. 69, no. 3–4, p. 352–359.

Usery, E.L., Choi, Jinmu, and Finn, M.P., 2010, Modeling sea-level rise and surge in low-lying urban areas using spatial data, geographic information systems, and animation methods, *in* Showalter, P.S., and Lu, Y., eds., Geospatial techniques in urban hazard and disaster analysis: Netherlands, Springer, Geotechnologies and the Environment, p. 11–30.

U.S. Fish and Wildlife Service, 2012, Application of the Sea-Level Affecting Marshes Model (SLAMM 6) to St. Marks NWR: U.S. Fish and Wildlife Service, 52 p. [Also available at http://catalog.data.gov/dataset/application-of-the-sea-level-affecting-marshes-model-slamm-6-to-st-marks-nwr.]

Voinov, Alexey; Costanza, Robert; Maxwell, Thomas; and Vladich, Helena, 2007, Patuxent Landscape Model—4. Model application: Water Resources, v. 34, no. 5, p. 501–510.

Voinov, Alexey; Costanza, Robert; Wainger, Lisa; Boumans, Roelof; Villa, Ferdinando; Maxwell, Thomas; and Voinov, Helena, 1999, Patuxent Landscape Model—Integrated ecological economic modeling of a watershed: Environmental Modelling & Software, v. 14, no. 5, p. 473–491.

Wang, Hongqing, Hsieh, Y.P., Harwell, M.A., and Huang, Wenrui, 2007, Modeling soil salinity distribution along topographic gradients in tidal salt marshes in Atlantic and Gulf Coastal regions: Ecological Modelling, v. 201, no. 3–4, p. 429–439, doi:10.1016/j.ecolmodel.2006.10.013.

Warrick, R.A., 2006, Climate change impacts and adaptation in the Pacific—Recent breakthroughs in concept and practice, *in* Chapman, R., Boston, J., and Schwass, M., eds., Confronting climate change—Critical issues for New Zealand: Wellington, New Zealand, Victoria University Press.

Warrick, R.A., and Cox, G., 2007, New developments of SimCLIM software tools for risk-based assessments of climate change impacts and adaptation in the water resource sector, *in* Heinonen, M., ed., Proceedings of the Third International Conference on Climate and Water: Helsinki, Finland, Finish Environmental Institute (SYKE), p. 518–524.

Weiss, J.L., Overpeck, J.T., and Strauss, B.H., 2011, Implications of recent sea level rise science for low-elevation areas in coastal cities of the conterminous U.S.A.: Climatic Change, v. 105, no. 3–4, p. 635–645.

Appendixes

Appendix 1. Effect of Steric Temperature Functions on Ocean Volume

The change in seawater volume for a given change in temperature can be calculated from the change in the water density (ρ, in kilograms per cubic meter [kg/m^3]). If the water pressure is constant, the water density depends on the practical salinity (S, in parts per thousand [ppt]) and temperature (t, in degrees Celsius [°C]).

Seawater density is given by the following formula, according to Fofonoff and Millard (1983):

$$\rho\,(S, t, 0) = \rho_w + (b_0 + b_1 t + b_2 t^2 + b_3 t^3 + b_4 t^4)S + (c_0 + c_1 t + c_2 t^2)S^{3/2} + d_0 S^2 \quad (1)$$

where

ρ_w = density of reference pure water,
b_0 = $+8.24493 * 10^{-1}$,
b_1 = $-4.0899 * 10^{-3}$,
b_2 = $+7.6438 * 10^{-5}$,
b_3 = $-8.2467 * 10^{-7}$,
b_4 = $+5.3875 * 10^{-9}$,
c_0 = $-5.72466 * 10^{-3}$,
c_1 = $+1.0227 * 10^{-4}$,
c_2 = $-1.6546 * 10^{-6}$, and
d_0 = $+4.8314 * 10^{-4}$.

The density of the reference pure water is given by the following formula:

$$\rho_w = a_0 + a_1 t + a_2 t^2 + a_3 t^3 + a_4 t^4 + a_5 t^5 \quad (2)$$

where

a_0 = +999.842594,
a_1 = $+6.793952 * 10^{-2}$,
a_2 = $-9.095290 * 10^{-3}$,
a_3 = $+1.001685 * 10^{-4}$,
a_4 = $-1.120083 * 10^{-6}$, and
a_5 = $+6.536332 * 10^{-9}$.

The formulas have been implemented as MATLAB code by James Manning (http://globec.whoi.edu/globec-dir/sigmat-calc-matlab.html) and Python code by Bjørn Ådlandsvik (http://www.imr.no/~bjorn/python/seawater/index.html). The two implementations are based on the SeaWater library (http://www.cmar.csiro.au/datacentre/ext_docs/seawater.htm) of EOS-80 seawater properties (Millero and others, 1980). For example, if the reference column of water is 100 centimeters (cm) (1 meter) in height at 0 °C and 35 ppt salinity, the height of the column (proportional to the water volume) changes with the temperature and the salinity as presented in table 1–1 (computed with Python code).

If the seawater pressure is a variable, then similar polynomial formulas containing 26 coefficients (Fofonoff and Millard, 1983) are added to the above formulas to compute the water density for a given temperature, salinity, and pressure.

The SeaWater library of EOS-80 seawater properties has been superseded by the Gibbs SeaWater (GSW) Oceanographic Toolbox of the International Thermodynamic Equation of Seawater 2010 (TEOS-10; http://www.teos-10.org/). The density of seawater in the GSW toolbox is given by a formula involving 48 coefficients (IOC, SCOR, and IAPSO, 2010). The values in table 1–1 remain the same under the new equations.

Table 1–1. Height of water column at different temperatures and salinities.

[cm, centimeter]

Temperature, in degrees Celsius	Height of water column	
	Salinity, in parts per thousand	
	0	35
0	102.827 cm	100.000 cm
34	103.392 cm	100.765 cm

References Cited

Fofonoff, N.P., and Millard, R.C., Jr., 1983, Algorithms for computation of fundamental properties of seawater: UNESCO Technical Papers in Marine Science, no. 44, 53 p.

IOC, SCOR, and IAPSO, 2010, The international thermodynamic equation of seawater—2010—Calculation and use of thermodynamic properties: Intergovernmental Oceanographic Commission, Manuals and Guides, no. 56, UNESCO (English), 196 p.

Millero, F.J., Chen, Chen-Tung, Bradshaw, Alvin, and Schleicher, Karl, 1980, A new high pressure equation of state for seawater: Deep-Sea Research, v. 27A, p. 255–264.

Appendix 2. Published Sea-Level Trends for U.S. Tide Gages

Table 2–1. Published sea-level trends for U.S. tide gages.

[Measurements are in millimeters per century; -, value not available]

Station identification	City, port, State	Start year	End year				
			1972 (Hicks and Crosby, 1974)	1986 (Lyles and others, 1988)	Up to 1999 (Flick and others, 2003)	1999 (Zervas, 2001)	2006 (Zervas, 2009)
	East Coast, United States						
8410140	Eastport, Maine	1929	360	270	224	212	200
8413320	Bar Harbor, Maine	1947	-	270	219	218	204
8418150	Portland, Maine	1912	230	220	194	191	182
8419870	Seavey Island, Maine	1926	-	180	-	175	176
	Portsmouth, N.H.	-	242	-	169	-	-
8443970	Boston, Mass.	1921	289	290	269	265	263
	Sandwich, Mass.	-	-	-	80	-	-
8447930	Woods Hole, Mass.	1932	346	271	262	259	261
	Buzzards Bay, Mass.	-	117	-	-	-	-
8449130	Nantucket, Mass.	1965	-	-	315	300	295
8452660	Newport, R.I.	1930	304	270	255	257	258
8454000	Providence, R.I.	1938	237	180	217	188	195
8461490	New London, Conn.	1938	263	210	208	213	225
8467150	Bridgeport, Conn.	1964	-	210	244	258	256
8510560	Montauk, N.Y.	1947	231	190	248	258	278
8514560	Port Jefferson, N.Y.	1957	362	270	215	244	244
8516945	Kings Point, N.Y.	1931	-	240	243	241	235
	New Rochelle, N.Y.	-	310	60	-57	54	-
8518750	The Battery, N.Y.	1856	287	270	319	277	277
8531680	Sandy Hook, N.J.	1932	492	410	397	388	390
8534720	Atlantic City, N.J.	1911	390	390	415	398	399
8536110	Cape May, N.J.	1965	-	-	365	388	406
8545240	Philadelphia, Pa.	1900	267	260	-	275	279
8557380	Reedy Point, Del.	1919	-	-	-	-	346
8551910	Lewes, Del.	1956	354	310	304	316	320
8570283	Ocean City, Md.	1975	-	-	-	-	548
8571892	Cambridge, Md.	1943	-	-	-	352	348
8573927	Chesapeake City, Md.	1972	-	-	-	-	378
8574680	Baltimore, Md.	1902	339	320	313	312	308
8575512	Annapolis, Md.	1928	423	360	374	353	344
8577330	Solomons, Md.	1937	387	330	-	329	341
8594900	Washington, D.C.	1924	328	320	308	313	316
8632200	Kiptopeke, Va.	1951	-	-	367	359	348
8635150	Colonial Beach, Va.	1972	-	-	-	527	478

Table 2–1. Published sea-level trends for U.S. tide gages.—Continued

[Measurements are in millimeters per century; -, value not available]

Station identification	City, port, State	Start year	End year				
			1972 (Hicks and Crosby, 1974)	1986 (Lyles and others, 1988)	Up to 1999 (Flick and others, 2003)	1999 (Zervas, 2001)	2006 (Zervas, 2009)
East Coast, United States—Continued							
8635750	Lewisetta, Va.	1974	-	-	-	485	497
8637624	Gloucester Point, Va.	1950	-	-	-	395	381
8638610	Sewells Point, Va.	1927	-	-	-	442	444
	Hampton Roads, Va.	-	463	430	435	-	-
8638660	Portsmouth, Va.	1935	381	370	-	376	376
8638863	Bridge Tunnel, Va.	1975	-	-	744	701	605
8652587	Oregon Inlet, N.C.	1977	-	-	-	-	282
8656483	Beaufort, N.C.	1953	-	-	-	371	257
8658120	Wilmington, N.C.	1935	-	-	201	222	208
8659084	Southport, N.C.	1933	-	-	-	-	207
8661070	Springmaid Pier, S.C.	1957	-	-	-	517	409
8665530	Charleston, S.C.	1921	361	340	318	328	315
8670870	Fort Pulaski, Ga.	1935	265	300	297	305	298
8720030	Fernandina, Fla.	1897	184	190	216	204	202
8720218	Mayport, Fla.	1928	269	220	234	243	240
8721120	Daytona Beach, Fla.	1925	-	-	-	-	232
8723170	Miami Beach, Fla.	1931	250	230	218	239	239
8723970	Vaca Key, Fla.	1971	-	-	227	258	278
Atlantic Caribbean							
2695540	Bermuda	1932	-	-	-	183	204
9731158	Guantanamo, Cuba	1937	-	-	285	164	164
9751401	Lime Tree Bay, Virgin Islands	1977	-	-	-	-	174
9751639	Charlotte Amalie, Virgin Islands	1975	-	-	-	50	120
9755371	San Juan, Puerto Rico	1962	-	-	152	143	165
9759110	Mayagues, Puerto Rico	1955	-	-	-	124	135
	Cristobal, Panama	-	124	-	-	-	-
Gulf Coast, United States							
8724580	Key West, Fla.	1913	210	220	192	227	224
8725110	Naples, Fla.	1965	-	-	133	208	202
8725520	Fort Myers, Fla.	1965	-	-	-	229	-
8726520	St. Petersburg, Fla.	1947	-	230	239	240	236
8726724	Clearwater Beach, Fla.	1973	-	-	269	276	243
8727520	Cedar Key, Fla.	1914	204	190	137	187	180
8728690	Apalachicola, Fla.	1967	-	-	-	153	138
8729108	Panama City, Fla.	1973	-	-	-	30	75
8729840	Pensacola, Fla.	1923	236	240	214	214	210
8735180	Dauphin Island, Ala.	1966	-	-	-	293	298

Table 2–1. Published sea-level trends for U.S. tide gages.—Continued

[Measurements are in millimeters per century; -, value not available]

Station identification	City, port, State	Start year	End year				
			1972 (Hicks and Crosby, 1974)	1986 (Lyles and others, 1988)	Up to 1999 (Flick and others, 2003)	1999 (Zervas, 2001)	2006 (Zervas, 2009)
			Gulf Coast, United States—Continued				
8761724	Grand Isle, La.	1947	-	1,050	-	985	924
8764311	Eugene Island, La.	1939	921	970	-	974	965
8770570	Sabine Pass, Tex.	1958	-	1,320	-	654	566
8771450	Galveston Pleasure Pier, Tex.	1908	-	640	653	739	684
8771510	Galveston Pier 21, Tex.	1957	595	750	708	650	639
8772440	Freeport, Tex.	1954	-	1,400	1,099	587	435
8774770	Rockport, Tex.	1948	-	400	564	460	516
8778490	Port Mansfield, Tex.	1963	-	-	-213	205	193
8779751	Padre Island, Tex.	1958	-	510	-	344	348
8779770	Port Isabel, Tex.	1944	-	310	327	338	364
			West Coast, United States				
9410170	San Diego, Calif.	1906	199	210	231	215	206
9410230	La Jolla, Calif.	1924	191	200	229	222	207
9410580	Newport Beach, Calif.	1955	-	190	-	222	222
9410660	Los Angeles, Calif.	1923	66	80	91	84	83
9410840	Santa Monica, Calif.	1933	-	180	161	159	146
9411270	Rincon Island, Calif.	1962	-	-	-	322	322
9411340	Santa Barbara, Calif.	1973	-	-	-	277	125
9412110	Port San Luis, Calif.	1945	-	120	196	90	79
9413450	Monterey, Calif.	1973	-	-	302	186	134
9414290	San Francisco, Calif.	1854	197	130	145	141	201
9414290	San Francisco, Calif.	1906	-	-	-	213	-
9414523	Redwood City, Calif.	1974	-	-	-	-	206
9414750	Alameda, Calif.	1939	45	100	81	89	82
9415020	Point Reyes, Calif.	1975	-	-	405	251	210
9415144	Port Chicago, Calif.	1976	-	-	727	-	208
9418767	North Spit, Calif.	1977	-	-	-	-	473
9419750	Crescent City, Calif.	1933	-49	-60	-50	-48	-65
9431647	Port Orford, Ore.	1977	-	-	-	-	18
9432780	Charleston, Ore.	1970	-	-	207	174	129
9435380	South Beach, Ore.	1967	-	-	369	351	272
9437540	Garibaldi, Ore.	1970	-	-	-	-	198
9439040	Astoria, Ore.	1925	5	-30	6	-16	-31
9440910	Toke Point, Wash.	1973	-	-	-	282	160
9443090	Neah Bay, Wash.	1934	-86	-110	-103	-141	-163
9444090	Port Angeles, Wash.	1975	-	-	-	149	19
9444900	Port Townsend, Wash.	1972	-	-	-	282	198

Table 2–1. Published sea-level trends for U.S. tide gages.—Continued

[Measurements are in millimeters per century; -, value not available]

Station identification	City, port, State	Start year	End year				
			1972 (Hicks and Crosby, 1974)	1986 (Lyles and others, 1988)	Up to 1999 (Flick and others, 2003)	1999 (Zervas, 2001)	2006 (Zervas, 2009)
West Coast, United States—Continued							
9447130	Seattle, Wash.	1898	193	200	212	211	206
9449424	Cherry Point, Wash.	1973	-	-	189	139	82
9449880	Friday Harbor, Wash.	1934	115	140	138	124	113
9450460	Ketchikan, Alaska	1919	0.3	-10	-4	-11	-19
9451600	Sitka, Alaska	1924	-231	-220	-211	-217	-205
9452210	Juneau, Alaska	1936	-1,346	-1,240	-1,248	-1,269	-1,292
9452400	Skagway, Alaska	1944	-	-1,730	-1,636	-1,668	-1,712
9453220	Yakutat, Alaska	1940	-533	-460	-552	-575	-1,154
9454050	Cordova, Alaska	1964	-		706	697	257
9454240	Valdez, Alaska	2006	-	-	5	-34	-492
9455090	Seward, Alaska	1925	-	-	2,069	-146	-174
9455500	Seldovia, Alaska	1964	-	-820	-997	-993	-945
9455760	Nikiski, Alaska	1973	-	-	-	-1,071	-98
9455920	Anchorage, Alaska	1972	-	-	381	276	88
9457292	Kodiak Island, Alaska	1949	-	-	-	-1,208	-1,042
9459450	Sand Point, Alaska	1972	-	-	108	7	92
9461380	Adak Island, Alaska	1943	-	0	-60	-263	-275
9462620	Unalaska, Alaska	1957	-	-710	-565	-644	-572
Pacific Islands							
1611400	Nāwiliwili, Hawaii	1955	-	200	162	153	153
1612340	Honolulu, Hawaii	1905	156	160	129	150	150
1612480	Mokuoloe, Hawaii	1957	-	360	-	112	131
1615680	Kahului, Hawaii	1947	-	-	234	209	232
1617760	Hilo, Hawaii	1927	-	-	340	336	327
1619000	Johnston Atoll	1947	-	40	55	68	75
1619910	Midway Atoll	1947	-	-60	8	9	70
1630000	Guam, Marianas Islands	1948	-	-120	-36	10	845
1770000	Pago Pago, American Samoa	1948	-	150	199	148	207
1820000	Kwajalein, Marshall Islands	1946	-	100	87	105	143
1840000	State of Chuuk, Caroline Islands	1947	-	100	-	68	60
1890000	Wake Island	1950	-	80	155	189	191

References Cited

Flick, R.E., Murray, J.F, and Ewing, L.C., 2003, Trends in United States tidal datum statistics and tide range: Journal of Waterway, Port, Coastal, and Ocean Engineering, v. 129, no. 4, p. 155–164.

Hicks, S.D., and Crosby, J.E., 1974, Trends and variability of yearly mean sea level, 1893–1972: Rockville, Md., National Ocean Survey, National Oceanic and Atmospheric Administration.

Lyles, S.D., Hickman, L.E., and Debaugh, H.A., 1988, Sea-level variations for the United States 1855–1986: Rockville, Md., U.S. Department of Commerce.

Zervas, Chris, 2001, Sea level variations of the United States 1854–1999: National Oceanic and Atmospheric Administration Technical Report NOS CO-OPS 36.

Zervas, Chris, 2009, Sea level variations of the United States 1854–2006: National Oceanic and Atmospheric Administration Technical Report NOS CO-OPS 53.

Appendix 3. Elevation and Vegetation Data Sources for Sea-Level Rise Modeling

The recent advent of geospatial software, digital modes of cartographical referencing, and remote sensing applications has greatly expanded the scope of data visualization and spatial modeling critical to the study and analysis of Earth-climate systems and sea-level rise. Fundamental to the process of assessing the impact of rising sea levels on a natural or cultural feature, park or refuge, ecosystem or species range, or coastline or continent is knowing where you are and whether you are above or below a past, present, or future waterline. Geographic information systems (GIS) and the Global Positioning System (GPS) are common tools on the job, in the home, or on mobile phones and are useful for placing oneself or any physical or natural feature in time and space. Most sea-level rise analyses or applications have some spatial context and depend on geospatial data sources and software to make assessments and predictions. Fundamental geospatial data inputs include model boundaries or study area; land, water, or feature elevations; and cover type, usually vegetation, species, ecosystem, or cultural. This appendix provides a basic overview of commonly used geospatial datasets of sea-level rise models and an evaluation of data utility for sea-level vulnerability assessments.

Topography and bathymetry are key parameters of the process and consequence of coastal change based on elevation above or below past, present, or future sea level. Relating the surface elevation of the terrestrial to the marine environment requires a compatible reference datum with respect to sea surface (such as mean high water [MHW] or mean higher high water [MHHW]). Historically, the records and datums for land and water have been collected and referenced differently in orthometric and tidal datums that are not directly comparable without rectification or transformation from one to the other. Depending on the date, age, and process of data gathering, the records also may be of different orthometric and tidal datums of different eras, thereby requiring additional rectification to match modern datums. The subject of datum transformations is critically important but beyond the scope of this handbook except to educate potential users and modelers of the need to rectify all data sources and elevations into a compatible format and the same reference plane.

The choices of digital data for surface elevations and habitat type are becoming increasingly diverse and are generally improving in detail, spatial resolution, and accuracy. In this appendix, we describe various public-domain topographic and bathymetric data products of global, national, and regional significance that have been or can be used for sea-level rise modeling. Important considerations are addressed regarding the data source, spatial resolution, temporal period, and the data vertical and horizontal accuracies (table 3–1). Evaluations of the different data sources are contrasted to describe the utility and limitations of the data for coastal change analysis. Widespread and readily available elevation sources discussed herein include Shuttle Radar Topography Mission (SRTM) data, various versions of the National Elevation Dataset (NED) (for example, NED 1 arc-second, NED 1/3 arc-second, and NED 1/9 arc-second), and mission-based light detection and ranging (lidar) data collections, photogrammetry, and topographic surveys.

Digital Elevation Models

A digital elevation model (DEM) is defined as an electronic file or database containing elevation points over a contiguous area. The data files are generally raster-based grids or vector-based triangular irregular networks (TINs). On the basis of models we have reviewed, raster-based DEMs are more prevalent in sea-level rise models; TINs are common in more advanced engineering applications involving elevation analyses and are beyond the scope of this handbook. Two types of DEMs are digital surface models (DSMs) and digital terrain models (DTMs). DSMs are models that contain the elevations of all features found on the surface of the Earth, including vegetation, buildings, or other structures. DTMs represent elevation data of bare-earth only and are more commonly used for sea-level rise modeling applications. Each data product is specified to the particular datum on which it is based or referenced (horizontal and vertical, as previously described).

Shuttle Radar Topography Mission (SRTM)

The SRTM (Bamler, 1999; Farr and others, 2007) was a collaborative mission by the National Aeronautics and Space Administration (NASA), the National Imagery and Mapping Agency (NIMA), the German Space Agency (DLR), and the Italian Space Agency (ASI) to collect synthetic aperture radar data from two radar antennas on an 11-day mission in February 2000 for more than 80 percent of the Earth's surface. Differences in data received from the two radar antennas were analyzed to estimate surface topography.

SRTM data are available in two spatial resolutions: 3 arc-seconds (approximately 90 meters [m]) globally and 1 arc-second (approximately 30 m) for the United States and its territories. Rodríguez and others (2005, 2006) assessed SRTM errors globally. For North America, more than 90 percent of errors were within 12.6 m for absolute horizontal accuracy, 9 m for absolute vertical accuracy, and 7 m for relative height accuracy. The errors were roughly consistent globally. The vertical datum for SRTM data is the World Geodetic System 1984 (WGS 84) ellipsoid. It is important to note that SRTM elevation data do not always map the ground surface because radar cannot penetrate dense tree canopy or can be reflected off man-made structures or objects. The elevation

Table 3–1. Sources, attributes, and accuracies of publicly available digital elevation models.

[RMSE, root mean square error; lidar, light detection and ranging]

Elevation dataset	Source(s)	Spatial resolution, in meters	Time period(s)	Horizontal accuracy, in meters	Vertical accuracy, in meters
Shuttle Radar Topography Mission (SRTM)	Satellite-based radar data collection	30; 90	February 2000	12.6	9 Relative: 7
National Elevation Dataset (NED) 1 arc-second	Stereo photogrammetry and linear interpolation of cartographic contours	30	1925–present	Variable on the basis of source data	2.44 RMSE Relative (average): 1.64
NED1/3 arc-second	Simple linear interpolation of cartographic contours, digital photogrammetry, and polynomial interpolation of lidar data	10	Variable on the basis of source data; typically 1960s–present	Variable on the basis of source data	Variable on the basis of source data
NED 1/9 arc-second	Polynomial interpolation of lidar data and digital photogrammetry	3.3	Variable on the basis of source data; typically 2000s–present	Variable on the basis of source data	Variable on the basis of source data
Photogrammetry	Overlapping aerial photography	Variable on the basis of mission specifications	Variable on the basis of mission specifications	Variable on the basis of mission specifications	Variable on the basis of mission specifications
Lidar	Aerial lidar collection	Variable by mission specifications; typically 3–5	Variable on the basis of mission specifications; typically 2000s–present	Variable on the basis of mission specifications; typically submeter	Variable on the basis of mission specifications; typically submeter
Topographic survey	Field data collection	Spot elevations	Variable	Typically several centimeters	Typically several centimeters

data from SRTM, therefore, can be considered more of a DSM than a "bare-earth" DEM. There are multiple versions of the SRTM data. Version 1, released in 2003, is considered "research grade" data and should be avoided for sea-level rise applications for several reasons, including the following: (1) these data are unedited and may contain areas with no data or anomalous data, (2) coastlines are typically not well delineated, and (3) these data have not been evaluated for conformance with National Mapping Accuracy Standards. Version 2.0, also known as the SRTM finished data, was released in 2005 and contains edits to fill voids and to better delineate coastlines and water bodies, specifically oceans, lakes, and rivers. Version 2.1 was released in 2009 and had a low filter (3×3) applied to clean remaining voids from version 2.0 data. Version 2.1 is available for only SRTM 3-arc-second (approximately 90-m) data. The accuracy associated with SRTM is notable considering the scale of a near global mapping effort; however, these data are not recommended for local, regional, or national sea-level rise modeling.

National Elevation Dataset (NED)

NED (Gesch and others, 2002) is a seamless DEM produced by the U.S. Geological Survey (USGS) for the entire United States and its territories. NED is a dynamic dataset that is continually updated as new elevation data, particularly lidar data, become available. NED data are referenced to a 1-by-1 degree latitude/longitude index. NED products are available at various spatial resolutions. NED 1 arc-second is a DEM product with a spatial resolution of 30 m, whereas NED 1/3 arc-second and NED 1/9 arc-second are interpolated at finer resolutions of 10 m and 3.3 m, respectively. The vertical datum for these products is the North American Vertical Datum of 1988 (NAVD 88). NED source data vary by DEM product and by geographic area. NED 1-arc-second data are created by using stereophotogrammetry of aerial photographs and linear interpolation of cartographic contours. NED 1/3-arc-second and 1/9-arc-second data are resampled with different degrees and combinations

of simple linear interpolation of cartographic contours, digital photogrammetry, and polynomial interpolation of lidar data. The accuracy of these NED products is variable depending on the actual data sources used by geographic location. The absolute vertical accuracy of the NED 1-arc-second DEM products was assessed by using control points from the National Geodetic Survey (NGS) and has been found to have a root mean square error (RMSE) of 2.44-m horizontal accuracy and 1.64-m vertical accuracy. Although this accuracy assessment provides a useful baseline, it was conducted by using about 13,000 control points for the entire conterminous United States. If possible, a separate assessment is recommended for more localized accuracy estimates for any NED product. Accuracy assessment is particularly important for NED 1/3-arc-second and NED 1/9-arc-second data, for which there is not a reported accuracy. Another way to determine the vertical accuracy is to investigate the vertical accuracy of the source data. To check availability of NED products, updates, methods and source data, and currency of data, visit the USGS National Elevation Dataset Viewer (http://viewer.nationalmap.gov/viewer/?p=ned).

Light Detection and Ranging (Lidar)

In 1960, the first optical laser was developed by Hughes Aircraft, Inc. (the technology is similar to sonar and can gage distance below), and shortly thereafter, early lidar technology was used to develop topographic profiles (Jensen, 2007). Modern lidar system surface elevation data are generated by firing a laser beam from an airplane-based instrument and recording the time increment required for the beam return. Elevations are calculated on the basis of the time it takes for the laser beam to bounce from the surface and return to the aircraft, the position of which is recorded by highly accurate GPS. Lidar data provide both horizontal positions in planimetric geographic coordinates (x,y) and vertical (or elevation) coordinates (z).

Lidar sensors can receive one or more returns from one pulse of light. If multiple returns exist for a sample area, then the first return is considered the elevation of the first object that the light contacts, and the last return is often some point below the first return and sometimes considered to be bare earth. Raw data (often received as files in LASer file format [.las]) contain all returns. DSMs can be created from lidar data containing first returns (that is, tree canopy and structures). Lidar products are commonly available in raw format (as .las files) containing all returns and as lidar-derived products (for example, DEMs or contour maps) that have undergone advanced postprocessing to ensure that elevations represent bare earth.

There are two main types of lidar systems. Terrestrial lidar systems fire laser pulses that have a spectral resolution of near-infrared (0.75–1.4 micrometers [μm]). Near-infrared light is absorbed by water and therefore may not record elevations below the surface of the water. Bathymetric lidar systems use a laser-visible, green band length in addition to the infrared band length. The return pulse of the infrared laser indicates the surface of the water body, and the return pulse of the green laser indicates the bottom of the water body (Fowler, 2001).

Lidar data availability in the United States is increasing. Although much of the lidar data available are topographic lidar data collected for mapping floodplains, some bathymetric lidar data are available for coastal areas. Lidar data are obtained on a mission-by-mission basis by agencies and organizations such as Federal agencies (for example, the USGS, National Oceanic and Atmospheric Administration [NOAA], and U.S. Army Corps of Engineers) or State and local governments (for example, county or city governments). The spatial resolution, accuracy, and temporal resolution, therefore, vary by dataset. Generally, the spatial resolution of lidar-based DEMs is less than 5 m, and the reported horizontal and vertical accuracies are highly accurate and are 0.25 m or less. For information pertaining to the spatial resolution and horizontal and vertical accuracies of individual products, check the metadata that accompany the product, contact the vendor, or contact the entity that provided the data.

Lidar data have limitations in areas with dense canopy or vegetative cover. Generally, if one is standing under dense tree canopy and cannot see the sky, then it is unlikely that a laser pulse will strike the ground there. Accuracy estimates are reported over the entire mission area, which can be large and include a large number of different land covers. It is recommended, therefore, that if possible the lidar data and related products are assessed locally for relevant accuracy estimates for the area of interest in any modeling effort. Recently, easy to use portals such as the United States Interagency Elevation Inventory and the NOAA Coastal Lidar Portal have been developed to view and obtain readily available lidar data.

Bathymetric Data

Seafloor topographic data are often combined with terrestrial DEMs (see section “Digital Elevation Models”) to create a DEM that extends above and below the water surface (that is, a topobathy DEM). Multiple sources of bathymetry data exist, including NOAA nautical charts radar, marine geophysical trackline surveys, multibeam sound navigation and ranging (sonar) surveys, bathymetric lidar, and satellite altimetry. The NOAA National Geophysical Data Center has an extensive archive of bathymetric data collected by various sources and methods. For some areas, NOAA National Geophysical Data Center has created DEMs containing topography and ocean bathymetry for coastal areas. Bathymetric data sources can be found in the United States Interagency Elevation Inventory. Bathymetric data were collected during the SRTM; however, the data (known as SRTM Plus) have a coarser resolution (that is, 1.85-km resolution) than do the SRTM topographic data. A few considerations for selecting bathymetric data include the objective(s) of the sea-level rise application, the extent of the study area, and the scale and limitations of the existing data used (that is, topographic elevation data, land cover data).

Topographic Survey

Topographic surveys conducted with a total station or GPS equipment may be available for certain localized areas along a coast or within managed lands where a topographic survey may have been conducted. These data may be used to enhance an existing DEM, but because of the time-consuming nature and cost of these surveys, they would rarely be done at a scale large enough for a sea-level rise modeling effort.

Vertical Accuracy and Uncertainty

Vertical accuracy of elevation data is one of the most critical elements in sea-level rise applications. The National Standard for Spatial Data Accuracy (NSSDA) uses the RMSE to estimate the linear error with a 95-percent confidence level by multiplying the RMSE by 1.96. As previously mentioned, uncertainty can present critical limitations to sea-level rise applications, particularly regarding modeling a sea-level rise rate (such as 50 cm by 2100) for relatively small time steps (such as 2040, 2060, 2080, and 2100) (Gesch, 2013). Elevation data with the lowest amount of uncertainty (that is, highest vertical accuracy), therefore, should be used for modeling inundation associated with sea-level rise.

Land Cover Data

Numerous sources of land cover data may be available for any given area where one may want to conduct sea-level rise modeling. In this section, we introduce and discuss a few widespread and readily available land cover sources. We identify where these datasets may be obtained and sources of supplementary information. Important considerations regarding land cover data include the classes mapped (that is, vegetation types, habitats), scale of source data, spatial resolution of the data, temporal period of the data, minimum mapping unit (that is, area of the smallest features mapped), and the accuracy of the land cover dataset (table 3–2).

Classification Systems

Classification systems provide standards for a land cover mapping product in regards to classes and the definitions of classes. A few common classification systems include Anderson Level I and II (Anderson and others, 1976), the classification of wetlands and deepwater habitats (Cowardin and others, 1979), and NatureServe's Terrestrial Ecological Systems (http://www.natureserve.org/library/usEcologicalsystems.pdf). The objectives and focus of the sea-level rise application should determine the level of detail in a classification system required.

Methodology for Commonly Used Land Cover Data

There are numerous land cover products that are available throughout the conterminous United States. The methodology used to create these land cover datasets can be lumped into two different categories: (1) photointerpretation of aerial photography (for example, U.S. Fish and Wildlife Service National Wetlands Inventory [NWI] and Florida Land Use, Cover, and Forms Classification System [FLUCCS]) and (2) image classification from automated and manual classification of satellite imagery (for example, National Land Cover Dataset [NLCD] and NOAA Coastal Change Analysis Program [C-CAP]).

Photointerpretation Land Cover Classifications

Photointerpretation is a manual process that typically involves mapping features in a highly detailed manner by using expert opinion, aerial photography, and ancillary data. Features are delineated by using heads-up digitizing (that is, manual digitizing by tracing over features displayed on a computer monitor) or created by using a more robust vectorization of imagery (that is, segmentation by using image properties such as spectral bands, texture, and hue) and then are assigned a class in a classification system via photointerpretation. Some examples of photointerpretation land cover maps include the NWI, some State land cover mapping efforts, particularly FLUCCS, and localized habitat maps (for example, park maps and maps developed by ecologists of habitat for managed lands). By using the Cowardin and others (1979) classification system, NWI maps not only differentiate a wide spectrum of wetland types but also classify wetland water regime (for example, saturated, seasonally flooded, permanently flooded) and in some cases apply special modifiers to wetlands to indicate special characteristics of the wetland (for example, presence of mangroves, salinity concentration). The date and scale of photography used for NWI maps vary by area. In some cases, the NWI has been updated recently, and in other cases, the NWI may be from the 1980s or earlier. If NWI is incorporated into a sea-level rise application, it is important therefore to assess the date and scale of source imagery for NWI maps available for the study area (http://www.fws.gov/wetlands/data/mapper.HTML). The spatial resolution of these classifications makes them better suited for more localized sea-level rise applications.

Satellite-Imagery-Based Land Cover Classifications

Many of the other land cover classifications that are widely available are created from automated or manual classification of satellite-based imagery with a moderate spatial resolution of 5–30 m. In most cases, these types of classifications tend to be less detailed than those created with photointerpretation of aerial photography. Satellite-imagery-based classifications include NLCD, NOAA C-CAP land cover, National Gap

Table 3–2. Landcover class descriptions, data attributes, and sources for publicly available datasets.

[<, less than; %, percent; ft, foot; m, meter; TM,Thematic Mapper; ETM+, Enhanced Thematic Mapper Plus; m^2, square meter; NOAA, National Oceanic and Atmospheric Administration; GAP, National Gap Analysis Program]

Land cover/ vegetation dataset	Source(s)	Spatial resolution, in meters	Temporal period	Minimum mapping unit	Classification system	Accuracy (overall thematic accuracy unless specified otherwise)[1]
National Wetlands Inventory	Aerial photography at various scales (<1:40,000, 1:40,000, 1:50,000, and 1:80,000)	Vector data (such as polygons)	1970s–present; varies by geography	1 acre	(Cowardin and others, 1979)	Thematic: 90% features at 95% Positional: 33 ft/10 m
Localized habitat maps	Variable (such as aerial photographs and field data collection/survey)	Variable	Variable	Variable	Variable	Variable
State landcover classification (such as Florida Land Use, Cover, and Forms Classification System [FLUCCS] or Texas Ecological Classification Systems)	Varies by dataset (such as aerial photography, Landsat TM/ ETM+ Imagery)	Varies by dataset; Florida: Vector data Texas: 10	Varies by dataset; Florida[2]: 2000s Texas: 2005–07	Varies by dataset; Florida[2]: 2 acres Texas: 1 hectare (about 2.5 acres)	Variable; Florida and Texas: NatureServe's Terrestrial Ecological Systems	Varies by dataset
National Land Cover Dataset (NLCD)	Landsat 5 TM and Landsat 7 ETM+	30	1992, 2001, 2006, 2011	4,500 m^2 (1.11 acre)	Modified Anderson (Anderson and others, 1976)	1992: 80% 2001: 79% 2006: 78%
NOAA Coastal Change Analysis Program	Landsat 5 TM	30	1996, 2001, 2006, 2011	3,600 m^2 (1 acre)	Modified Anderson (Anderson and others, 1976) with increased number of wetland classes	85% Varies by geography and date
GAP	Landsat 7 ETM+	30	1999–2001	Varies by geography	NatureServe's Terrestrial Ecological Systems	Varies by geography
LANDFIRE Existing Vegetation Cover	Landsat 7 ETM+	30	2008	Not specified	NatureServe's Terrestrial Ecological Systems	Eastern United States: 63% Western United States: 40%
Commission for Environmental Cooperation North America Land Cover	Moderate Resolution Imaging Spectroradiometer (MODIS)	250	2005	Not specified	Modified Anderson (Anderson and others, 1976)	59%

[1]Reported accuracy assessments are for a sampled area within data or maps. Actual accuracy may vary by geography within dataset.

[2]May vary by water management district.

Analysis Program (GAP), LANDFIRE Existing Vegetation Cover, and the Commission for Environmental Cooperation North America Land Cover (table 3–2). C-CAP land cover was developed for coastal areas of the United States with a goal of increasing the level of detail at which coastal wetlands were mapped in the NLCD. Table 3–3 contains a comparison between Anderson Level I (Anderson and others, 1976), NLCD, and C-CAP classification systems for wetlands, open water, and barren land classes. Similarly, GAP and LANDFIRE Existing Vegetation Cover are classified by using NatureServe's Terrestrial Ecological Systems and contain many more wetland classes common in the southeastern region of the United States (for example, bottomland forests, pondshore, peat swamp, seepage fen). It is important to note that GAP data are mapped at a State and regional level by different agency offices and personnel; therefore, the accuracy and quality of data may vary.

Table 3–3. Comparison among Anderson Level I, National Land Cover Database (NLCD), and National Oceanic and Atmospheric Administration (NOAA) Coastal Change Analysis Program (C-CAP) classification systems.

Anderson Level 1[1]	NLCD category	C-CAP category
Wetlands	Woody wetlands	Palustrine forested wetlands. Palustrine scrub shrub wetlands. Estuarine forested wetlands. Estuarine scrub shrub wetlands.
	Emergent herbaceous wetlands	Palustrine emergent wetlands. Estuarine emergent wetlands.
Open water	Open water	Open water. Palustrine aquatic bed. Estuarine aquatic bed.
Barren land	Barren land	Unconsolidated shore. Barren land.

[1]Anderson and others (1976).

References Cited

Anderson, J.A., Hardy, E.E., Roach, J.T., and Witmer, R.E., 1976, A land use and land cover classification system for use with remote sensor data: Washington D.C., U.S. Geological Survey Professional Paper 964. [Also available at http://landcover.usgs.gov/pdf/anderson.pdf.]

Bamler, Richard, 1999, The SRTM mission—A world-wide 30 m resolution DEM from SAR interferometry in 11 days: Photogrammetric Week, p. 145–154.

Cowardin, L.M., Carter, Virginia, Golet, F.C., and LaRoe, E.T., 1979, Classification of wetlands and deepwater habitats of the United States (FWS/OBS–79/31): Washington, D.C., U.S. Fish and Wildlife Service.

Farr, T.G., Rosen, P.A., Caro, Edward; Crippen, Robert; Duren, Riley; Hensley, Scott; Kobrick, Michael; Paller, Mimi; Rodriguez, Ernesto; Roth, Ladislav; Seal, David; Shaffer, Scott; Shimada, Joanne; Umland, Jeffrey; Werner, Marian; Oskin, Michael; Burbank, Douglas; and Alsdorf, D.E., 2007, The shuttle radar topography mission: Reviews of Geophysics, v. 45, doi:10.1029/2005RG000183.

Fowler, R.A., 2001, Topographic lidar, chap. 7 *of* Digital elevation model technologies and applications—The DEM users manual (1st ed.): Bethesda, Md., American Society for Photogrammetry and Remote Sensing, p. 207–236.

Gesch, D.B., 2013, Consideration of vertical uncertainty in elevation-based sea-level rise assessments—Mobile Bay, Alabama case study: Journal of Coastal Research, v. 63, p. 197–210.

Gesch, D.B., Oimoen, Michael, Greenlee, Susan, Nelson, Charles, Steuck, Michael, and Tyler, Dean, 2002, The National Elevation Dataset: Photogrammetric Engineering & Remote Sensing, v. 68, no. 1, p. 5–11.

Jensen, J.R., 2007, Remote sensing of the environment—An Earth resource perspective: Upper Saddle River, N.J., Pearson Prentice Hall.

Rodríguez, Ernesto, Morris, C.S., and Belz, J.E., 2006, A global assessment of the SRTM performance: Photogrammetric Engineering & Remote Sensing, v. 72, p. 249–260.

Rodríguez, Ernesto, Morris, C.S., Belz, J.E., Chapin, E.C., Martin, J.M., Daffer, W., and Hensley, Scott, 2005, An assessment of the SRTM topographic products: Pasadena, Calif., Jet Propulsion Laboratory, Technical Report JPL D–31639, 143 p.

Appendix 4. Recommended Reading

Alley, R.B., 2002, The two-mile time machine—Ice cores, abrupt climate change, and our future: Princeton University Press.

Arkema, K.K., Guannel, Greg; Verutes, Gregory; Wood, S.A.; Guerry, Anne; Ruckelshaus, Mary; Kareiva, Peter; Lacayo, Martin; and Silver, J.M., 2013, Coastal habitats shield people and property from sea-level rise and storms: Nature Climate Change, v. 3, p. 913–918.

Barry, R.G., and Chorley, R.J., 1998, Atmosphere—Weather and climate: London, Routledge.

Bassinot, F.C., Labeyrie, L.D., Vincent, Edith, Quidelleur, Xavier, Shackleton, N.J., and Lancelot, Yves, 1994, The astronomical theory of climate and the age of the Brunhes-Matuyama magnetic reversal: Earth and Planetary Science Letters, v. 126, no. 1, p. 91–108.

Berger, A.L., 1978, Long-term variations of caloric insolation resulting from the Earth's orbital elements: Quaternary Research 9, no. 2, p. 139–167.

Berner, R.A., 1999, A new look at the long-term carbon cycle: GSA Today, v. 9, no. 11, p. 1–6.

Bradley, R.S., 1999, Paleoclimatology—Reconstructing climates of the Quaternary: San Diego, Calif., Harcourt Academic Press, International Geophysics Series, v. 64.

Bradley, R.S., and Jones, P.D., 1992, Climate since A.D. 1500: Chapman Hall.

Bradley, R.S., Mann, M.E., and Hughes, M.K., 1999, Northern hemisphere temperatures during the past millennium—Inferences, uncertainties, and limitations: Geophysical Research Letters, v. 26, no. 6, p. 759–762.

Cox, P.M., Betts, R.A., Jones, C.D., Spall, S.A., and Totterdell, I.J., 2000, Acceleration of global warming due to carbon-cycle feedbacks in a coupled climate model: Nature, v. 408, no. 6809, p. 184–187, doi:10.1038/35041539.

Crowley, T.J., 1992, North Atlantic deep water cools the southern hemisphere: Paleoceanography, v. 7, no. 4, p. 489–497.

Davis, R.A., 2011, Sea-level change in the Gulf of Mexico: Texas A&M University Press.

Douglas, B.C., Kearney, M.S., and Leatherman, S.P., eds., 2001, Sea level rise—History and consequences: New York, Academic Press.

Emery, K.O., and Aubrey, D.G., 1991, Sea levels, land levels, and tide gauges: New York, Springer-Verlag.

FitzGerald, D.M., Fenster, M.S., Argow, B.A., and Buynevich, I.V., 2008, Coastal impacts due to sea-level rise: Annual Review of Earth and Planetary Sciences, v. 36, no. 1, p. 601–647, doi:10.1146/annurev.earth.35.031306.140139.

Grove, J.M., 2003, The little ice age: Psychology Press.

Hays, J.D., Imbrie, John, and Shackleton, N.J., 1976, Variations in the Earth's orbit—Pacemaker of the ice ages: Science, v. 194, p. 1121–1132.

Imbrie, John, and Imbrie, K.P., 1986, Ice ages—Solving the mystery: Harvard University Press.

Imbrie, John, and Imbrie, J.Z., 1980, Modeling the climatic response to orbital variations: Science, v. 207, no. 4434, p. 943–953, doi:10.1126/science.207.4434.943.

International Geosphere-Biosphere Programme, 2013, accessed August 2013 at www.igbp.net.

Karl, T.R., Melillo, J.M., and Peterson, T.C., eds., 2009, Global climate change impacts in the United States: Cambridge University Press.

Kennett, J.P., 1977, Cenozoic evolution of Antarctic glaciation, the circum-Antarctic Ocean, and their impact on global paleoceanography: Journal of Geophysical Research, v. 82, no. 27, p. 3843–3860.

Mann, M.E., Zhang, Zhihua, Hughes, M.K., Bradley, R.S., Miller, S.K., Rutherford, Scott, and Ni, Fenbiao, 2008, Proxy-based reconstructions of hemispheric and global surface temperature variations over the past two millennia: Proceedings of the National Academy of Sciences, v. 105, no. 36, p. 13252–13257.

Miller, K.G., Fairbanks, R.G., and Mountain, G.S., 1987, Tertiary oxygen isotope synthesis, sea level history, and continental margin erosion: Paleoceanography, v. 2, no. 1, p. 1–19.

Miller, K.G., Kominz, M.A., Browning, J.V., Wright, J.D., Mountain, G.S., Katz, M.E., Sugarman, P.J., Cramer, B.S., Christie-Blick, Nicholas, and Pekar, S.F., 2005, The Phanerozoic record of global sea-level change: Science, v. 310, no. 5752, p. 1293–1298.

Nerem, R.S., Chambers, D.P., Choe, C., and Mitchum, G.T., 2010, Estimating mean sea level change from the TOPEX and Jason altimeter missions: Marine Geodesy, v. 33, no. S1, p. 435–446.

Oglesby, R.J., and Saltzman, Barry, 1992, Equilibrium climate statistics of a general circulation model as a function of atmospheric carbon dioxide, I—Geographic distributions of primary variables: Journal of Climate, v. 5, no. 1, p. 66–92.

PAGES - Past Global Changes Project, 2013, accessed August 2013 at www.pages-igbp.org.

Peltier, W.R., 1994, Ice age paleotopography: Science, v. 265, no. 5169, p. 195–201.

Penland, Shea, and Ramsey, K.E., 1990, Relative sea-level rise in Louisiana and the Gulf of Mexico—1908–1988: Journal of Coastal Research, p. 323–342.

Pugh, D.T., 1987, Tides, surges and mean sea-level—A handbook for engineers and scientists: Chichester, United Kingdom, Wiley, 472 p.

Raymo, M.E., 1997, The timing of major climate terminations: Paleoceanography, v. 12, no. 4, p. 577–585.

Raymo, M.E., Ruddiman, W.F., and Froelich, P.N., 1988, Influence of late Cenozoic mountain building on ocean geochemical cycles: Geology, v. 16, no. 7, p. 649–653.

Rind, David, and Peteet, Dorothy, 1985, Terrestrial conditions at the Last Glacial Maximum and CLIMAP sea-surface temperature estimates—Are they consistent?: Quaternary Research, v. 24, no. 1, p. 1–22.

Rind, David; Peteet, Dorothy; Broecker, Wallace; McIntyre, Andrew; and Ruddiman, W.F., 1986, The impact of cold North Atlantic sea surface temperatures on climate—Implications for the Younger Dryas cooling (11–10 k): Climate Dynamics, v. 1, no. 1, p. 3–33.

Roberts, Neil, 2009, The Holocene—An environmental history (2): Wiley, 344 p.

Ruddiman, W.F., 2003, The anthropogenic greenhouse era began thousands of years ago: Climatic Change, v. 61, no. 3, p. 261–293.

Ruddiman, W.F., 2008, Earth's climate—Past and future (2): W.H. Freeman, 388 p.

Ruddiman, W.F., 2010, Plows, plagues, and petroleum—How humans took control of climate: Princeton University Press.

Sigman, D.M., and Boyle, E.A., 2000, Glacial/interglacial variations in atmospheric carbon dioxide: Nature, v. 407, no. 6806, p. 859–869.

Strauss, Ben; Tebaldi, Claudia; and Ziemlinski, Remik, 2012, Surging seas—Sea level rise, storms & global warming's threat to the U.S. coast—A Climate Central Report, March 14, 2012: Climate Central. [Also available at http://sealevel.climatecentral.org/research/reports/surging-seas.]

Stuiver, Minze, and Braziunas, T.F., 1993, Sun, ocean, climate and atmospheric $^{14}CO_2$—An evaluation of causal and spectral relationships: The Holocene, v. 3, no. 4, p. 289–305.

Tebaldi, Claudia, Strauss, B.H., and Zervas, C.E., 2012, Modelling sea level rise impacts on storm surges along U.S. coasts: Environmental Research Letters, v. 7, no. 1, doi:10.1088/1748-9326/7/1/014032.

Thurman, H.V., and Burton, E.A., 1997, Introductory oceanography: New Jersey, Prentice Hall.

Vail, P.R.; Mitchum, R.M., Jr.; and Thompson, S., III, 1977, Seismic, stratigraphy and global sea level changes of sea level part 4—Global cycles of relative changes in sea level, *in* Payton, C.E., ed., Seismic stratigraphy—Applications to hydrocarbon exploration: AAPG Memoir 26, American Association of Petrology Geology, Tulsa, Okla., p. 83–97.

Wright, H.E., ed., 1993, Global climates since the last glacial maximum: University of Minnesota Press.

Zachos, James; Pagani, Mark; Sloan, Lisa; Thomas, Ellen; and Billups, Katharina, 2001, Trends, rhythms, and aberrations in global climate 65 Ma to present: Science, v. 292, no. 5517, p. 686–693.

Publishing support provided by
Lafayette Publishing Service Center

ISSN 2330-7102 (online)
http://dx.doi.org/10.3133/pp1815